

✓
1N-91-CR
86 P

Final Report
on
PIONEER VENUS DATA ANALYSIS
FOR THE
RETARDING POTENTIAL ANALYZER

NASA/AMES contract NAS2-12902

Aug. 1, 1988 - SEP. 30, 1993

William C. Knudsen
Knudsen Geophysical Research, Inc.
18475 Twin Creeks RD.
Monte Sereno, CA 95030

Date: Oct. 5, 1993

(NASA-CR-194673) PIONEER VENUS
DATA ANALYSIS FOR THE RETARDING
POTENTIAL ANALYZER Final Technical
Report, Aug. 1988 - Sep. 1993
(Knudsen Geophysical Branch) 86 p

N94-17292

Unclas

G3/91 0193599

TABLE OF CONTENTS

	<u>page</u>
SUMMARY	3
INTRODUCTION.....	3
MISSION OPERATIONS.....	4
ORPA HEALTH	5
PROJECT OFFICE SUPPORT	5
DATA REDUCTION.....	5
NSSDC DATA SUBMISSIONS.....	6
DATA ANALYSIS RESULTS PRIOR TO ENTRY	6
Improvement of Reduction Algorithms	6
Solar Cycle Changes in the Venus Ionosphere.....	7
Additional Ionospheric Results	7
Suprathermal Electron Measurements.....	7
 PV SPACECRAFT ENTRY RESULTS	 8
PUBLICATIONS AND PRESENTATIONS.....	9
Publications	9
Presentations.....	9
CONCLUSIONS.....	10
APPENDIX A	11
APPENDIX B	12
APPENDIX C	13
REFERENCES.....	14

SUMMARY

This report describes the results of the data reduction, data analysis, and data archiving of the Pioneer Venus (PV) Retarding Potential Analyzer (ORPA) experiment for the period Aug. 1, 1988 to Sep 30, 1993. The ORPA was one of twelve instruments carried on the PV spacecraft and one of sixteen experimental investigations. The Principal Investigator of the ORPA experiment was William C. Knudsen of Knudsen Geophysical Research Inc. He has been responsible for representing the interests of the ORPA at PV Project Office meetings, directing the data reduction and archiving activities which were performed by NASA/Ames, analyzing the reduced ORPA data, and reporting and publishing the scientific results of the analysis. In addition, he has provided data, software, and assistance to Prof. Douglas Jones of the Brigham Young University, and Dr. Karl Spenner of the German Fraunhofer Institute during approximately the last two years of the contract period. Prof. Jones and Dr. Spenner are analyzing ORPA solar wind electron data and entry ionospheric data, respectively.

Periapsis altitude of the PV spacecraft descended slowly from approximately 1900 km in Aug. 1988 to approximately 130 km in Oct. 1992 at which time communication with the spacecraft ceased. The spacecraft was above the ionosphere for most of the contract period, dipping into the ionosphere in the nightside hemisphere primarily during the last three months prior to loss of the spacecraft. Because of this sampling restriction, the ORPA was commanded into its suprathermal electron mode during most of the contract period, a mode in which it measured solar wind electron data, and was commanded into its ionospheric measuring modes only when the spacecraft began dipping into the ionosphere toward the end of the mission.

The quantity of data recorded during the last, approximately four years of the PV spacecraft lifetime covered by this contract was reduced considerably from that obtained previously because of the reduction in power available for operating the science instruments as a result of spacecraft solar cell deterioration, loss of half of the spacecraft solid state memory for storing science data during occultations, and partial failure of the ORPA during the last two years of spacecraft life.

Despite the reduction in available data, especially ionospheric data, important scientific discoveries resulted from this contract. The most significant was the discovery of a strong solar cycle change in the size of the dayside ionosphere and the resulting 'shutoff' of flow of dayside ions into the nightside hemisphere. The large topside O⁺ F2 ionospheric layer observed in both the day- and nightside hemispheres during the first three years of the Pioneer Venus mission is essentially absent during the solar minimum activity period.

INTRODUCTION

The Pioneer Venus retarding potential analyzer instrument (ORPA) is one of eleven instruments that was flown on the Pioneer Venus spacecraft, a spacecraft that was launched May 20, 1978 by the United States National Aeronautics and Space Administration (NASA), was inserted into orbit about Venus on December 4, 1978, and ceased transmitting data to earth following the periapsis pass of orbit 5056. The last data recovered was from a periapsis period from orbit 5055 on Oct. 7, 1992. The purpose of the Pioneer Venus (PV) Mission was to significantly increase our knowledge of the plasma environment, atmosphere, surface, and interior of planet Venus.

The ORPA was selected for the PV mission to measure several important ionospheric plasma quantities as the spacecraft swept through the ionosphere near the orbit periapsis. Quantities measured uniquely by the ORPA include ion temperature, ion bulk velocity (vector), and suprathermal electron temperature. Quantities measured in common with other instruments include total ion (plasma) density, major ion concentrations, electron temperature, and spacecraft potential. The ORPA has also proven capable of

measuring the solar wind electron temperature and density, a capability which has proven to be of great value in defining plasma properties in the boundary layer between the solar wind and ionosphere.

The PV mission data acquisition, reduction, analysis and dissemination activities since December 4, 1978 have been separated into four programmatic time periods, Prime Mission, May 1978 - Sept. 1979; Extended Mission I, Oct. 1979 - Mar. 1981; Extended Mission II, Mar. 1981 - Sept. 1986; and Extended Mission III, Sept. 1986 - Sept. 1993. The data reduction and analysis activities reported herein began Aug. 1, 1988 and extended through Sept. 1993 and covered most of the Extended Mission III period. For scientific purposes, the mission has been divided into three mission phases. Phase I began at the time of insertion of the PV spacecraft into orbit about Venus and ended to approximately Dec. 1980 at which time spacecraft fuel ceased to be used to maintain periapsis altitude at low altitude (Fig. 1). Phase II extended from approximately Dec. 1980 to April 1991. Phase III extended from April 1991 to termination of communication with the spacecraft which occurred on Oct. 8, 1992. The data acquisition period covered by this final report is from Aug. 1 1988 through Oct. 7 1992.

Solar conditions changed during this data acquisition period from solar cycle minimum at the beginning (1988) to solar cycle maximum, 1989-1990, and back down toward solar cycle minimum at the end. Periapsis altitude decreased from its maximum value of approximately 2300 km at the beginning of the contractual period to altitudes as small as approximately 130 km during the final low altitude maintenance period. This combination of conditions prevented in situ measurements of the ionosphere during solar minimum conditions existing during phase II but provided a short period of in situ measurements at low altitude in the nightside ionosphere during solar conditions approaching that of solar minimum during the final entry period of the mission.

Despite the paucity of in situ measurements of the ionosphere during solar minimum conditions, the measurements that were made provided the clues and, later, the evidence for the "breathing" of the Venus ionosphere that occurs through a solar cycle. This breathing was not anticipated at the end of the prime mission and is probably the most significant contribution to the overall mission that was made during the contractual period covered by this final report.

The ORPA data analysis and reporting activities for the subject contract have been performed by William C. Knudsen (WCK). The data reduction has been performed at NASA/Ames Research Center under the supervision of WCK with Joe Goosby, a contract employee with Sterling Software performing programming and computer operations.

MISSION OPERATIONS

The mission operations during this contract affected ORPA mode commanding and data recovery in the following way: The declining power output of the spacecraft solar cells dictated that the ORPA be turned on during a limited portion of each orbit. Hence, it was necessary to turn the ORPA off and on at least once each orbit. During the early years of the mission, the ORPA was left on at all times, and commanding it consisted of sending mode reconfiguration commands only. The spacecraft data storage unit lost half its data storage capacity which cut in half the data that could be stored during short occultations (periods when the spacecraft was shadow from the Earth by Venus). The orbit periapsis altitude was above the ionosphere except for the last year of the mission. The consequences of these conditions were that the ORPA was commanded into its suprathermal electron mode most of the time except for the last year. During the last year, It was commanded into its thermal electron and ion modes during short periods around periapsis. Because of the limited power output of the solar cells, the loss of half the data storage unit, competition among principle investigators for data formats and bit rates, and a partial failure of the ORPA, ionospheric data obtained by the ORPA during the final eclipse season of the mission was severely limited.

ORPA HEALTH

The ORPA operated within its specifications until June 1990 at which time it began to respond to commands erratically. The data stream from the instrument was observed on some occasions to be anomalous after turn-on and mode configuration by ground command. At this phase of the mission, the ORPA, as well as other instruments, was turned off during portions of the orbit to conserve power. After experimentation over a period of approximately one year, I determined, with the cooperation of the Pioneer operations center, that the ORPA was accepting ground commands correctly approximately 50% of the time. The remainder of the times, the ground commands were implemented incorrectly, and the bit stream from the instrument was anomalous. A procedure was implemented with the operations center such that if the bit stream was observed to be anomalous after ORPA turn-on, the ORPA would be turned off and then re-commanded. Because of the two-way time delay between sending a command and receiving the instrument response, this procedure was possible only once per orbit and, then, not on all orbits. With this procedure, we achieved approximately 70% data recovery of the total possible recovery during the last year of spacecraft operation.

PROJECT OFFICE SUPPORT

WCK attended all Science Study Group meetings conducted during this contract period and presented the results of his analyses therein. He also attended all of the Orbiter Mission Operations Planning (OMOP) meetings and contributed to the deliberations as they affected the ORPA.

DATA REDUCTION

The reduction of the ORPA bit stream to engineering numbers and, thence, to geophysical quantities such as ion temperature and density, the computer manipulation and plotting of the geophysical quantities to aid analysis, and the submission of the geophysical quantities in appropriate format to the National Space Science Data Center (NSSDC) was performed at NASA/Ames Research Center under the direction of a NASA appointed PV ORPA data manager. The PV ORPA data manager was Robert C. Whitten, initially, and, thereafter, John Mihalov. The programming and computer operations required to accomplish the reduction were performed primarily by Mr. Joseph Goosby, a contract employee of Sterling Software.

The programming and data reduction activities performed by Mr. Goosby has been disappointing. I have been unable to accomplish all the analysis activities that I could have accomplished had the programming and data reduction been performed more effectively. I have had to restrict my requests for data analysis because of delays and lack of accomplishing the programming and routine data reduction.

All of the ORPA data from orbit 1 to orbit 5055 have been re-reduced during this contract period with revised reduction software programs that were written by WCK to improve the accuracy of the derived geophysical quantities. With the exception of the thermal electron mode, derivation of geophysical quantities from the I-V curves returned by the ORPA requires that the I-V curves be fit with a theoretical expression that predicts the ion or electron current that should be observed as a function of retarding potential. The theoretical expression depends on instrument parameters as well as the ambient plasma geophysical parameters. WCK spent a substantial fraction of his efforts during this contract modifying and improving the theoretical expressions for the ion current when the ORPA is operating in its ion mode and for the electron current when it is operating in the suprathermal electron mode.

NSSDC DATA SUBMISSIONS

The first product that has been submitted to the National Space Science Data Center (via the Planetary Data System (PDS) Node at the University of California) is called the RDR files and contains the ORPA current-voltage (I-V) data for all retarding potential sweeps for all orbits. The I-V data are in engineering quantities, Amperes and Volts, and are associated with a status word which describes the instrument mode in which the data were taken and a set of ephemeris quantities which describe the time of measurement and the orientation and location of the instrument and spacecraft. The RDR files will be essential for verifying the accuracy of the least-squares fits from which the geophysical quantities to be submitted as the Tables files and UADS files were derived. PDS has transcribed the RDR files from 9 track magnetic tapes to CD ROMS for convenient use by the scientific community. The RDR files for the final entry period of the PV mission are presently being used by Dr. Karl Spenner of the German Fraunhofer institute in Freiburg to derive the geophysical quantities for the entry period. Dr. Spenner was a Co-investigator on the ORPA experiment during the prime PV mission period, and was responsible for supplying the sensor head for the ORPA.

Two additional products which are to be submitted to NSSDC are called the Tables File and the UADS File. The Tables File contains all the geophysical quantities derived from the ORPA for the entire PV mission. It is complete and archived at NASA/Ames Research Center at the present time. The UADS File will contain ORPA geophysical quantities for +/- one half hour about periapsis for each orbit and will conform to the format specified by the PV Science Study Group for this File. The UADS file contains a subset of the geophysical quantities stored in the Tables file. The PV ORPA data manager has been instructed to submit the ORPA UADS file consistent with the "letter to distribution" by Lawrence Colin dated Sept. 7, 1983, the report referred to therein and titled "Pioneer Venus Mission, Instructions for Data Submissions to the National Space Science Data Center, A Committee Report" by Roger Craig, NASA Ames Research Center dated Aug. 11 1983, and the document "Pioneer Venus Orbiter Retarding Potential Analyzer NSSDC Submission Documentation" by William C. Knudsen Dated Nov. 4, 1993. The letter, report and document are reproduced in Appendix C. Submission of the ORPA reduced data in the UADS form satisfies the contract requirement for data submission to NSSDC.

ANALYSIS RESULTS

Improvement of Reduction Algorithms

A substantial fraction of WCK's efforts during this contract has been expended on improving the least-squares algorithms used to obtain geophysical quantities from the suprathermal electron and ion modes of the ORPA. The algorithms used prior to the re-reduction of all orbits, which took place in the Spring of 1993, were based on the assumption that the grid walls of the ORPA were infinite in radius and the grid thicknesses were zero. He believed that these assumptions were most likely to be affecting the density and, to a smaller extent, the temperature of the suprathermal electrons derived from the I-V curves. In an early publication containing ORPA solar wind electron densities and orbiter plasma analyzer (OPA) solar wind ion densities, it was evident that the ORPA densities were consistently a factor of 2 below the OPA ion densities. To try and improve the agreement of the densities from the two instruments, he undertook a numerical analysis of the reduction of the electron current to an RPA having the geometry and grid thicknesses of the ORPA caused by the existence of a finite wall radius and finite thickness of grids. The results of this analysis have been published [Knudsen, 1992a] and incorporated into the ORPA data reduction program. The new algorithm is now providing solar wind densities that are approximately a factor of two larger than those obtained without the correction for finite wall radius and grid thickness. Professor Douglas Jones, of the Brigham Young University, is currently analyzing solar wind electron density and temperature data from the ORPA and will publish a detailed comparison of densities derived from the ORPA and OPA.

Solar Cycle Changes in the Venus Ionosphere

The most significant achievement of this contract effort is the discovery by WCK of a rather dramatic solar cycle variation in the size of the Venus ionosphere. The Venus ionosphere, as initially measured early in the PV mission, typically extended from below 150 km altitude to 300 km altitude at low solar zenith angles (SZA) and to 900 km at 90 deg SZA. In the nightside hemisphere, an upper ionospheric layer of atomic ions existed which extended over 900 km in altitude and had a density of the order of $1 \times 10^3 \text{ cm}^{-3}$. This was the picture generally held of the Venus ionosphere prior to his discoveries reported in publications [Knudsen, et al. 1986; Knudsen et al. 1987; Knudsen, 1988; and Knudsen, 1992b]. A summary of the Venus ionosphere as understood up through 1991 is presented in the publication "The Venus Ionosphere from In-situ Measurements" [Knudsen, 1992b] and is included in this report as Appendix A. The solar cycle variation as described therein is now generally accepted and has been verified by the reentry data obtained in the last 50 orbits of the PV mission and which are currently being reported in presentations and publications by several of the PV principal investigators.

Additional Ionospheric Results

Two additional papers on ionospheric topics, "Role of Hot Oxygen in Venusian Ionospheric Ion Energetics and Supersonic Antisunward Flow" [Knudsen, 1990a] and "The Venus Transterminator Ion Flux at Solar Maximum" [Knudsen and Miller, 1992], were also published during this contract. The first paper drew attention to the role of hot oxygen in heating the Venus ionosphere and in affecting the transterminator flow of dayside O^+ ions. The second paper presented a more detailed and accurate measurement of the average transterminator flux of O^+ ions during solar maximum activity than had been presented in an early paper. In the second paper, evidence was again presented in favor of the belief that the major source of ionization of the nightside ionosphere during solar maximum activity is transterminator O^+ transport.

Suprathermal Electron Measurements

One of the important goals of this contract was to obtain as much information from the suprathermal electron mode measurements as possible since the PV orbit periapsis was above the sensible ionosphere most of the contract period. Valuable suprathermal electron data could be obtained in the mantle, in the solar wind in the dayside hemisphere, and in the ionotail (wake of the planet).

Possible mass loading of the solar wind up stream of the Venus bow shock has been an interesting subject because of the relatively close proximity of the Venus bow shock (approximately 2000 km above the Venus surface in the sub solar region). Brace et al. [1985] and Brace [1987] observed increased electron current to the electron temperature probe (ETP) upstream of the Venus bow shock in the sub solar region and referred to this region as the precursor region. They suggested that mass loading of the solar wind upstream of the bow shock through charge exchange and photo ionization of the neutral, hot atomic oxygen halo was responsible for the increased current. Knudsen [1985] presented observations by the ORPA of a smooth increase in solar wind electron density and temperature in the same region and assumed the cause to be mass loading of the solar wind. In a subsequent paper titled "The Venus Precursor: An Environmental Effect on the Pioneer Venus Spacecraft", Knudsen et al. [1989] concluded that both the increase in current observed by the ETP and the increase in density of a relatively cold (about 1 eV in temperature) electron population measured by the ORPA were caused by an increase in the density of secondary electrons trapped in the potential well surrounding the PV spacecraft. The increase in Solar wind electron density and temperature which had been reported by Knudsen [1985] was shown to be caused by the grazing passage of the PV spacecraft into and through the bow shock transition region. Knudsen et al. [1989] concluded, further, that there was no evidence in their data for a mass loading of the upstream solar wind density that exceeded a few percent.

The source of the suprathermal electrons observed in the Venus umbra with an energy distribution characterized by a temperature of about 14 eV has been an intriguing question ever since the electrons were

first measured by Gringauz et al. [1979] with a retarding potential analyzer carried on the Venera 9 spacecraft in 1976. The same population has been measured by the PV ORPA, and the source of the electrons has remained unknown. However, measurements of the suprathermal electron temperature and density as the PV spacecraft travels from the magnetosheath into the planet umbra strongly suggest that the source of the electrons is the solar wind. The temperature of the suprathermal electron distribution decreases smoothly from that of the shocked solar wind flowing in the magnetosheath to that of the suprathermal electrons co-located with the ionospheric plasma in the umbra. Frequently, but not always, the density decreases in like manner. This variation of the suprathermal electrons with location strongly suggests that the suprathermal electrons are solar wind electrons that have infiltrated the nightside ionosphere and ionotail. This suggestion and the measurements supporting it have been presented at an annual meeting of the American Geophysical Union [Knudsen, 1990b]. A paper containing these results will be published in due time.

The results of a study of the suprathermal electron flux in ionospheric holes are presented in Appendix B. The results, titled "Suprathermal Electron Flux in Venus Ionospheric Holes" was submitted for publication but was rejected, because only two examples were presented. From these two examples and additional examples not presented, WCK concluded that the suprathermal electron flux observed in ionospheric holes is similar to that observed outside the holes and that the holes are not formed by the existence of a significant electric field parallel to the field as has been suggested by Grebowsky and Curtis [1981]. The cause or causes of ionospheric holes remains a significant unsolved problem, and WCK intends to pursue this problem by examining additional examples.

WCK contributed data and analysis to two studies undertaken by Dr. Devrie Intriligator. One study resulted in the publication of a paper "Evidence for Unusually high densities of Plasma in the Venus Ionosheath" [Intriligator et al., 1991]. This study attributed the high density of hot plasma to ionospheric plasma that had been drawn into and heated in the ionosheath. The second study, "Evidence for Ion Transport on the Venus Ionotail" is an effort to report on the first believable low energy ion fluxes measured by the Plasma analyzer and relate these measurements and related measurements by the other in situ instruments to a narrow plasma feature observed on orbit 4574. This paper has not been accepted for publication at the present time.

PV SPACECRAFT ENTRY RESULTS

Descent of the PV orbit periapsis altitude into the ionosphere during the last few weeks prior to spacecraft burnup was a particularly important event of the PV mission. The periapsis passes occurred in the nightside ionosphere during a period of time when the Sun's activity was approaching a minimum, and the periapsis altitude was permitted to get smaller than it was during the early years of the mission since the risk of losing the spacecraft was of little consequence. The significance of the entry occurring at a time of near-minimum solar activity is that in situ measurements could confirm predictions that the transport of dayside O⁺ ions across the terminator would be reduced a factor of ten during solar minimum. WCK and his co-authors had predicted in 1986 and 1987 that the nightside topside O⁺ layer density would be reduced a factor of ten as a result of the reduction in transterminator O⁺ flow [Knudsen et al., 1986; 1987]. Preliminary analysis of a few ORPA orbits and reported results from the orbiter ion mass spectrometer and electron temperature probe instruments for the entry period confirm the accuracy of the prediction.

Unfortunately, the amount of ORPA data obtained during this period was severely limited by the reduced interval of time that the spacecraft could store data, the limited bit rate, and the partial failure of the ORPA. Nevertheless, significant results will be forthcoming from the ORPA entry data. Analysis of the ORPA entry data may not be accomplished under this contract because of slow progress in processing of ORPA data at Ames Research Center. If no results are forthcoming from this contract, results will be forthcoming from an analysis effort by Dr. Karl Spenner sponsored by the German government. The effort is a three year effort and is in support of analysis of ORPA data obtained during the entry period. Dr. Spenner has

been supplied our data reductions programs and the entry ORPA data. He is currently reducing the data by interactively performing least-squares fit of the theoretical ion current algorithm, mentioned above, to the entry ORPA I-V data. Interactive fitting of the algorithm to the data is essential because of the meager amount of ORPA data and the low level of the currents.

PUBLICATIONS AND PRESENTATIONS

Publications

The scientific papers written and completed during this contractual period are:

Phillips, J. L., J. G. Luhmann, W. C. Knudsen, and L. H. Brace, Asymmetries in the location of the Venus ionopause, *J. Geophys. Res.*, **93**, 3927-3941, 1988

Knudsen, W. C., Solar cycle changes in the morphology of the Venus ionosphere, *J. Geophys. Res.*, **93**, 8756-8762, 1988.

Knudsen, W. C., J. G. Luhmann, C. T. Russell, F. L. Scarf, The Venus precursor: An environmental effect on the Pioneer Venus spacecraft, *J. Geophys. Res.*, **94**, 197-207, 1989.

Knudsen, W. C., Role of hot oxygen in Venusian ionospheric ion energetics and supersonic antisunward flow, *J. Geophys. Res.*, **95**, 1097-1101, 1990.

Singhal, R. P., R. C. Whitten, and W. C. Knudsen, Comparative dynamics of the ionospheres of Venus and Mars at large solar zenith angles, *Indian J. Rad. and Space Sci.*, **9**, 88-102, 1990.

Intriligator, D. S., L. Brace, S. H. Brecht, W. C. Knudsen, F. L. Scarf, R. J. Strangeway, and H. Taylor, Evidence for unusually high densities of plasma in the Venusian ionosheath, *Geophys. Res. Lett.*, **18**, 61-64, 1991.

Knudsen, W. C., Finite grid radius and thickness effects on RPA- measured suprathermal electron density and temperature, *J. Geophys. Res.*, **97**, 13,767, 1992a.

Knudsen, W. C., The Venus Ionosphere from In-situ Measurements, in *Venus and Mars: Atmospheres, Ionospheres, and Solar Wind Interactions*, J. G. Luhmann, M. Tatrallyay, and Robert O. Pepin, Eds., pp. 237 - 263, AGU Geophysical Monograph 66, The American Geophysical Union, Wash. DC., 1992b.

Knudsen, W. C. and K. L. Miller, The Venus transterminator ion flux at solar maximum, *J. Geophys. Res.*, **97**, 17,165, 1992.

Knudsen, W. C., Venus' internal magnetic field and its reconnection with the IMF, *J. Geophys. Res.*, submitted 1993.

Presentations

The presentations of scientific results derived from the data reduction and analysis of ORPA and other PV instruments are as follows:

Knudsen, W. C., Current picture of the Venus ionosphere from Pioneer-Venus and major unknowns, Twenty-seventh Plenary Meeting of COSPAR, ABSTRACTS, p237, Espoo, Finland, July, 1988.

Knudsen, W. C., Role of hot oxygen in Venusian ionospheric ion energetics and antisunward flow, *EOS*, 70, 1177, 1989

Knudsen, W. C., The Venus Ionosphere from In Situ Measurements, AGU Chapman Conference on Comparative Study of Venus and Mars, Balatonfured, Hungary, June 3-9, 1990.

Knudsen, W. C., Origin of Suprathermal Electrons in the Venus Ionosphere, *EOS*, 71, 1431, 1990.

Knudsen, W. C., Pioneer Venus Mission and Venus Plasma Environment, presented at the April 23 American Institute of Aeronautics and Astronautics, San Francisco Section, April 23, 1992a.

Knudsen, W. C., Venus internal magnetic field and its interaction with the interplanetary magnetic field, p 60, International Colloquium on Venus, Aug. 10 -12, 1992b, Pasadena, CA.

Knudsen, W. C., Venus' Internal Magnetic Field and its Interaction with the Interplanetary Magnetic field, *EOS, Trans., Amer. Geophys. Union*, 74, 111, 1993.

CONCLUSIONS

The PV mission has been an outstanding success, and the results from the ORPA have contributed greatly to that success despite the fact that it had a small -probably the smallest- share of the spacecraft bit stream. Significant experimental contributions made by the ORPA include planet-wide measurement of the ionospheric electron and ion temperature fields, ion bulk velocity field, total and major ion densities, ionopause altitude, and photoelectron energy distribution. The ORPA has also contributed suprathermal electron density and energy distribution measurements in the region immediately adjacent to the ionosphere but dominated by the solar wind plasma.

Major scientific discoveries resulting from ORPA measurements and published by ORPA team members include: supersonic bulk flow of the ionospheric plasma across the Venus terminator, acceleration of the supersonic flow by the thermal pressure gradient of the ionosphere across the terminator, maintenance of the nightside ionosphere during solar activity maximum conditions primarily by the supersonic flow of the dayside ionospheric plasma into the nightside hemisphere, existence of a transition region named the mantle above the ionopause, and compression of the ionopause to low, median altitude by the solar wind dynamic pressure during solar activity minimum conditions with consequent large reduction in the density of the nightside O⁺ layer.

APPENDIX A
THE VENUS IONOSPHERE FROM IN SITU MEASUREMENTS
BY
WILLIAM C. KNUDSEN

Reproduced from:

Venus and Mars: Atmospheres, Ionospheres, and Solar Wind Interactions, J. G. Luhmann, M. Tatrallyay,
and Robert O. Pepin, Eds., pp 237-263, AGU Geophysical Monograph 66, The American Geophysical
Union, Washington D.C. 1992.

THE VENUS IONOSPHERE FROM IN SITU MEASUREMENTS

WILLIAM C. KNUDSEN

Knudsen Geophysical Research, Inc., Monte Sereno, California

A current picture of the Venus ionosphere is presented with emphasis placed on those features revealed by the Pioneer Venus orbiter (PVO) in situ ionospheric particle measuring instruments. The PVO mission has extended over a complete cycle of solar activity and has revealed a striking change in the typical ionospheric morphology from solar maximum to solar minimum. However, the periapsis altitude history has been such that the ionosphere was sampled by the PVO in situ experiments only during periods of solar maximum. At solar maximum the typical ionosphere, in both the day and nightside hemispheres, consists of a lower F_1 -type layer composed primarily of O_2^+ ions overlain by a substantial F_2 -type layer composed primarily of O^+ ions. The dayside O^+ layer is terminated above in a narrow layer called the ionopause across which the plasma origin changes from that of the planet Venus to that of the sun. The median altitude of the dayside ionopause at solar maximum increases from approximately 300 km to 900 km as the solar zenith angle (SZA) increases from 0° to 90° and is determined by pressure balance between the ionospheric particle pressure and the normal component of the solar wind dynamic pressure for low to moderate values of the dynamic pressure. The ionopause descends to a lower altitude limit of approximately 220 km for high solar wind dynamic pressure. The principal source of ionization in the dayside ionosphere during both solar maximum and solar minimum is solar extreme ultraviolet (EUV) radiation. The principal source of ionization in the nightside ionosphere during solar maximum is a downward flux of O^+ ions originating in the day side ionosphere and transported across the nightside hemisphere by a supersonic ion wind. The Venus electron temperature is hotter than that of the earth's ionosphere, exhibits little variation with SZA, and is believed to require an external source of heat such as heat flow through the ionopause for its explanation. The ion temperature is also hotter than that of the earth's ionosphere and is also believed to require an external heat source such as heat flow through the ionopause. At higher altitudes in the central nightside hemisphere, a substantial increase in ion temperature occurs and is believed to result from conversion of directed bulk ion kinetic energy into thermal energy. Narrow regions of low density plasma and enhanced magnetic field directed parallel to the sun-Venus axis, called holes, are frequently observed in the nightside ionosphere. The dayside ionosphere contains fluxes of suprathermal electrons with energy spectra consistent with the fluxes originating from EUV photo production. Temporally and spatially variable suprathermal electron fluxes are observed in the nightside hemisphere during both solar maximum and solar minimum with a median energy spectrum similar to a 14 eV thermal distribution. These suprathermal electron fluxes are the principal ionization source of the nightside ionosphere during solar minimum and are responsible for the observed nightside aurora. Although the ionosphere was not sampled by in situ experiments during solar minimum, radio occultation measurements and inferences drawn from solar maximum in situ measurements reveal a solar minimum ionosphere that consists primarily of an F_1 -type O_2^+ layer in both the day- and nightside hemispheres. The ionopause altitude is approximately 250 km or less at all SZA, and the F_2 -type O^+ layer is missing.

INTRODUCTION

The Venus ionosphere has been sampled for over 12 years by several particle measuring instruments mounted on the NASA Pioneer-Venus orbiter (PVO) spacecraft [Colin, 1980] and, as a

**Venus and Mars: Atmospheres, Ionospheres,
and Solar Wind Interactions**
Geophysical Monograph 66
Copyright 1992 American Geophysical Union

consequence, is the most extensively explored ionosphere in the Solar System next to that of the earth. The intent in this paper is to present a current picture of the Venus ionosphere as revealed by those instruments. The presentation would be incomplete without some reference to important features revealed by the PVO magnetometer and radio occultation experiments and, also, radio occultation and in situ particle experiments carried on Russian Venera missions prior to insertion of the Pioneer Venus Orbiter spacecraft into orbit. Previous reviews of the Venus ionosphere

covering some of the same material include Brace et al. [1983a], Bauer et al. [1985], Luhmann [1986], Brace and Kliore [1991], Miller and Whitten [1991], and Luhmann and Cravens [1991].

The PVO ionospheric particle instruments include the electron temperature probe (OETP), the ion mass spectrometer (OIMS) and the retarding potential analyzer (ORPA). The OETP consists of two cylindrical Langmuir-type probes, each located at the end of a boom approximately one meter long. The instrument measures electron temperature, electron density, and total ion density [Krehbiel et al., 1980]. The OIMS is a radio frequency Bennett ion mass spectrometer capable of resolving ions differing in mass by one atomic mass unit (amu). The mass range covered is 1 to 56 amu. The OIMS also measures the component of the ion drift velocity parallel to the instrument axis which is parallel to the spacecraft spin axis. When the kinetic energy of the ions relative to the spacecraft becomes large, 20-90 eV, the ions are considered superthermal, and the density, masses, and kinetic energy of the ions are inferred from a harmonic peak analysis method [Taylor et al., 1980a, 1980b]. The ORPA is composed of several parallel,

plane grids followed by a collector. By applying appropriate control voltages on the grids, electrons or ions can be selected for energy analysis. The ORPA measures electron temperature, ion temperature, major ion composition, ion vector velocity, and the suprathermal electron energy distribution [Knudsen et al., 1980c].

OVERVIEW

An overview of Venus's ionospheric morphology at solar maximum is illustrated schematically in Figure 1 together with some of the processes that have been observed. As a first approximation, the ionosphere may be considered symmetric about the sun-Venus axis (the x axis, positive toward the sun in Figure 1). A bow shock is formed upstream of Venus in the supersonically flowing solar wind and the flow is diverted around the planet. The idealized surface separating the planetary ionosphere and the solar wind is called the ionopause. The region between the bow shock and the ionopause is referred to as the ionosheath or, alternatively, the magnetosheath. Just above the ionopause is a region called the mantle, a region in which the properties of the ionosheath are

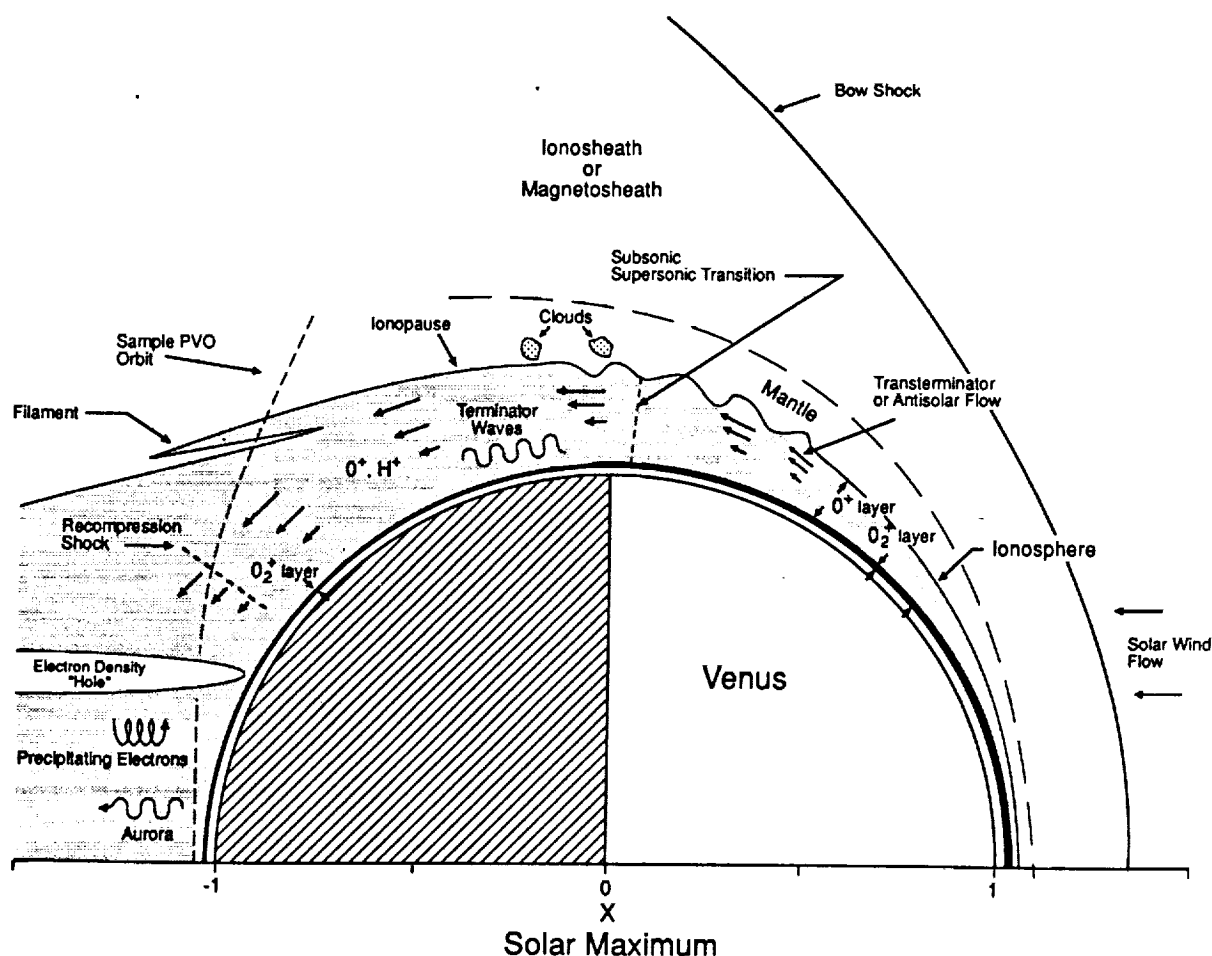


Fig. 1. Schematic representation of the Venus plasma environment during solar maximum. The identified plasma subregions are drawn approximately to scale, and several identified processes affecting the the plasmas are shown in their approximate location.

altered by the presence of neutral atoms extending above the ionopause. The ionosphere itself extends from the ionopause down to an altitude of approximately 130 km. The main or peak ionospheric layer is predominantly O_2^+ and lies between altitudes of approximately 130 and 180 km in the dayside hemisphere and between 130 and 160 km altitude in the nightside hemisphere. Above the O_2^+ layer, O^+ ions are the dominant constituent in the dayside hemisphere. The O^+ and H^+ ion densities are comparable in the nightside hemisphere. The median locations of the bow shock and ionopause in Figure 1 are drawn approximately to scale.

Some of the prominent features and processes characterizing the ionosphere at solar maximum include waves on the ionopause, elongated filaments of plasma attached to the ionosphere proper, clouds of plasma above the ionopause, the acceleration of dayside ionospheric plasma across the terminator into the nightside hemisphere at supersonic speeds, the generation of plasma waves nightward of the terminator at low altitude, the formation of relatively narrow magnetic tubes of low density plasma, called holes, oriented approximately parallel to x axis, and the precipitation of approximately 14 eV suprathermal electrons into the nightside neutral atmosphere, producing ionization and auroral emissions (see the papers by Fox and Paxton, this volume).

The present picture of the solar minimum Venus ionosphere is illustrated in Figure 2. Figure 3 shows that the PVO spacecraft periapsis altitude has been above 1800 km during the years of solar minimum. For this reason, we have no in situ measurements of the main ionospheric layer during this phase of the solar cycle so that the picture in Figure 2 is based largely on extrapolation and remote sensing. The dimensions of the solar minimum main layer has been revealed primarily by radio occultation electron density profiles recorded during solar minimum (see the paper by Kliore, this volume). However, some inferences concerning the composition and dimensions of the ionosphere at solar minimum have been made from in situ measurements made at solar maximum during periods of extreme solar wind dynamic pressure.

The solar minimum dayside layer is expected to be composed primarily of O_2^+ ions and is confined between approximately 130 and 300 km altitude. The nightside layer is also believed to be composed primarily of O_2^+ ions and is confined between approximately 130 and 200 km altitude. The in situ measurements made above 1800 km reveal that the wake consists of what are presumed to be elongated filaments of ionospheric plasma with a density of a few times 10^2 cm^{-3} . O^+ is a major ion constituent, and H^+ , although not directly measured, is also presumed to be a

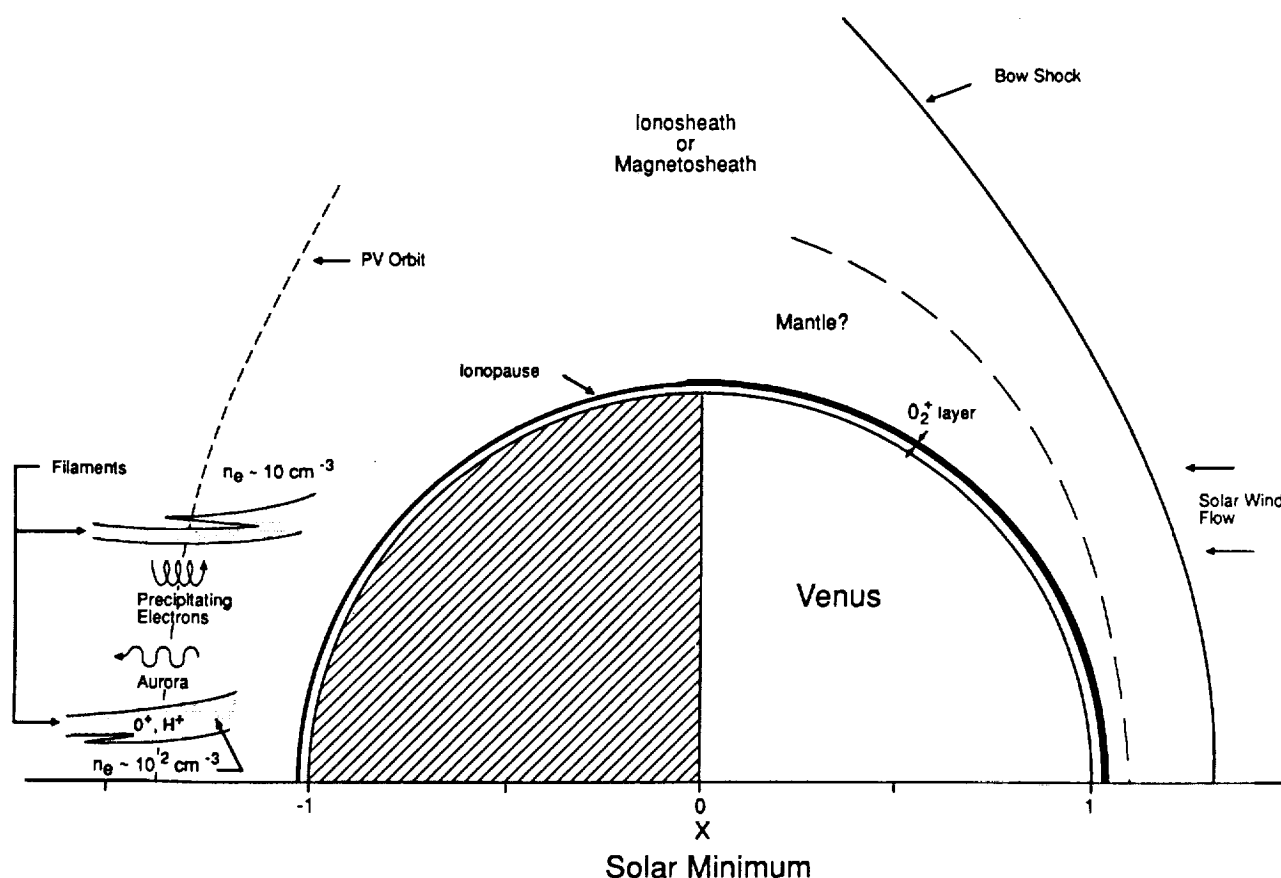


Fig. 2. Schematic representation of the Venus plasma environment during solar minimum. The PVO orbiter periapsis altitude was above 1900 km, and in situ observations of the ionosphere were limited to the relatively high altitude wake region.

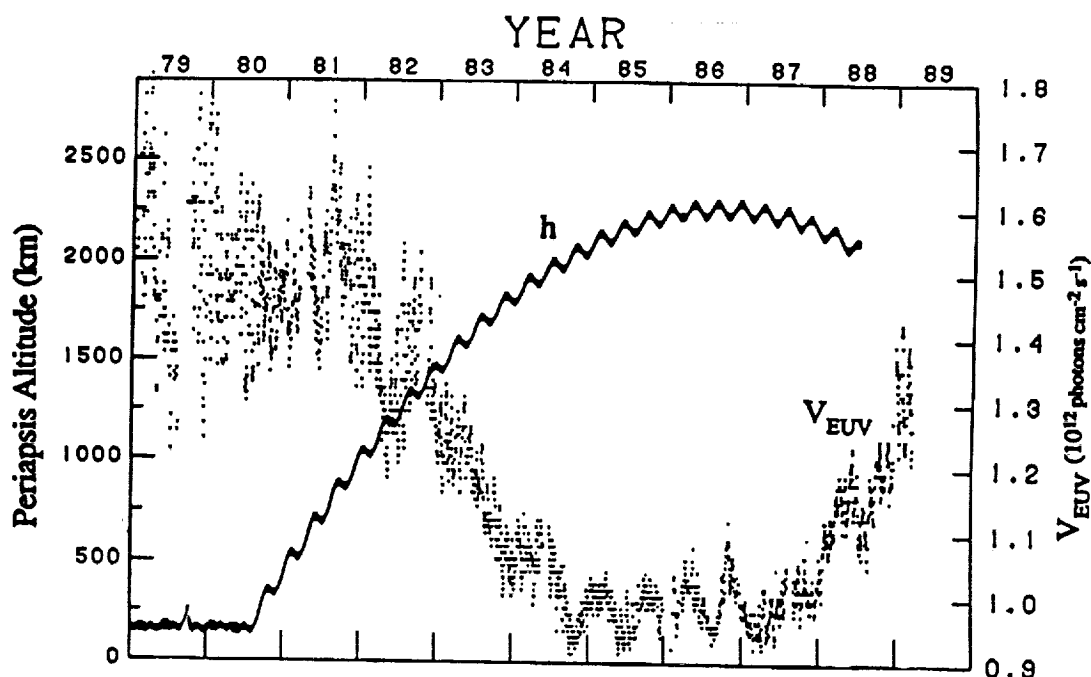


Fig. 3. PVO periapsis altitude (h) and the OETP daily measurements of the solar EUV flux (V_{EUV}) between 1979 and 1989 (from [Brace et al., 1990]). Up to the present time (April 1991), the PVO periapsis altitude has been below 500 km only during solar maximum, and it has been above 1900 km only during solar minimum.

significant constituent. Between the filaments the density is of the order of 10 cm^{-3} , a value comparable to that of the ionosheath in the wake. The magnetic field within the troughs is parallel to the x axis and is stronger than it is within the filaments. A mantle region should be present, but its existence has not been determined by measurement. Although Figures 1 and 2 illustrate what is believed to be the typical morphology of the Venus ionosphere at solar maximum and solar minimum, respectively, the solar maximum ionospheric morphology is believed to look like that of Figure 2 during periods of extreme solar wind dynamic pressure, and the solar minimum ionospheric morphology can presumably look like that of Figure 1 during periods of very low solar wind dynamic pressure.

THE SOLAR MAXIMUM IONOSPHERE

Ionopause

One of the Venus ionospheric structures that has no counterpart in the ionosphere of the earth is the relatively narrow transition region between the solar wind plasma and the ionospheric plasma called the ionopause. Figure 4 illustrates the variation in density of O^+ and O_2^+ ions measured by the PVO ion mass spectrometer as the spacecraft passed through the ionopause at a time when the solar wind dynamic pressure was low (1.8 nanoPascals (nPa), where $1 \text{ nPa} = 1 \times 10^{-8} \text{ dynes cm}^{-2}$) relative to the median effective ionospheric peak particle pressure of 6 nPa, and at a time when the solar wind dynamic pressure was high (8.5 nPa) relative to the peak ionospheric particle pressure [Mahajan and Mayr, 1989]. Both of these orbits were recorded under solar maximum conditions in the

subsolar region. At low solar wind dynamic pressure, a thick F_2 type O^+ layer overlies the O_2^+ layer, and the transition between the solar wind plasma and the O^+ layer is characterized by a drop in O^+ density by two to three orders of magnitude over an altitude interval of a few tens of kilometers. The density scale height within the ionopause is small in comparison with the approximately diffusive equilibrium O^+ scale height just below the ionopause. In this type of transition, the total pressure just above the ionopause is principally magnetic field pressure and just below the ionopause is principally thermal particle pressure. This thin type of ionopause was the most frequent type during the years of solar maximum in 1979-1981, a period during which the PVO periapsis altitude was below 500 km altitude. For large dynamic pressure, the O^+ layer is eroded down upon the O_2^+ layer, and the density scale height within the transition layer is larger than that in the low dynamic pressure case. The ionospheric plasma density scale height is approximately equal to the neutral atomic oxygen scale height [Elphic et al., 1981; Shinagawa et al., 1987; Mahajan and Mayr, 1989]. This type of ionopause layer was observed occasionally during solar maximum and is typical during solar minimum.

While it is generally agreed that the ionopause is a layer of finite thickness across which the plasma changes from that originating predominantly in the sun to that originating predominantly in the planet Venus, some experimenters have been more specific in defining the ionopause as a surface which lies within the ionopause layer. For example, Knudsen et al. [1982b] used the term, top of the ionosphere, to refer to the bottom of the ionopause layer for low solar wind dynamic pressure transitions and the term, top of the

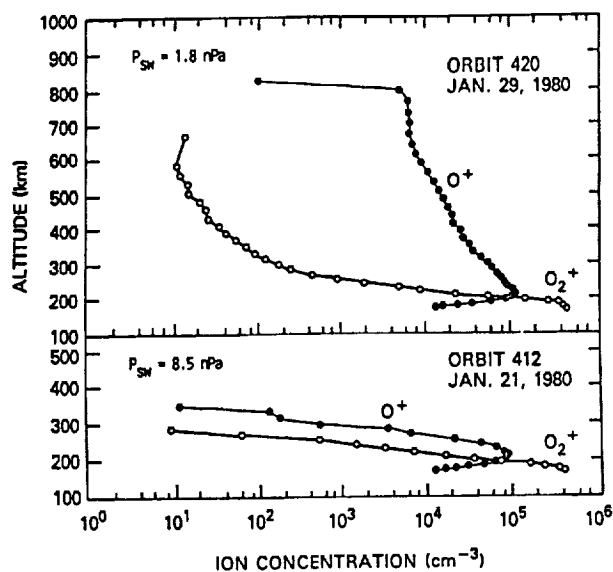


Fig. 4. Altitude profiles of the major ions O^+ and O_2^+ measured on the outbound legs of two orbits. The normal component of the solar wind dynamic pressure, obtained from magnetometer measurements, was low, 1.8 nPa, for orbit 420 and high, 8.5 nPa, for orbit 412 (adapted from [Mahajan and Mayr, 1989]).

ledge to refer to the top of the layer. Brace et al. [1980] have defined the ionopause as the altitude where the plasma density decreases below approximately 100 cm^{-3} . This location is approximately equivalent to Knudsen's top of the ledge. Elphic et al. [1980] and Phillips et al. [1988] define the ionopause altitude as that at which the magnetic pressure in the overlying magnetosheath first equals the thermal pressure of the ionospheric plasma.

The dynamic pressure of the solar wind is transmitted to the ionosphere primarily through the pressure of the magnetic barrier. As the shocked solar wind approaches the ionopause, the embedded magnetic field lines become draped around the ionopause and lose much of their plasma [Zwan and Wolf, 1976]. The region of large magnetic pressure and small particle pressure at the top of the ionopause (top of the ledge) is called the magnetic barrier. Figure 5 illustrates the variation of magnetic and ionospheric thermal pressure during one periapsis pass of the PVO spacecraft through the ionosphere. At an altitude above 400 km, the pressure is essentially all magnetic. At the bottom of the transition layer, the magnetic pressure has become negligible when compared to the ionospheric thermal pressure. At the lowest altitudes in this example, the magnetic field pressure again builds up to about 30% of the total, but this field plays no important role in the structure of the ionopause layer. Figure 5 illustrates the behavior of the magnetic field and ionospheric plasma in the ionopause transition layer for cases of moderate to low solar wind dynamic pressure. For cases with high solar wind dynamic pressure, the magnetic field remains large within the ionosphere down to the altitude of periapsis and can affect the ionospheric plasma [Luhmann et al., 1980].

The variation of the "pressure balance" ionopause altitude with ionopause pressure is illustrated in Figure 6. Total ionopause

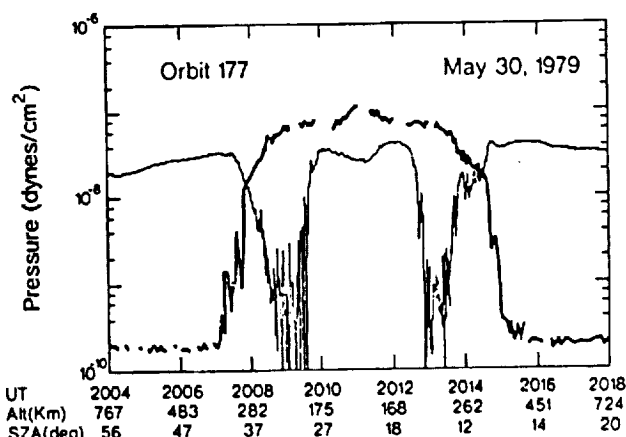


Fig. 5. Magnetic pressure $B^2/8\pi$ (light trace) and ionospheric thermal pressure (heavy trace) for a subsolar periapsis pass at solar maximum (adapted from [Elphic et al., 1980]).

pressure for this figure is the sum of magnetic pressure and ionospheric thermal pressure measured at the ionopause height. The total pressure is presumed to be equal to the component of the solar wind dynamic pressure normal to the ionopause surface reduced by the factor $K (= 0.86)$. For total pressure less than about 4 nPa, the median ionopause altitude decreases approximately linearly with increase in the logarithm of the total pressure. This is the behavior expected if the ionospheric particle pressure is balancing the total ionopause pressure. The logarithm of the ionospheric thermal pressure decreases approximately linearly with altitude (Figure 7). As the total pressure increases above 4 nPa, the median ionopause altitude approaches a lower limit of approximately 250 km. The large solar wind dynamic pressure case illustrated in Figure 3 is an example of an ionopause at the low altitude limit. For total ionopause pressures of approximately 4 nPa and larger, the ionospheric particle pressure is evidently unable by itself to balance the total ionopause pressure.

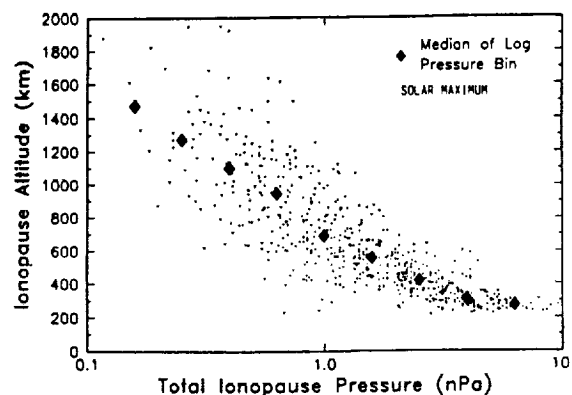


Fig. 6. Variation of the ionopause height with total ionopause pressure at solar maximum (adapted from [Phillips et al., 1988]). Total ionopause pressure is the sum of magnetic and ionospheric thermal pressure at the height of equality. All crossings with SZA less than 120° are plotted. Solid diamonds are median altitudes of log pressure bins.

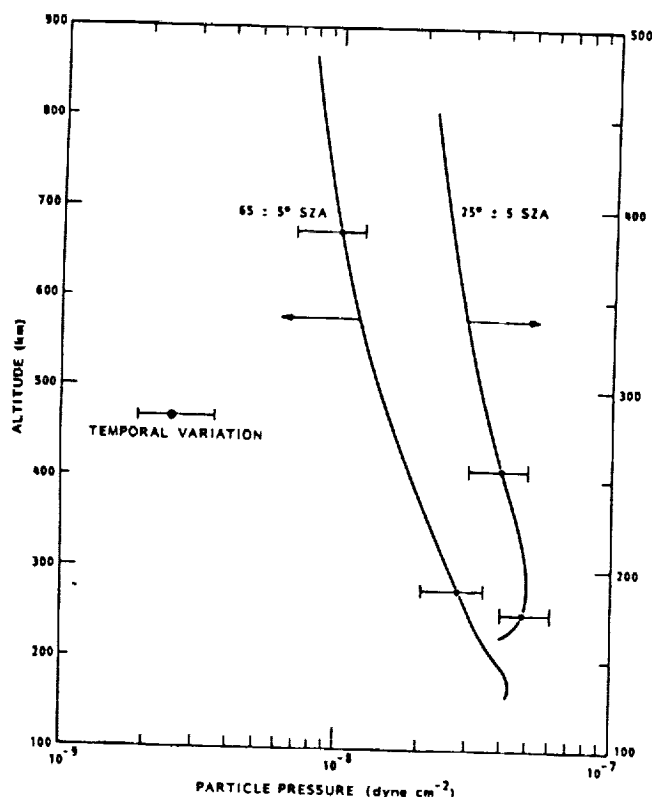


Fig. 7. Median profiles of the ionospheric particle pressure $n_i k(T_e + T_i)$ during solar maximum. Medians are medians of the local product and not the product of the medians. Note that the altitude scale is different for the two solar zenith angle intervals (from [Miller et al., 1984]).

The large variation in ionopause heights for a given total pressure illustrated in Figure 6 suggests that dynamical processes, such as the Kelvin-Helmholtz instability and other as yet unrecognized processes are operating to produce instantaneous ionopause heights that differ from that expected under steady state conditions.

Figure 8 illustrates the relative frequency of occurrence of the up-stream solar wind dynamic pressure during 1980, a period of solar maximum and the "effective" peak ionospheric pressure (6×10^{-8} dyne/cm²) for the same period. The "effective" peak ionospheric pressure is the median peak ionospheric particle pressure of Figure 7 divided by the factor K . Figure 8 illustrates that the up-stream solar wind dynamic pressure was less than the effective peak ionospheric particle pressure about 80% of the time during solar maximum.

The median shape of the ionopause during solar maximum can be accurately modeled by assuming that the ionopause altitude is determined by pressure balance between the sum of the solar wind dynamic and thermal pressures and the ionospheric thermal pressure. Figure 9 illustrates the computed altitude of the ionopause location and the measured median altitude at solar maximum for SZA between 0° and 125° [Knudsen et al., 1982b]. The ionospheric pressure field was derived from measured quantities. The computed and measured median ionopause heights agree well at solar maximum because the median up-stream solar wind dynamic pressure is moderate, and the ionospheric thermal pressure is able to stand off the solar wind most of the time (Figure 7).

Phillips et al. [1988] have recently shown that a small cylindrical asymmetry reported by Brace et al. [1980] and Knudsen et al. [1982b] in which the dawn ionopause altitude is higher than the

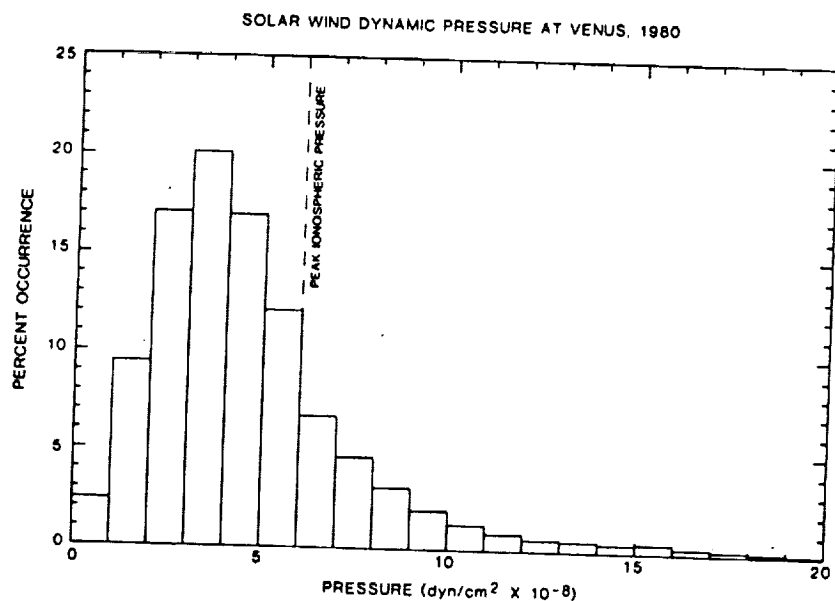


Fig. 8. Frequency of occurrence of solar wind dynamic pressure at Venus during 1980, a period of solar maximum. Dashed line is the median peak effective ionospheric particle pressure at low solar zenith angle from Figure 7 (from [Phillips et al., 1984]).

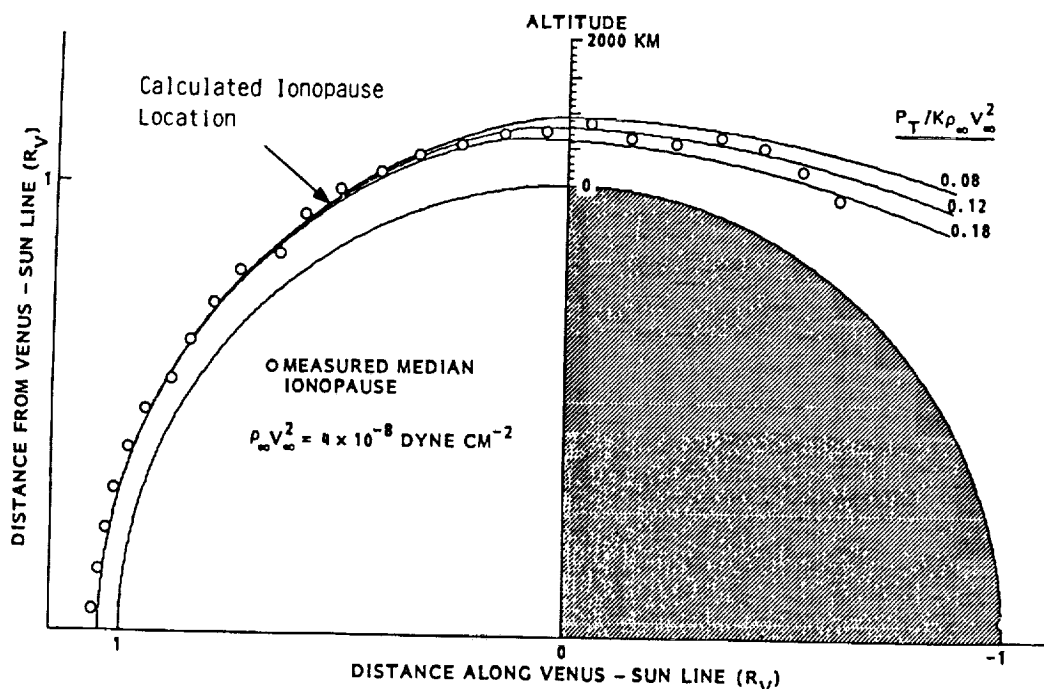


Fig. 9. Shape of the ionopause over the dayside hemisphere and terminator region during solar maximum (adapted from [Knudsen et al., 1982b]). The three different calculated shapes are for different nose to terminator pressure ratios.

dusk ionopause is largely the result of orbital bias and uneven sampling of solar wind dynamic pressure. However, they found an asymmetry in which the ionopause in the terminator region is displaced in a direction opposite to that of the motional electric field.

The solar maximum ionopause shape beyond about 125° SZA has not been determined experimentally because of measurement limitations imposed by the PVO orbit. However, using a gas dynamic numerical model, Moore et al. [1991] have recently derived an ionopause shape extending to a large distance down the Venus wake. Figure 10 illustrates the shape of the ionopause that he obtained by iteratively altering the shape until the solar wind normal pressure at the ionopause balanced the ionospheric pressure for x between 0 and -0.5.

Wave-like structure observed within but near the ionopause, as illustrated in the electron density and temperature and magnetic field for orbit 184 of Figure 11, has been interpreted as evidence for waves on the ionopause [Brace et al., 1980, 1982a]. In some instances a "cloud" of plasma, such as that occurring on the inbound leg of orbit 173, appears to be completely detached from the main body of the ionopause. The strong decrease in density, increase in magnetic field strength, and increase in T_e all suggest that the spacecraft has reentered the ionosheath after encountering a patch of ionospheric plasma. Some patches of plasma are encountered with a greater separation between the cloud and the ionopause than is indicated in orbit 173. Although there is separation of the cloud from the ionopause along the orbital tract, the clouds may not be completely detached from the ionosphere proper. The orbital track

is near-tangent to the ionopause and irregularities in ionopause height could also appear as detached plasma.

The OIMS has observed superthermal ions near and above the ionopause as illustrated in Figure 12. The behavior of the instrument current in the shaded region above 270 km altitude is interpreted as consisting of ions with a kinetic energy component parallel to the instrument axis in the range 30-80 eV. The inference is that O^+ ions in the shaded region have been accelerated antisunward into this energy range through interaction with the rapidly flowing solar wind plasma [Taylor et al., 1980a].

Spennner et al. [1980] found that the differential electron energy flux spectrum during solar maximum changed from one characteristic of the upper ionosphere photoelectron spectrum to one characteristic of the ionosheath solar wind electrons as the PVO spacecraft passed upward through the ionopause and into the ionosheath. Figure 13 illustrates spectra obtained in the ionosphere, in the ionosheath and in the transition layer. They called this layer the mantle (see Figure 1) and suggested that the upper surface of the mantle was the effective boundary diverting the shocked solar wind flow around the planet.

Density and Composition

Figure 14 illustrates the altitude and solar zenith angle dependence of the median ionospheric total ion density during solar maximum. The density varies approximately as the square root of SZA over most of the dayside hemisphere but drops rapidly by about an order of magnitude across the terminator. Figure 15 illustrates the order of magnitude drop in electron density (equal to

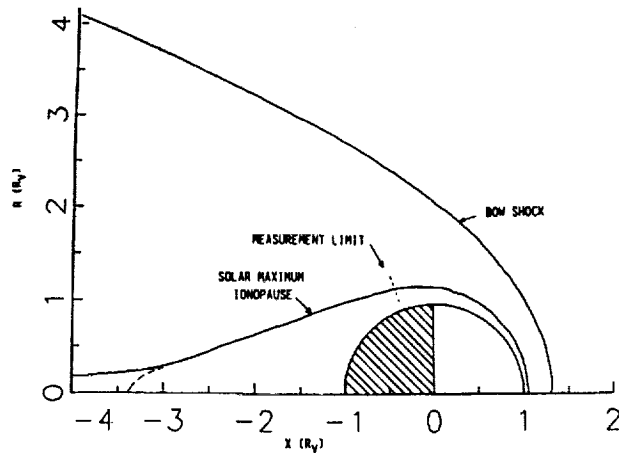


Fig. 10. Ionopause shape extrapolated into the near wake. The extrapolation is based on pressure balance between the ionospheric thermal pressure and solar wind thermal pressure over the region $0 > x > -0.5$ where x is measured in units of the Venus radius [Moore et al., 1991].

total ion density) across the terminator at three discrete altitudes. The dots are individual density measurements made during the first 600 orbits within the altitude intervals 160-170, 260-280, and 550-650 km. They reveal the strong increase in temporal density variability from the dayside to nightside hemispheres. The solid lines are empirical model values of the density [Theis et al., 1984].

The solar maximum dayside ionosphere of Venus consists principally of an upper layer of O^+ ions and a lower layer of O_2^+ ions. Other ions compose less than 10% of the total. Figure 16 illustrates the major ion composition measured by the ORPA for an SZA of 65° . The vertical profiles are smoothed median density profiles and the temporal variation bars indicate the interval within which two thirds of the measured values fall. Only measurements lying below the ionopause were included in the data base. The ion density labeled M29 $^+$ density is the sum of the densities of ions with mass 28 amu ($N_2^+ + CO^+$) and 30 amu (NO^+). The ORPA does not resolve M29 $^+$ from O_2^+ , and the density of these two individual ions is less certain than their sum. The O^+ , O_2^+ , and CO_2^+ densities vary as $\cos(SZA)^{1/2}$ across most of the dayside hemisphere [Miller et al., 1984]. Figure 17 illustrates the ion composition measured by the PVO OIMS during one subsolar orbit passage through periapsis [Taylor et al., 1980a]. The ion labeled H_2^+ in Figure 17a is now known to be D^+ [McElroy et al., 1982; Donahue et al., 1982; Hartle and Taylor, 1983]. The solar zenith angle variation of several ion species at an altitude of 200 km measured by the OIMS is presented in Figure 18. Perhaps the most interesting variation is the strong increase in H^+ ion density. The H^+ ion density becomes comparable to O^+ in a range of SZA centered on 130° in the dawn hemisphere in consequence of the enhanced neutral hydrogen density at this location and charge exchange between O^+ and H [Brinton et al., 1980].

During solar maximum, the nightside ionosphere, like the dayside ionosphere, typically consists of a layer of O^+ ions overlying a lower O_2^+ layer as illustrated by the median vertical profiles in Figures 19 and 20. The variance bars reflect the fact that

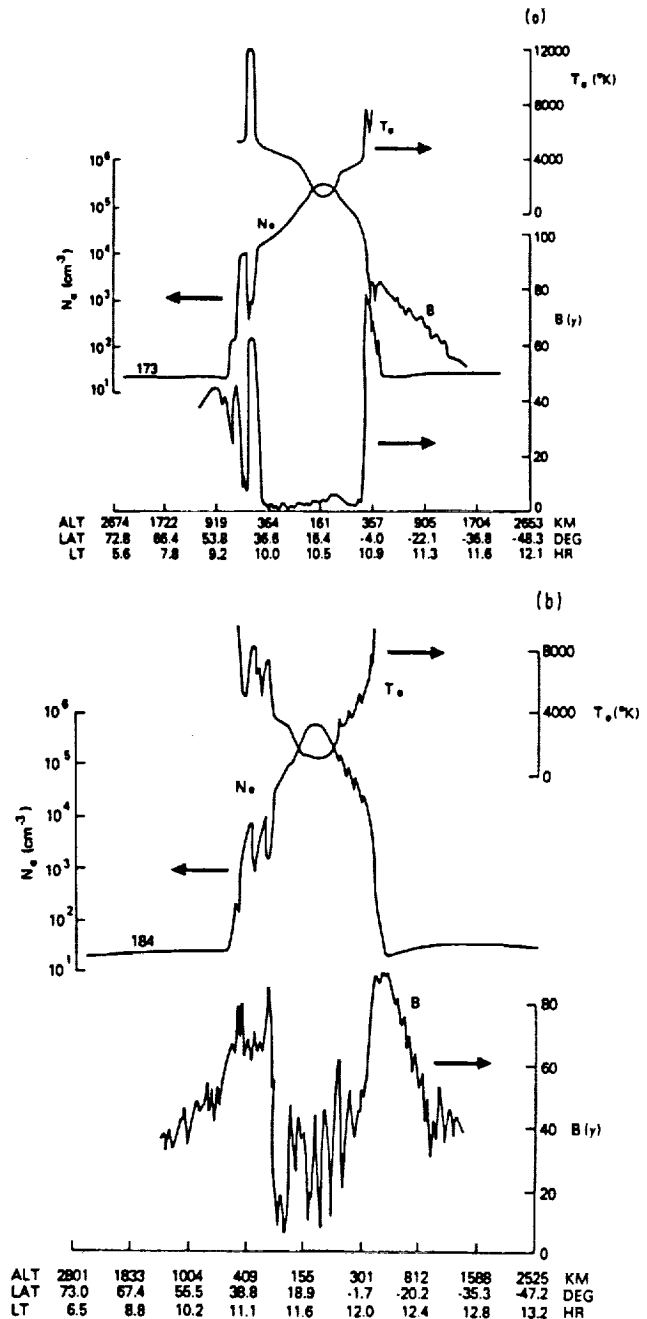


Fig. 11. (a) Measurements of N_e , T_e , and B from orbit 173 showing the passage of the PVO spacecraft back into the ionosheath (magnetic barrier?) for a short period of time after first encountering the ionosphere as the spacecraft entered the ionopause at a shallow angle. (b) Measurements of N_e , T_e , and B exhibiting wave like character as the spacecraft transited the ionopause inbound and outbound on orbit 184 (from [Brace et al., 1980]).

the temporal variability of the nightside ionospheric density is larger than that of the dayside ionospheric density (compare with Figure 15 and 16). In the SZA range 120° - 150° of the dawn hemisphere, the H^+ density becomes comparable to and greater than

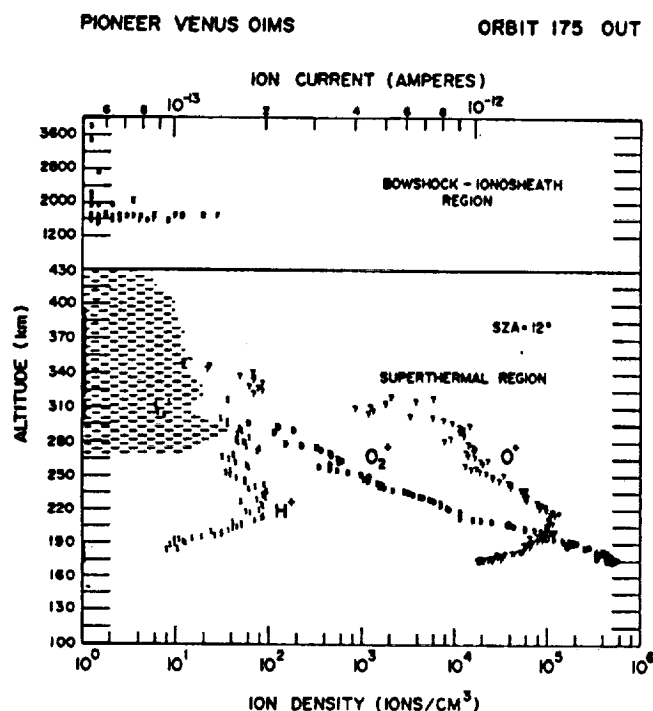


Fig. 12. A dayside example ($SZ = 11^\circ$) of the plasma measurements from the OIMS, including the bowshock-ionosheath, with energetic ion currents (energy > 100 eV) peaking near 1700 km, a region of superthermal (energy = 30-80 eV) ion flow (shaded) extending across the range 270-430 km, and the relatively undisturbed thermal ionosphere in the interval from 270 km down to periaapsis at 173 km. The ionopause is identified at approximately 270 km, the altitude above which the superthermal ions are observed. Within the shaded region thermal ion concentrations cannot be precisely determined owing to incomplete sampling of three dimensional plasma flow characteristics. The shaded area indicates qualitatively the height dimension and relative intensity (not calibrated in either density of species) of the superthermal flow (from [Taylor et al., 1980a]).

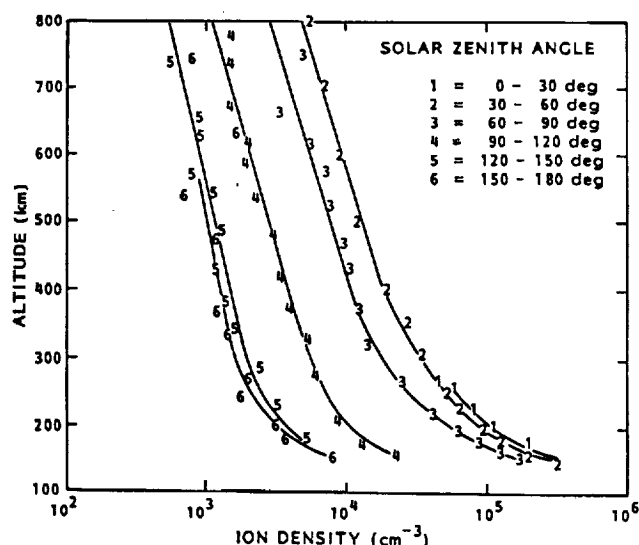


Fig. 14. Global variation of the median ionospheric ion density at solar maximum (after [Miller et al., 1980]).

the O^+ density as shown in Figure 18a for the reasons presented in the previous paragraph. A vertical profile of the median H^+ density in the region of enhancement is illustrated in Figure 21. In comparing the median H^+ vertical profile of Figure 21 with that of O^+ in Figure 19, note the difference in altitude scales of the two figures.

Figure 22 illustrates the ion composition measured by the OIMS along orbit 65 outbound from its periaapsis at $SZ = 162^\circ$. The composition on the nightside is, for the most part, similar to that on the dayside, but the density level is about a factor of ten less. The significantly higher density of H^+ is an exception. The similarity in composition, and the observation of large ion bulk velocity directed antisunward at the terminator led several of the PVO experimenters

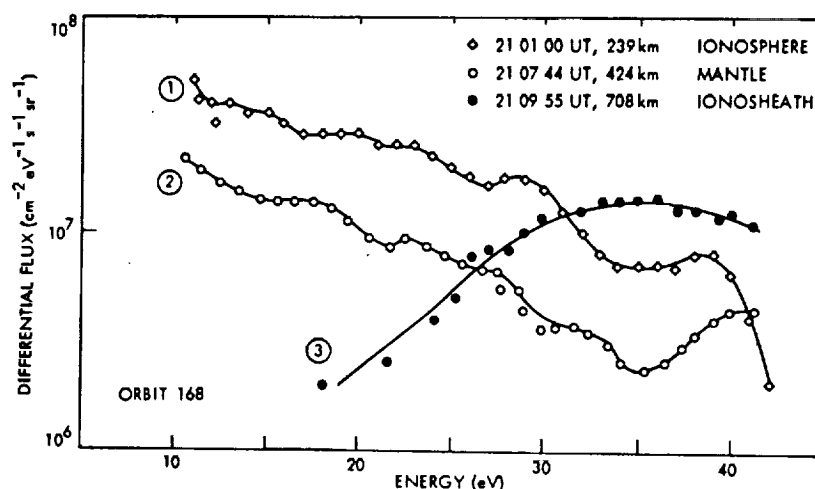


Fig. 13. Change in differential electron flux as the PVO spacecraft passed from the ionosphere into the ionosheath (magnetosheath) at solar maximum (from [Spencer et al., 1980]). The spectrum changed from one characteristic of ionospheric photoelectrons to one characteristic of the ionosheath electrons.

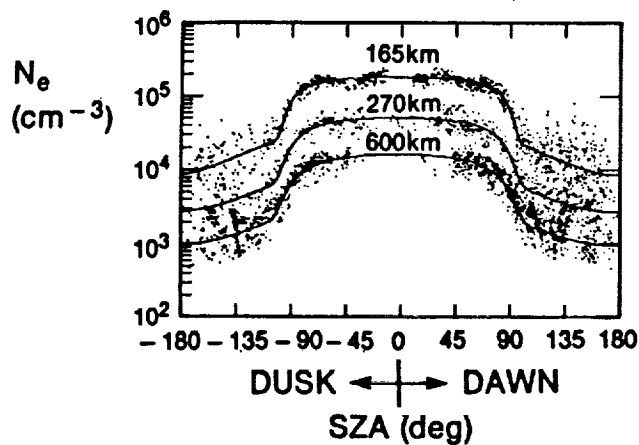


Fig. 15. Total electron density measured by the OETP within three altitude intervals, 160 - 170, 260 - 280, and 550 - 650 km as a function of SZA. The solid lines are empirical model values at the indicated altitudes derived from median values of the individual measurements, the latter indicated by the dots. The data base consists of measurements within the ionosphere from Dec 1978 to Dec 1982, the period of solar maximum (from [Theis et al., 1984]).

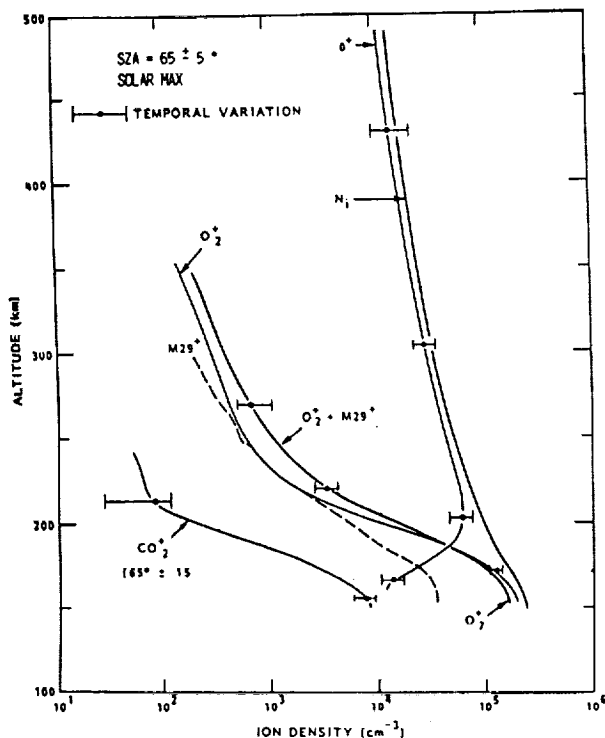


Fig. 16. Vertical profiles of the median density of the major ions measured in the dayside hemisphere by the PVO ORPA during solar maximum. M29⁺ represents the sum density of ions with masses 28 and 30 amu. Together, O⁺ and O₂⁺ compose in excess of 90% of the density (adapted from [Miller et al., 1984]).

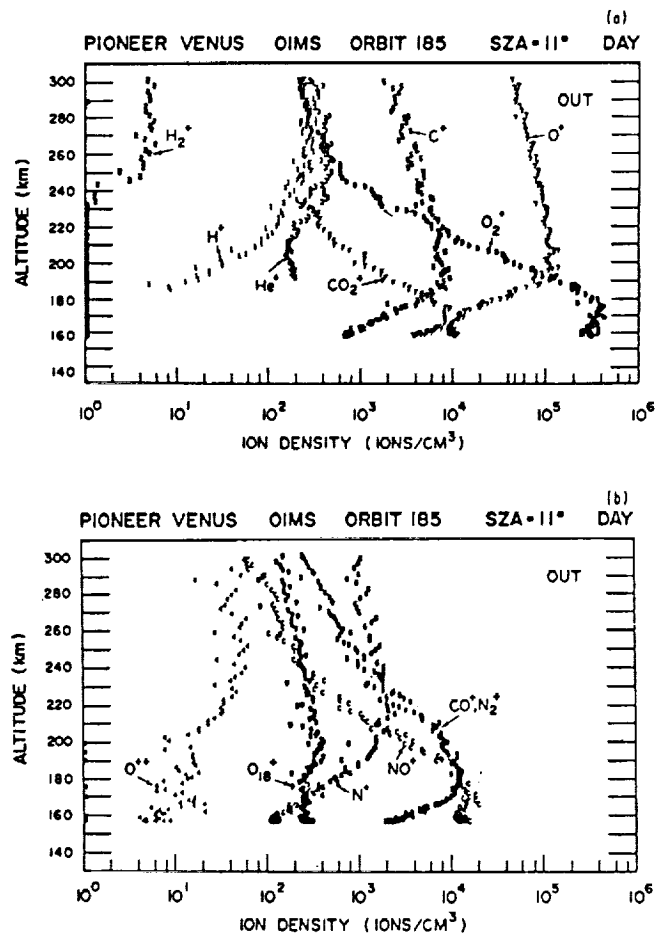


Fig. 17. A dayside example of the major and minor ions measured in the lower ionosphere of Venus by the PVO OIMS at solar maximum ([Taylor et al., 1980a]). Outbound pass occurred near local noon with SZA = 11° at the location of periapsis. Distributions are divided into panels (a) and (b) for clarity.

to postulate that transport of dayside ionospheric plasma into the nightside ionosphere was a significant source of the nightside ionosphere [Taylor et al., 1979a; Knudsen et al., 1980b].

The density and composition of the dayside ionosphere sunward of the terminator is reproduced reasonably accurately in one dimensional numerical models by assuming ion production from solar photon and photoelectron ionization of the neutral atmosphere and loss through a chain of chemical reactions. In modeling the behavior of ions above 170 km altitude, it is necessary to include vertical diffusion [Knudsen et al., 1979a; Nagy et al., 1979; Nagy et al., 1980]. At solar maximum, horizontal transport of ionization across the terminator is essential in modeling the nightside ionosphere, especially the O⁺ layer, and several two dimensional numerical models have been developed to predict the major ion densities as a function of SZA [Whitten et al., 1982; Cravens et al., 1983; Whitten et al., 1984; McCormich et al., 1987; Singhal and Whitten, 1987]. These authors recognized that electron impact

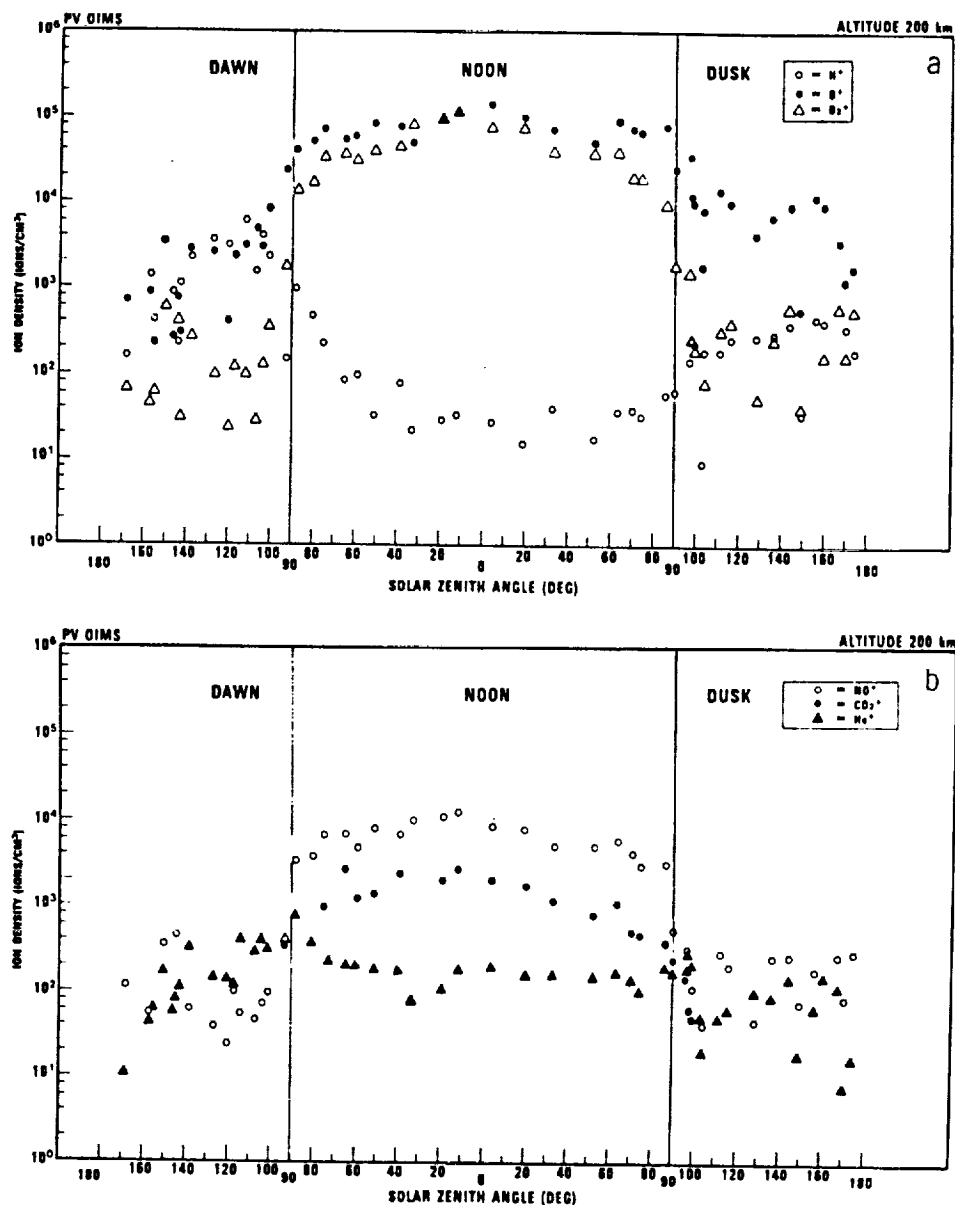


Fig. 18. (a,b) Variation of several ion species with SZA for a fixed altitude of 200 km as measured by the OIMS at solar maximum. The measurements were taken from the outbound leg of orbits at a latitude of 8° N and represent, for the most part, quiet conditions (from [Taylor et al., 1980a]).

contributes to the nightside ionization, but this source was not included in the models.

Energetics

The global variation of electron temperature (T_e) measured by the OETP at selected altitudes is presented in Figure 23. The dots are all the individual measurements from the first 600 orbits, a period of solar maximum, and the solid lines are from an empirical model derived from the medians of a subset of the data base. For comparison, Figure 24 illustrates a vertical profile of median values

of T_e measured by the ORPA in several SZA ranges. There is evidently little variation of the median T_e with SZA over the entire planet, although Figure 23 does exhibit a small decrease from the dayside to the nightside hemisphere. Numerical model calculations of T_e over the dayside hemisphere have shown that the measured T_e profile cannot be reproduced when solar EUV heating is the only heat source unless the thermal heat conductivity is greatly reduced by the presence of steady and fluctuating magnetic fields [Cravens et al., 1980, Kim et al., 1990]. By assuming a heat inflow at the ionopause of the order of a few times 10^{10} eV cm⁻²s⁻¹ it is possible

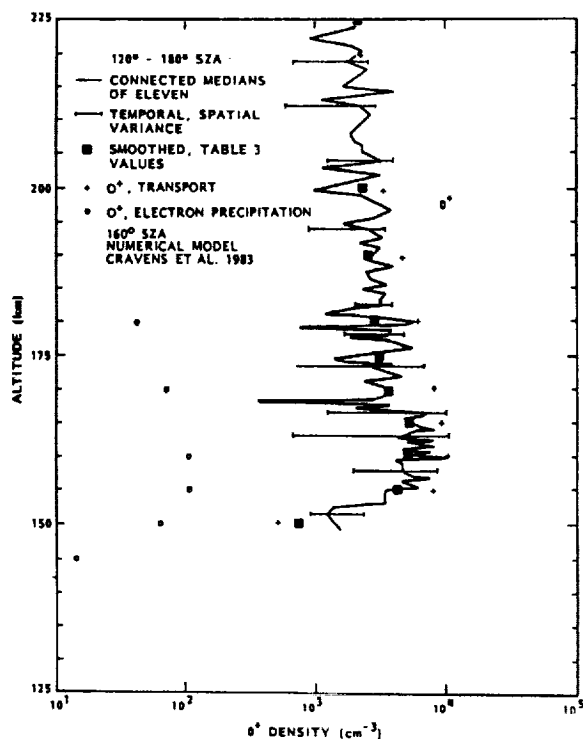


Fig. 19. Vertical profile of median O^+ density in the solar maximum nightside ionosphere and model computations of the O^+ layer expected from a downward flux of O^+ ions and from electron precipitation (from [Knudsen et al., 1986]).

to match the observed temperature profile [Knudsen et al., 1979b; Cravens et al., 1980; Kim et al., 1990].

Figure 23 illustrates the large temporal variability of T_e , especially in the night hemisphere. A significant part of this variability results from inclusions in the data base of T_e measurements when the electron density was very low, such as in holes and during periods of greatly depressed ionospheric density (disappearing ionosphere), topics to be discussed later.

The ion temperature T_i shows little variation with SZA over the dayside hemisphere, but changes substantially near the terminator and in the nightside hemisphere (Figure 25). The variation between 170 and 200 km altitude on the dayside requires the existence of a heat source localized in altitude and restricted to the dayside hemisphere. It has been identified as that due to chemical heating [Rohrbaugh et al., 1979; Cravens et al., 1979; Knudsen et al., 1979b; Kim et al., 1990]. Reproduction of observed dayside ion temperatures above 200 km altitude with numerical models requires a distributed heat source or a heat flux at the ionopause unless the ion heat conductivity is reduced by a horizontal and/or fluctuating magnetic field [Knudsen et al., 1979b; Cravens et al., 1980; Kim et al., 1990]. The increase of T_i with SZA in the altitude range 170-300 km at and beyond the terminator is probably due to decreased ion heat loss to the neutrals. (The neutral density and temperature decrease rapidly with SZA across the terminator.) The high altitude ionosphere flows supersonically across the terminator, as we shall discuss later, and advection of heat within the ion gas

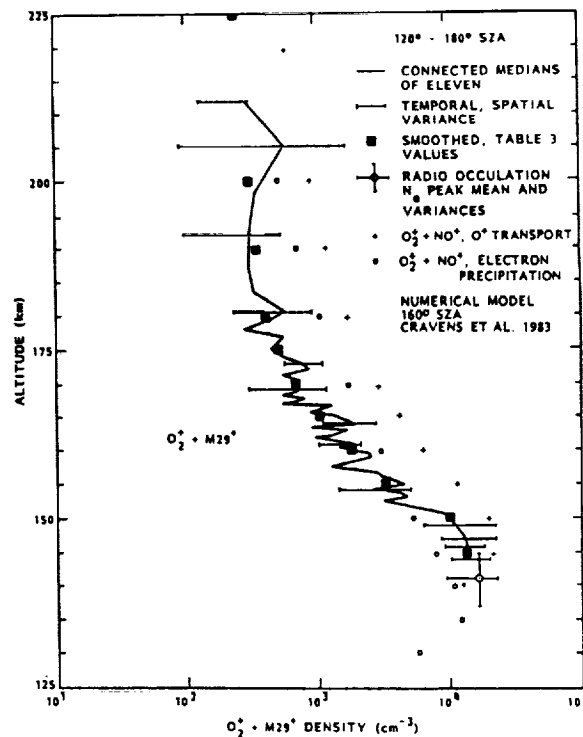


Fig. 20. Vertical profile of the median $O_2^+ + M29^+$ sum density in the solar maximum nightside ionosphere. The symbol $M29^+$ is defined in the Figure 16 caption (from [Knudsen et al., 1986]).

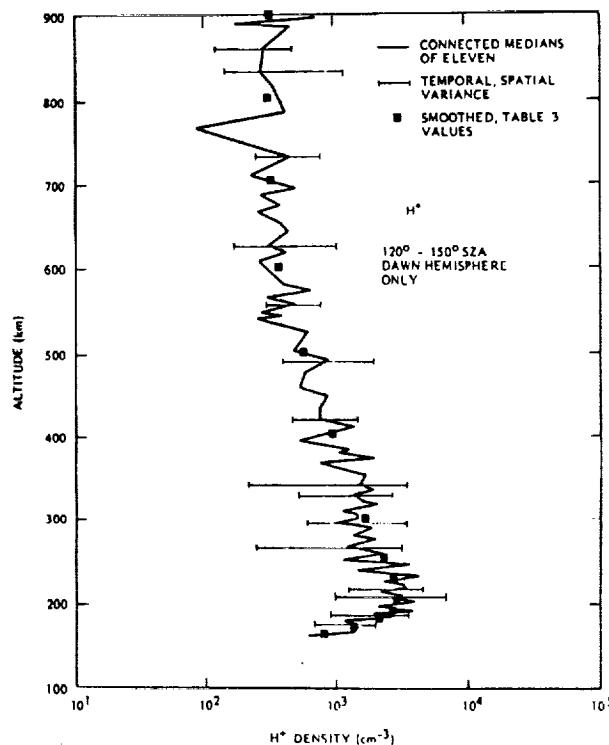


Fig. 21. Vertical profile of median H^+ density in solar maximum nightside dawn hemisphere between 120 and 150 SZA (from [Knudsen et al., 1986]).

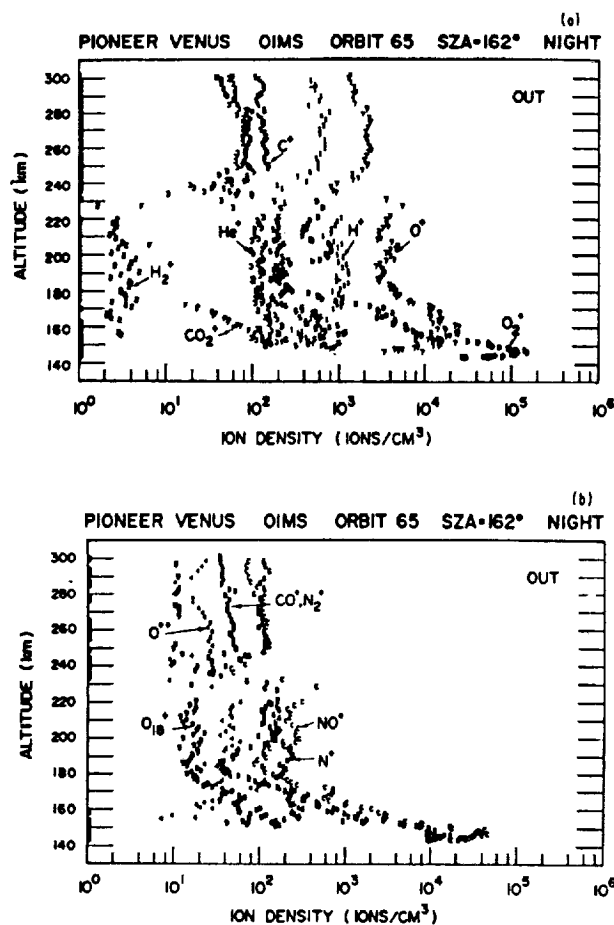


Fig. 22. A nightside (dusk hemisphere) example of the ion composition measured by the OIMS in the outbound leg of orbit 65. The SZA at periapsis was 162° . The strong decrease in density at 230 km altitude may result from passage through an ionospheric hole (from [Taylor et al., 1980a]).

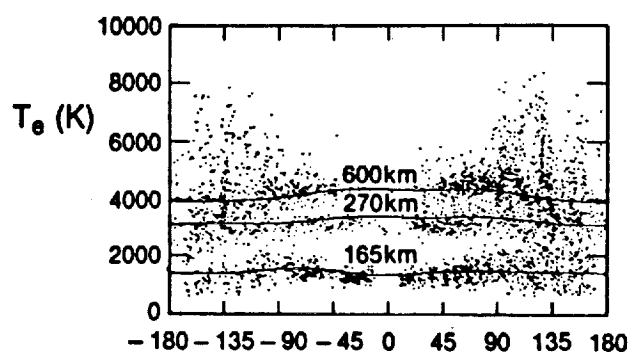


Fig. 23. Total electron temperature measured by the OETP within three altitude intervals, 160 - 170, 260 - 280, and 550 - 650 km as a function of SZA. The solid lines are empirical model values at the indicated altitudes derived from median values of the individual measurements, the latter indicated by the dots. The data base consists of measurements within the ionosphere from Dec 1978 to Dec 1982, the period of solar maximum (adapted from [Theis et al., 1984]).

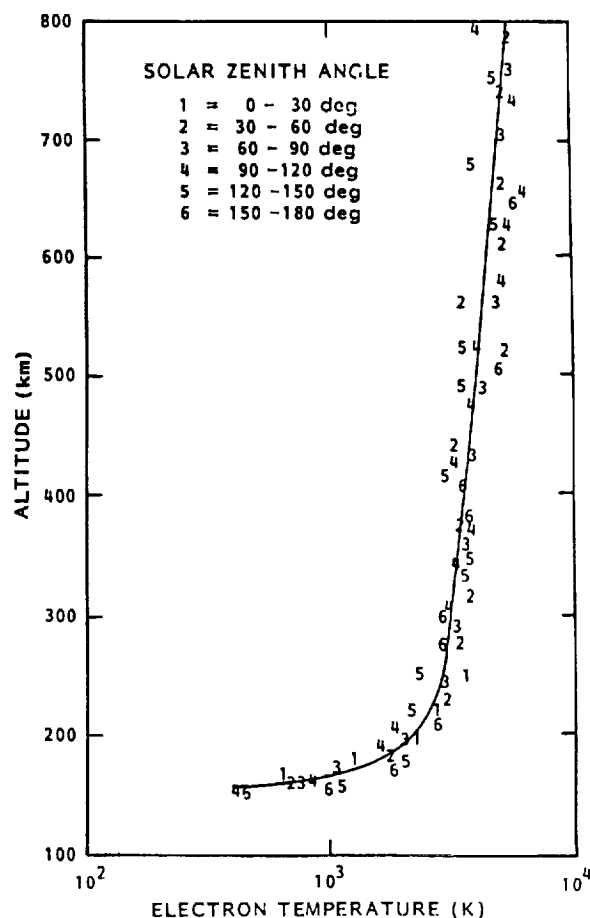


Fig. 24. Vertical profiles of median electron temperatures as a function of SZA at solar maximum (from [Miller et al., 1980]).

and conversion of the bulk kinetic energy into heat become important [Knudsen et al., 1981a; Bougher and Cravens, 1984; Whitten et al., 1986].

Velocity Field

Rapid advection of the near-terminator dayside O^+ layer into the nightside hemisphere plays a major role in the formation of the nightside ionosphere and in the nightside ion energetics. Figure 26 illustrates the median velocity field of O^+ ions measured on the outbound portion of orbits from periapsis to the ionopause. These data represent near-equatorial median results obtained from all solar hour angles over a period of approximately three and a half Venus years [Knudsen et al., 1982a]. The bulk velocity of the ions becomes reasonably well organized near the terminator and has a magnitude of the order of 3-4 km/s at higher altitude and antisunward of the terminator. The median velocity vectors are generally smaller and confused in the sub- and antisolar regions in this presentation.

Some of the confusion in the subsolar region disappears when the data are separated into dawn and dusk hemispheres before taking averages as shown in Figure 27. The altitude above the

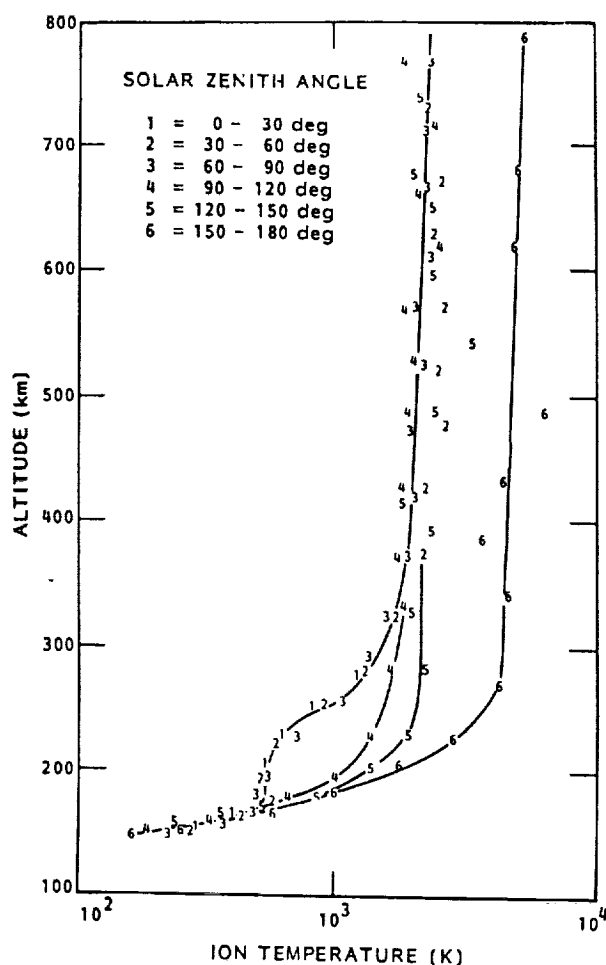


Fig. 25. Vertical profiles of median ion temperatures as a function of SZA at solar maximum (from [Miller et al., 1980]).

planet is exaggerated by a factor of four relative to the radius of the planet. In this analysis the flow in the subsolar region and at lower altitudes is seen to be westward and in the direction of planet rotation. The rotation of the cloud tops is in this direction and of the order of 0.1 km/s. If the thermosphere were super rotating at a speed of the order 1 km/s, we would expect this observed behavior. Because no corroborating evidence or theory for such a large super rotation exists, this result must be considered tentative. An uncertainty sphere of 0.3 km/s radius exists at the head of individually measured ORPA velocity vectors under the best of circumstances and some as yet undetected systematic error may also be present.

The measured average velocity vectors become chaotic beyond about 150° SZA in both Figures 26 and 27. The reason for this is not established at the moment but several factors may be contributing. The number of measurements at the higher altitudes with SZA greater than 150° is smaller than at lower SZA because of orbital coverage and also because of failure of the ORPA to detect O⁺ ion peaks at the low densities and high ion temperatures

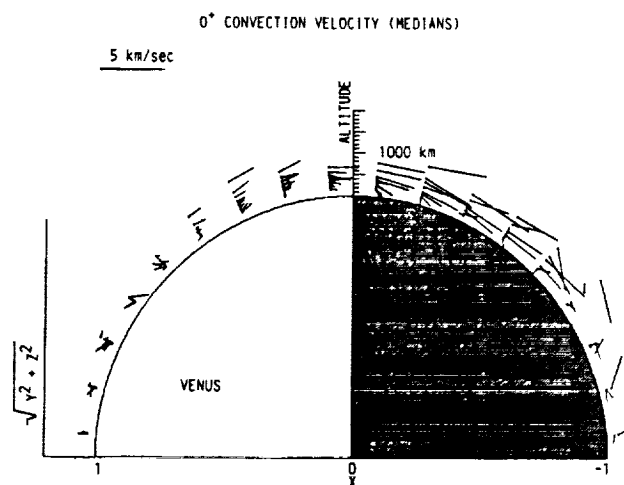


Fig. 26. Bulk ionospheric velocity field at solar maximum (from [Knudsen et al., 1982a]).

occurring in that region. The horizontal component of any cylindrically symmetric flow field about the sun-Venus axis should approach zero in the antisolar region. It is likely that the transterminator flow field is not cylindrically symmetric near the terminator and that the center of convergence of the flow wanders around in time. All these factors are probably contributing to the confused average flow near the antisolar axis.

Theis et al. [1984], Whitten et al. [1984] and Elphic et al. [1984], using two dimensional numerical models, have been able to reproduce reasonably well the measured velocity field. All models indicate that the measured pressure field is able to accelerate the plasma to the observed velocities. In the model by Whitten et al. [1984] the pressure field is produced entirely by EUV ionization. This result indicates that momentum transfer from the solar wind via viscous drag is not important in accelerating the ionospheric plasma [Knudsen et al., 1981b].

For flow speeds in excess of about 1 km/s, the flow is supersonic [Knudsen et al., 1980b]. Knudsen et al. [1980b] have suggested that a shock wave forms in the vicinity of 150° SZA which slows the flow, changes its direction and heats the ions in the central nightside region (Figure 28). This suggestion has recently been supported by observations of median ion temperature and density increases of the expected magnitude and at the expected SZA, and by the results of a model [Miller et al., 1990; Kim et al., 1990].

Nightside Ionospheric Holes

The term ionospheric hole has been given to an intriguing and unanticipated phenomenon discovered in the nightside Venus ionosphere by Brace et al. [1982b]. They observed that strong plasma density depletions frequently occurred within small time (or space) intervals during nightside periapsis passes. Outside these time intervals the plasma density was at its undisturbed value. Figure 29 illustrates the plasma density measured during several passes through the nightside ionosphere. The ionospheric holes are evident in several of these orbits. Two holes, one on either side of

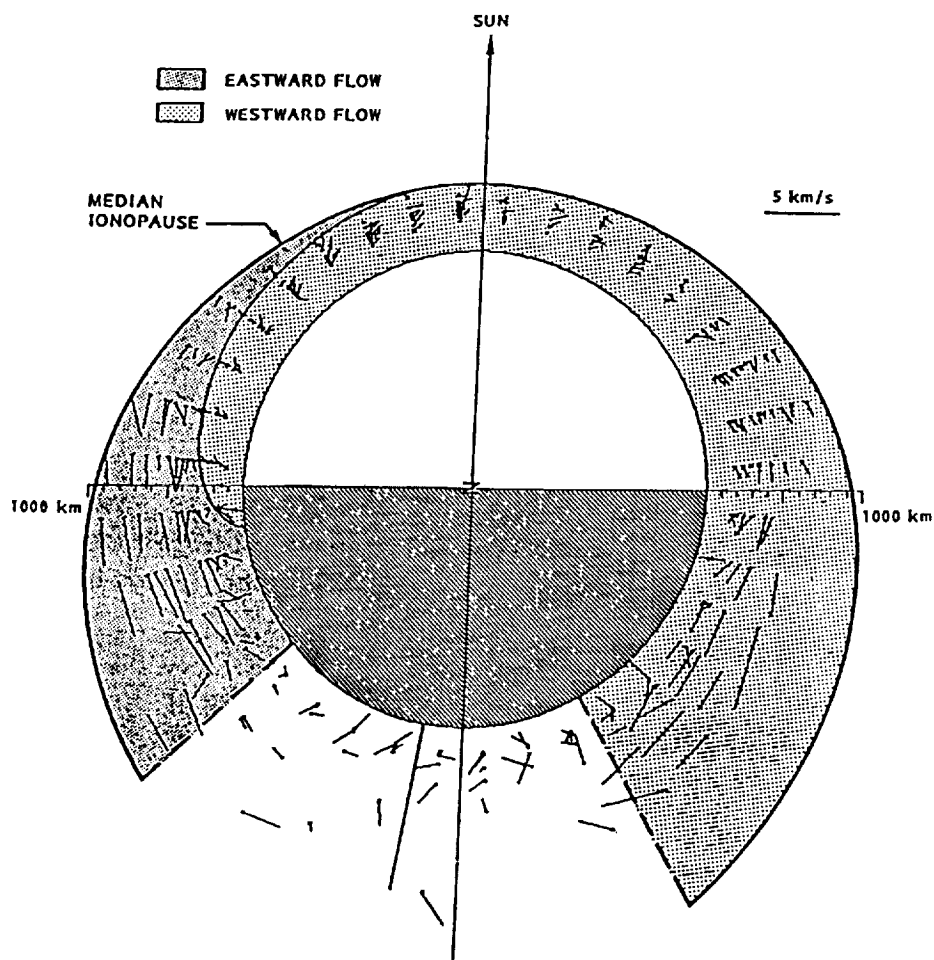


Fig. 27. Bulk ionospheric velocity field separated into dawn and dusk hemispheres. The altitude scale above the planet surface is four times that of the planet. The low altitude field in the dawn hemisphere suggests that a neutral atmospheric super rotation may be exerting an influence on the flow (from [Miller and Knudsen, 1987]).

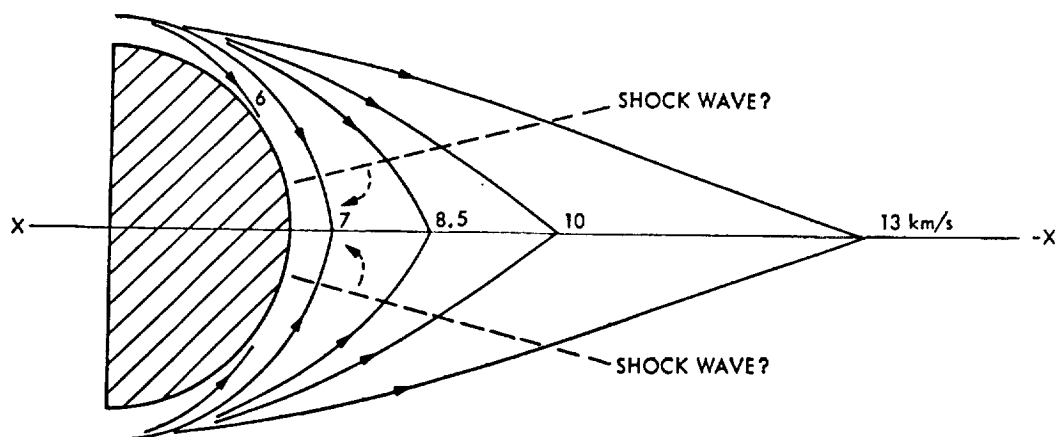


Fig. 28. Ballistic trajectory of ions with indicated bulk horizontal velocity at the terminator and at the median ionopause altitude. The flow is supersonic and a shock wave may form to slow and change the direction of the flow (from [Knudsen et al., 1980b]).

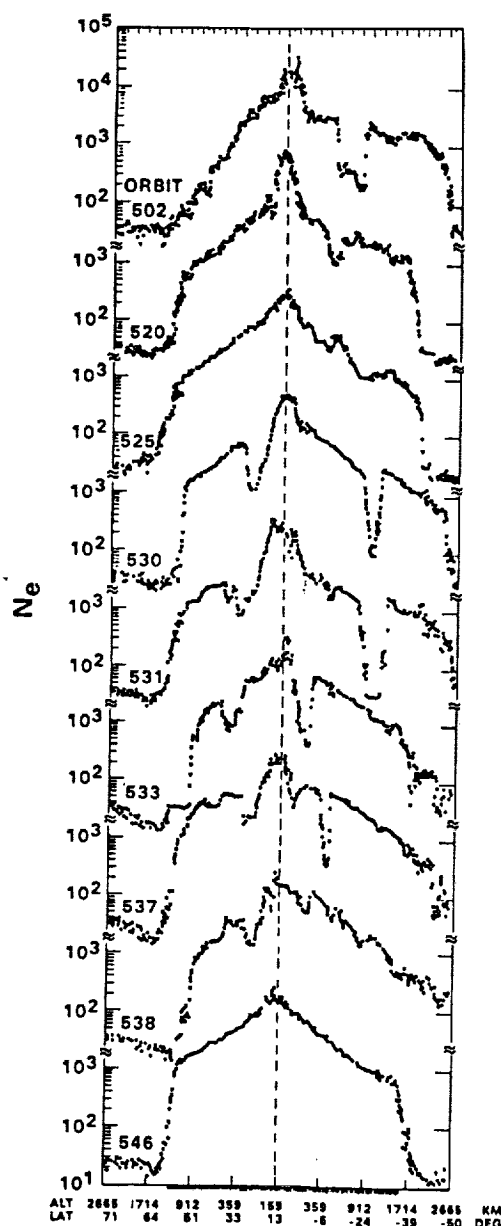


Fig. 29. Ionospheric holes present in several orbits that otherwise exhibit a fully established nightside ionosphere (from [Brace et al., 1982b]).

periapsis, are evident in each of the orbits 530, 531, 533 and 537. The holes are not seen in every passage and appear to move in latitude. The density depression tends to be greater in the holes occurring in the outbound portion of periapsis passes than those in the inbound portion which suggests that the holes disappear at altitudes near and below the nightside main peak altitude. Figure 30 illustrates the presence of an enhanced magnetic field within the holes directed predominantly along the sun-Venus axis.

Marubashi et al. [1985] have projected the location and polarity of the magnetic field observed in 55 holes onto the nightside planet

after rotation into a solar wind magnetic coordinate system so that the upstream Y component of the solar wind magnetic field is horizontal (Figure 31). Holes with sunward directed magnetic fields are plotted with crosses and holes with antisunward pointing fields with circles. This rotation orders the holes with sun-directed magnetic fields on the right and those with antisunward directed fields to the left of the $Y=0$ plane. This ordering is consistent with the fields having their origin in the draped magnetosheath field as indicated on the right. Processes responsible for the formation of the holes have been suggested by Grebowsky and Curtis [1981], Brace et al. [1982a], Luhmann et al. [1982], Grebowsky et al. [1983] and Marubashi et al. [1985].

Post Terminator Waves

Brace et al. [1983b] have reported the presence of wave-like structures in measurements of electron density, electron temperature, and magnetic field at low altitudes antisunward of the terminator. Figure 32 illustrates the waves and the anti-correlation between T_e and N_e , and correlation of peaks in N_e with sign changes in B_E , where the magnetic field components are radial B_R , eastward B_E and northward B_N . These waves first appear at the terminator, extend for at least another 30° SZA into the night hemisphere, and exist primarily below 200 km altitude. The waves are evidently not accompanied by waves in the neutral atmosphere [Brace et al., 1983b]. The generation mechanism for the waves is unknown, but the fact that they occur in a region of large plasma velocity shear suggest that a shear instability may be involved.

Suprathermal Electrons

Although the PVO spacecraft was not adequately instrumented to measure energetic particles within the ionosphere with energies above about 1 eV energy, the low energy ionospheric and neutral atmospheric instruments have been able to provide some measurements of considerable value for understanding the Venus energetic particle environment.

The ORPA has a mode of operation in which electron current is collected at several retarding voltages from 0 to 48 V. The differential photoelectron flux derived for the dayside solar maximum ionosphere from such measurements is illustrated in Figure 33. Comparison of the differential photoelectron fluxes computed numerically [Cravens et al., 1980] with the measured flux suggests that the measured flux is produced predominantly by solar photons and that the photoelectrons diffuse rather freely in the vertical direction.

Spenner et al. [1981] and Knudsen and Miller [1985] have reported on the suprathermal electron flux observed by the ORPA in the Venus nightside ionosphere during the 1980-1981 solar maximum and the following waning phase of the solar cycle. The measurements used in the study were restricted to the altitude interval of 1000-2000 km and to SZA greater than 130° , a region similar to that sampled by the Venera 9 and 10 suprathermal electron detectors during an solar minimum period [Gringauz et al., 1979]. The Venera instrument had a retarding potential range of 0-300 V. Figure 34 illustrates the median electron spectrum derived in the study by Knudsen and Miller and compares it with spectra reported by Gringauz et al. [1979] for the same region but measured

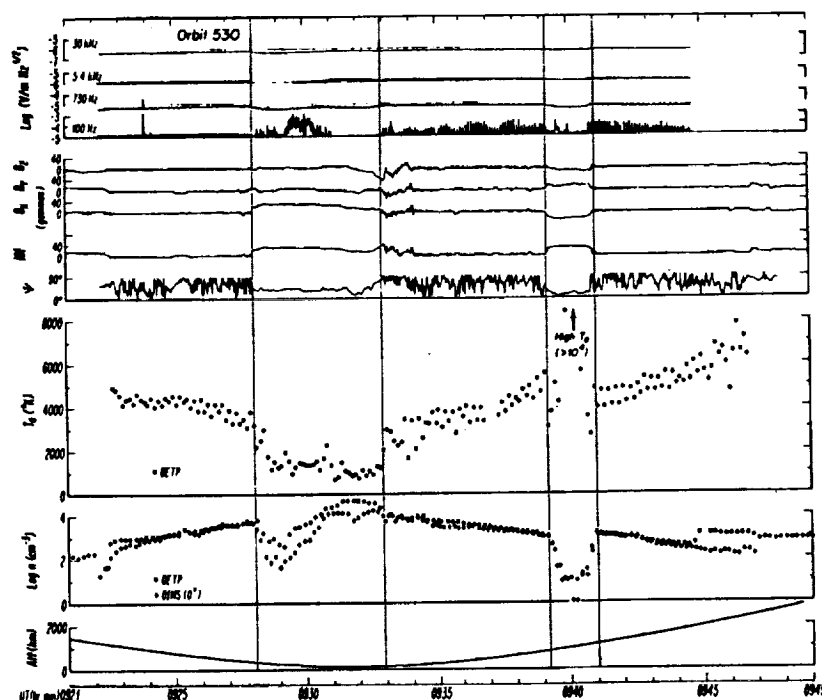


Fig. 30. Enhanced radial magnetic field in ionospheric holes. The magnetic field components are in solar ecliptic coordinate system; the angle Ψ is between the radial direction and the local magnetic vector. $\Psi = 0$ is radial. The magnetic field is enhanced within the holes and is oriented at a small angle to the radial. The vertical lines delineate the boundaries of the holes (from [Luhmann et al., 1982]).

during the preceding solar minimum period. Both Knudsen and Miller and Gringauz et al. found that the suprathermal flux could be approximated by a two component Maxwellian electron gas. Knudsen and Miller found that the most abundant component has a median density (n_2) of 3 cm^{-3} and a median temperature (T_2) of 14 eV. The density of the high temperature component (n_3)

depended on the assumed temperature (T_3). For an assumed T_3 temperature of 200 eV the density was 0.06 cm^{-3} . The median values of n_2 , T_2 and T_3 were found to be uniform over the altitude and SZA ranges covered by the study. Two thirds of the measured values of n_2 , T_2 and n_3 fell within a factor of ± 2 of the median values. Comparing the ORPA median omnidirectional flux with

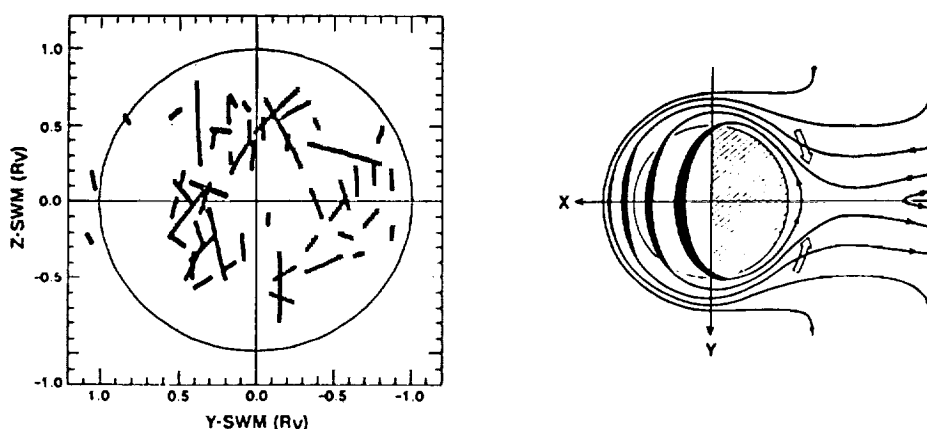


Fig. 31. PVO orbit segments where holes were detected are projected onto the nightside planet after rotation into the Y-Z plane of the solar wind magnetic coordinate system (left). Holes with magnetic field directed sunward are plotted with crosses, and holes with magnetic field directed antisunward, with circles. This organization of the segments is consistent with the hole magnetic fields originating in the draped solar wind magnetic field (right) (adapted from [Marubashi et al., 1985]).

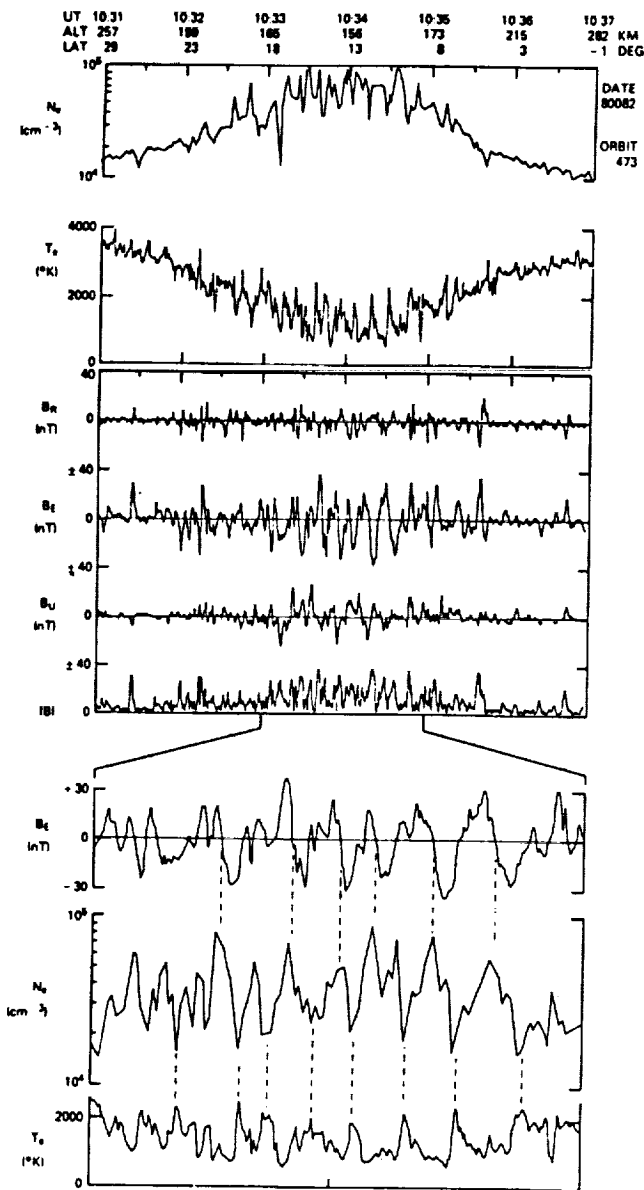


Fig. 32. The ionospheric and magnetic characteristics of post-terminator waves in orbit 473 (SZA=100° at periapsis). The upper five traces show a 6-minute segment of N_e , T_e , B_R , B_E , B_U , and $|B_I|$, while the lower panels display and expanded view of N_e , T_e , and B_E which show details of the wave patterns. Well ordered waves develop below about 175 km altitude. The vertical dashed lines draw attention to persistent phase relationships between B_E , N_e , and T_e (from [Brace et al., 1983b]).

some statistical data reported by Gringauz et al., Knudsen and Miller concluded that the ORPA median flux was about a factor of 2 larger than the Venera-measured fluxes within the lower energy range common to the two instruments. In both studies the omnidirectional flux was derived by assuming the flux to be isotropic.

Little directional information on the suprathermal flux is available. The effective solid angle of the ORPA is about pi

steradian, and its axis lies on a cone with a half angle of 25°. The axis of the cone is perpendicular to the earth ecliptic. The density and temperature of the suprathermal electrons are derived with the assumption that the electron flux is isotropic. No statistical studies have been conducted at the present of the ORPA suprathermal electron flux to look for a possible solar cycle variation or for flux anisotropies. The Venera electron detector has about the same solid angle as that of the ORPA, but the axis was fixed in the antisunward direction. Thus, all that can be inferred at the present is that the flux is probably approximately isotropic and that there is not a large solar cycle variation.

Nightside Ionization Sources

Two ionization sources play a significant role in maintaining the nightside ionosphere. The first to be recognized was the electron impact source, a source produced by the aforementioned suprathermal electron fluxes with energy of the order of 14 eV. Gringauz et al. [1979] were the first to recognize that the suprathermal electrons were a source of ionization and that the measured flux could produce the nightside electron density profiles measured by the Venera radio occultation experiments provided the electrons impacted a neutral CO₂ layer with appropriate scale height and density. The suprathermal electron fluxes are present in the nightside Venus hemisphere at solar maximum and solar minimum and contribute, therefore, to the maintenance of the nightside ionosphere at all phases of the solar cycle. The PVO measurements suggest that the median electron impact source may

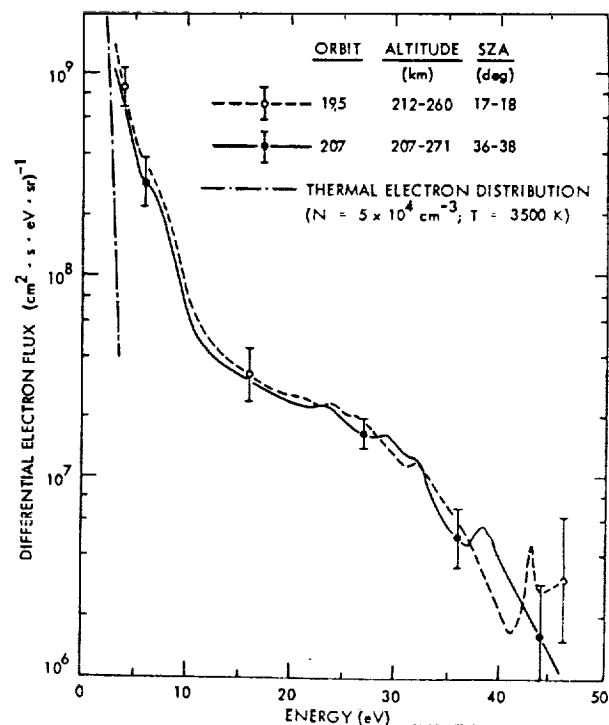


Fig. 33. Differential photoelectron flux in the solar maximum dayside ionosphere (from [Knudsen et al., 1980a]).

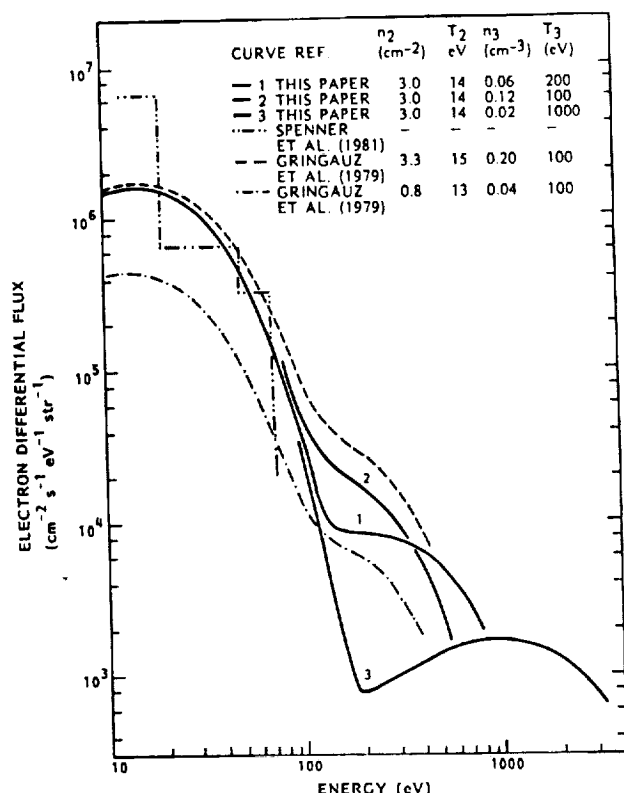


Fig. 34. Median suprathermal electron energy spectra measured in the Venus umbra at solar maximum in the altitude interval 1000-2000 km by the PVO ORPA and at solar minimum by the Venera 9 and 10 hemispherical retarding potential analyzer (adapted from [Knudsen and Miller, 1985]).

be larger by a factor of two at solar maximum than at solar minimum. Gringauz et al. and Knudsen and Miller [1985] have both reported considerable variability in the suprathermal electron fluxes. The variability, observed within single orbits as well as from orbit to orbit, may be reasonably assumed to result from temporal as well as spatial variations. Recent model computations of the ionization produced by the measured suprathermal electron fluxes impacting the solar maximum neutral nightside atmosphere demonstrate that these fluxes are primarily effective in producing an O_2^+ ionospheric layer [Spencer et al., 1981; Cravens et al., 1983]. The O^+ layer peak electron density produced by the flux is smaller by a factor of 10^2 than the O_2^+ layer peak electron density (see Figures 19 and 20). The computed column ion production rate from electron impact in both studies was of the order of $1 \times 10^7 \text{ cm}^{-2} \text{ s}^{-1}$.

The second ionization source to be recognized was the O^+ transport source. Taylor et al. [1979], observing that the nightside composition was similar to that in the dayside and that large horizontal ion velocities existed, concluded that transport of O^+ ions could produce the observed nightside ionization. The O_2^+ main peak would be produced through the reaction $O^+ + CO_2 \rightarrow O_2^+ + CO$. Knudsen et al. [1980b] established the importance of O^+ transport by making an ionization balance calculation. From early ORPA vector velocity and O^+ density

measurements, they calculated the median flux of O^+ ions crossing the terminator to be $8 \times 10^{26} \text{ s}^{-1}$ (Table 1). The median column source flux S_i that this transterminator flux would provide if distributed evenly across the the nightside hemisphere is $3 \times 10^8 \text{ cm}^{-2} \text{ s}^{-1}$. They also estimated the average column recombination rate L across the nightside hemisphere from the shape of the O_2^+ layer $s(r)$ and its peak density $n_m(\theta)$ as a function of SZA to be $2 \times 10^8 \text{ cm}^{-2} \text{ s}^{-1}$. Thus, the transterminator O^+ flux was sufficient to maintain the nightside hemisphere provided that most of the flux was being distributed appropriately across the entire nightside hemisphere and returning to the planet. Later studies have shown that the O^+ flow typically carries to at least 135° SZA (see Figure 26) and, hence, covers the bulk of the nightside hemisphere. Present evidence suggests that the planetary ionization escaping down the Venus wake is smaller by more than an order of magnitude than the cross terminator O^+ flux [Knudsen et al., 1980b; Mihalov and Barnes, 1982; and McComas et al., 1986]. Consequently, most of the transterminator O^+ flux recombines in the ionosphere. Numerical model studies, one dimensional as well as two dimensional, have demonstrated that formation of the nightside O^+ layer requires a downward flux of O^+ ions with magnitude of the order of $1 \times 10^8 \text{ cm}^{-2} \text{ s}^{-1}$, and that the flow will carry through most of the nightside hemisphere [Spencer et al., 1981; Cravens et al., 1983; Whitten et al., 1984; McCormick et al., 1986; and Nagy et al., 1991].

With the discovery of the O^+ transport source, the question arose as to the relative significance of the two sources. Spencer et al. [1981] concluded that the O^+ transport source was dominant with the O^+ transport source typically supplying three times the ionization that electron impact was supplying. The evidence cited above suggests that this conclusion was conservative for typical conditions existing during the first few years of the PVO mission. However, evidence is presented hereafter which shows that the O^+ transport source is typically large only during solar maximum and is probably insignificant during solar minimum. The two sources evidently alternate in being the dominant nightside ionization source.

TABLE 1. Nightside Ionospheric Ionization Balance

F (10^{26} s^{-1})	S_i ($10^8 \text{ cm}^{-2} \text{ s}^{-1}$)	S_e ($10^8 \text{ cm}^{-2} \text{ s}^{-1}$)	L ($10^8 \text{ cm}^{-2} \text{ s}^{-1}$)	Reference
8	3	-	2	Knudsen et al. 1980
-	-	~.02	2	Spencer et al. 1980
				Cravens et al. 1983

F: Integrated transterminator (O^+) flux = $\sum n v \cdot 2\pi r \Delta r$

S_i : Average column source = $F/(2\pi R_V^2)$

S_e : Column electron impact ionization rate

L: Nightside average column recombination rate

$$L = \frac{1}{2\pi R_V^2} \int_{\pi/2}^{\pi} \int_{R_V}^{\infty} \alpha n^2(\theta, r) 2\pi r^2 \sin \theta d\theta dr$$

$$n(\theta, r) \approx n_m(\theta) s(r)$$

Nightside Aurora

The Pioneer Venus ultraviolet spectrometer has observed 130.4 nm radiation, spatially and temporally variable in brightness and in coverage, emanating from the nightside hemisphere [Phillips et al., 1986]. The variability and energy spectrum of the suprathermal electrons observed in the nightside ionosphere are consistent with the suprathermal electrons being the source of the aurora [Fox and Bougher, 1991; Fox and Stewart, 1991]. No direct correlation of the 130.4 nm brightness with suprathermal electron flux is possible since the EUV observations are made when periapsis is in the dayside hemisphere and the suprathermal electron flux measurements when periapsis is in the nightside hemisphere.

Nightside Density Variability

After the first few passages of the PVO spacecraft periapsis through the night hemisphere, a period of solar maximum, it became evident that the ionosphere was substantial or "established" most of the time. However, it was almost unobservable at the PVO altitude on some occasions and intermediate on other occasions [Taylor et al., 1979; Knudsen et al., 1979b]. Figure 29, introduced earlier, illustrates the variation of N_e with time as the PVO spacecraft passed through the nightside hemisphere during periods when the ionosphere was established. For comparison, Figure 35 shows an extreme example of what has been called a "disappearing" nightside ionosphere. The greater variability of the nightside ionospheric density relative to that in the dayside hemisphere is evident in the scatter of points in Figure 15 and in the sizes of the temporal variance bars in Figures 16, 19 and 20.

The cause of the apparent nightside variability has to be variability in the two sources of ionization or in the loss processes. Gringauz et al. [1979] concluded that the variability in the nightside Venera radio occultation profiles, which were recorded during solar minimum, was caused by the observed variability of suprathermal electron fluxes. Since we now have evidence that the O^+ transport ionization source is greatly reduced at solar minimum, their conclusion seems reasonable.

Knudsen et al. [1980b] and Spenser et al. [1981], recognizing that trans terminator flow of ions from the dayside ionosphere was a dominant source of the nightside ionosphere at solar maximum, suggested that the relatively large variability of the nightside ionosphere was caused by temporal and spatial variations in the trans terminator O^+ flux. Since that flux depends on the ionopause height at the terminator, as well as on the velocity field, it is reasonable to assume that a correlation might exist between the density of the nightside ionosphere and the terminator ionopause height. Two dimensional model studies in which the height of the ionopause at the terminator has been varied confirmed this expectation [Cravens et al., 1983; Knudsen et al., 1987]. Miller and Knudsen [1987] investigated the correlation between ionopause height and nightside electron density experimentally. In Figure 36, the ionopause height measured near the terminator and normalized by the median ionopause at the same SZA is plotted against the ion density measured in the same orbit at an altitude between 170 and 200 km altitude and normalized by the local electron density of the empirical model of Theis et al. [1984]. The selected orbits had periapses in the central nightside hemisphere. By selecting the

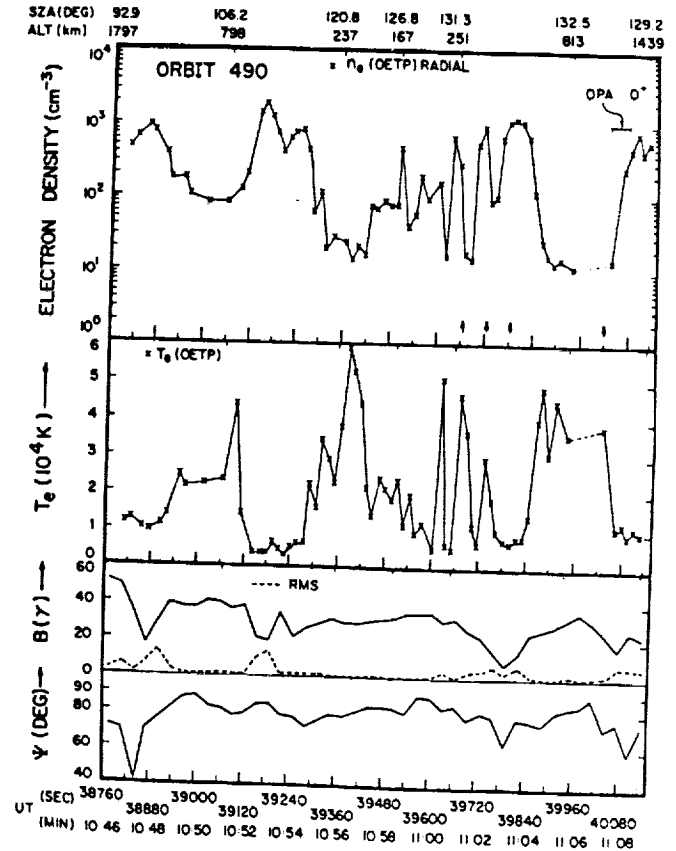


Fig. 35. Example of a disappearing nightside ionosphere at solar maximum. Ψ is the angle between the magnetic field vector and the vertical (from [Cravens et al., 1982]).

density in the 170 to 200 km height range, the density consists primarily of O^+ ions. A positive and approximately direct correlation is exhibited by the data, which were obtained during solar maximum.

As was discussed earlier, the ionopause height for moderate values of the solar wind dynamic pressure depends on a balance between the ionospheric particle pressure and the component of the solar wind dynamic pressure normal to the ionopause. Since the ionospheric particle pressure depends on the product of N_e and the sum $T_e + T_i$, we might logically assume that the ionopause height will depend on the magnitude of the solar EUV flux in addition to the solar wind dynamic pressure. Brace et al. [1990] have recently attempted to establish a correlation between the average electron density within several altitude intervals in the central Venus umbra and the solar wind dynamic pressure and between the electron density and the solar EUV flux. Over a solar cycle the expected correlation was obtained; the average nightside electron density was positively correlated with the EUV flux and negatively correlated with the solar wind dynamic pressure. With the data base restricted to solar maximum and low altitude, the nightside electron density was negatively correlated with the solar wind dynamic pressure, as expected, but showed a weak, negative correlation with EUV flux which was not expected.

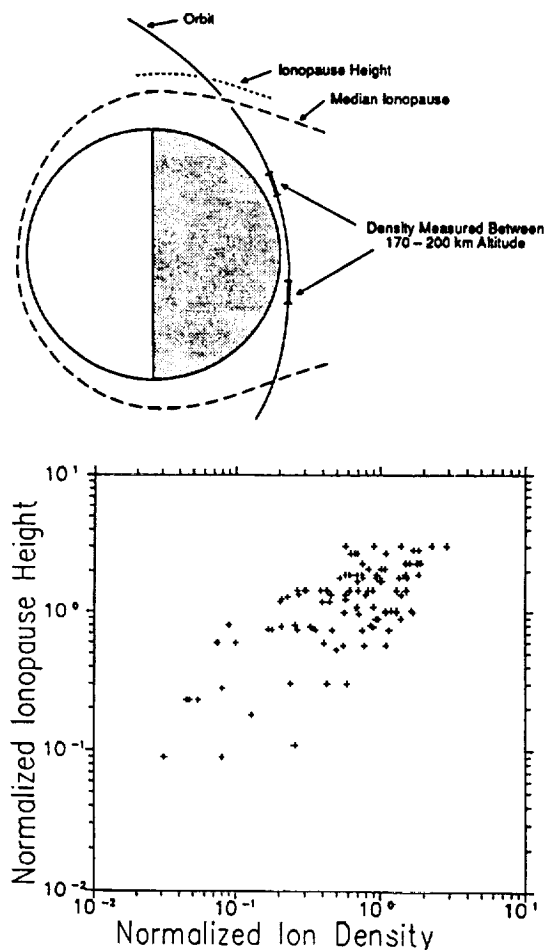


Fig. 36. Correlation of normalized nightside ion density and normalized ionopause height at solar maximum (adapted from [Miller and Knudsen, 1987]). The ion density, measured by the ORPA in the altitude interval 170-200 km, is predominantly O^+ and is normalized by dividing it by the empirical model density of Theis et al. [1984]. The measured ionopause altitude is normalized by dividing it by the median altitude modeled by Knudsen et al. [1982b].

THE SOLAR MINIMUM IONOSPHERE

Strong Solar Cycle Control of the Ionopause Altitude

The variation of the dayside ionospheric peak density with solar cycle phase consistent with Chapman's theory was to be expected and has been borne out by measurement [Bauer, 1983; Kliore and Mullen, 1989]. What was not anticipated or appreciated until 1987 was the rather dramatic depression of the dayside O^+ layer and the consequent depletion of the the nightside O^+ layer during solar minimum caused by the simultaneous reduction of the average solar EUV flux and increase of the average solar wind dynamic pressure [Knudsen et al., 1987]. In retrospect, it is rather surprising, that this process was not recognized from earlier clues.

One clue was the discrepancy in nightside density at and above 200 km altitude between Venera 9 and 10 radio occultation profiles obtained during solar minimum and PVO in situ measurements

made at solar maximum [Savich et al., 1982; Osmolovskii et al., 1984]. The discrepancy, which exceeds an order of magnitude, is illustrated in Figure 37. The densities measured at or near the nightside peak by both Venera and PVO radio occultation experiments and PVO in situ experiments were comparable. Honoring the discrepancy as real, Knudsen et al. [1986] suggested that the difference could be understood if at solar minimum the transterminator O^+ flux is reduced by an order of magnitude from that measured at solar maximum and the electron impact ionization produced by suprathermal electrons remained the same. With these conditions satisfied, the O^+ layer density would be reduced a factor of ten, but the O_2^+ layer would be reduced only a small amount. However, they failed to recognize how steady shutoff of the O^+ transport was being effected.

A final clue came in the form of PVO radio occultation profiles in the SZA range $60^\circ - 70^\circ$ at solar maximum and solar minimum. Figure 38 illustrates the average electron density profiles derived from several radio occultation profiles measured at solar maximum (1980) and at solar minimum (1986). The solar minimum average density profile is formed from 10 individual profiles lying between 60° and 70° SZA. The solar maximum average profile is formed from 6 individual profiles falling between 60° and 70° SZA. The average solar wind dynamic pressure for the 10 solar minimum profiles is 4.8 nPa and is 5.1 nPa for the 6 solar maximum profiles. If we assign the ionopause altitude as that at which the density decreases below $1 \times 10^4 \text{ cm}^{-3}$, the ionopause altitude, as inferred from Figure 39, would be at 225 km at solar minimum and at 575 km at solar maximum. The solar maximum density at and above 250 km is more than an order of magnitude larger than that at solar minimum.

Knudsen et al. [1987] attributed this solar cycle change to a decrease in the ionospheric pressure by a factor of 3 from solar

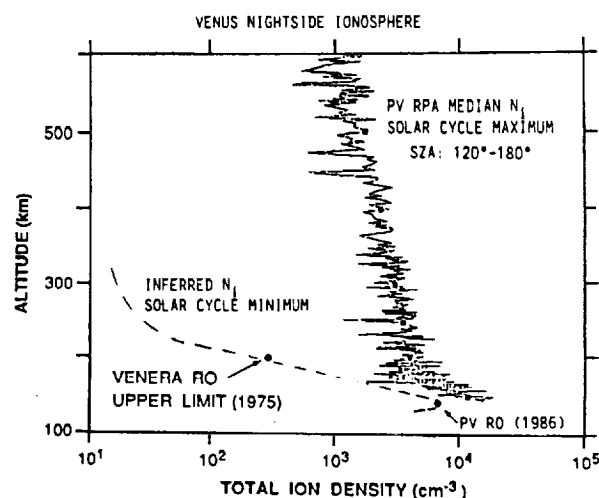


Fig. 37. Comparison of the solar maximum median nightside ion density altitude profile measured by the PVO ORPA, the solar minimum average peak electron density measured by the PVO radio occultation experiment [A. J. Kliore, private communication, 1987], and upper limit of the electron density at and above 200 km altitude at solar minimum inferred from Venera 9 and 10 radio occultation profiles [Savich et al., 1982].

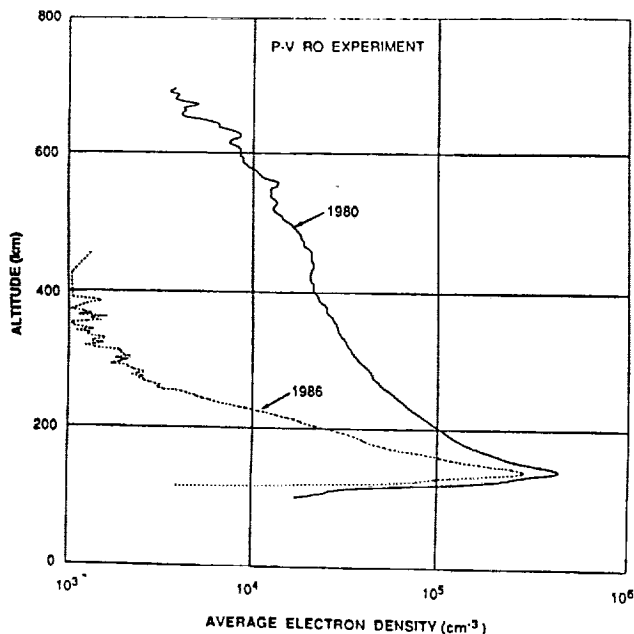


Fig. 38. Average electron density altitude profiles derived from PVO radio occultation profiles recorded at solar maximum and solar minimum (from [Knudsen et al., 1987]). Each average is derived from several profiles all of which were recorded between 60° and 70° SZA.

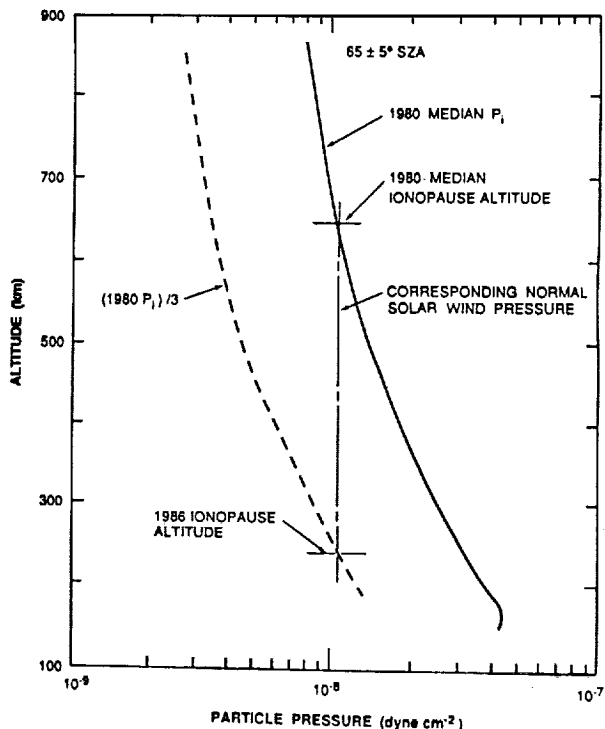


Fig. 39. The median ionospheric thermal pressure P_i measured at solar maximum measured by the PVO ORPA and the inferred thermal pressure at solar minimum $P_i/3$ (from [Knudsen et al., 1987]). For constant normal solar wind pressure, the median ionopause height decreases from 650 km at solar maximum to below 250 km at solar minimum.

maximum to solar minimum. Figure 39 illustrates the median ionospheric thermal pressure P_i measured by the PVO ORPA at solar maximum at 65° SZA. The dashed curve is the predicted curve that would be observed at solar minimum in the absence of a solar wind. The altitude of pressure balance changes from 650 km at solar maximum to 250 km at solar minimum for a constant normal component of solar wind dynamic pressure equal to 1 nPa. A reduction of the solar maximum pressure profile by a factor of three at solar minimum is reasonable because of its nonlinear response to the reduction of the solar EUV flux by a factor of two or more. The O^+ density, which is directly proportional to the O^+ ion production rate, would be decreased a factor of three by a 40% decrease in the neutral O density [Keating et al., 1985] and by a 50% decrease in the EUV flux. The reduction of the ionospheric pressure by a factor of three should, of itself, be sufficient to cause the observed reduction of typical ionopause height. However, the solar wind also contributes to the decrease. The solar wind average dynamic pressure at solar minimum (1985-1987) was approximately 50% larger than it was during solar maximum (1979-1981) according to the data shown in Figure 40.

That the ionopause would be compressed to its limiting altitude most of the time at solar minimum may be readily understood by referring back to Figure 8. If the peak effective ionospheric pressure is reduced by a factor of three, and the center of the solar wind dynamic pressure histogram intervals is moved to the right by a factor of 1.5, (I am assuming the histogram retains its solar maximum form), the percentage of time that the solar wind dynamic pressure is less than the ionospheric peak effective pressure changes from approximately 78% at solar maximum to something less than 10% at solar minimum.

The Dayside Ionosphere

No in situ measurements of the solar minimum dayside ionosphere exist, but from the available solar minimum radio occultation profiles and solar maximum PVO periapsis passes that

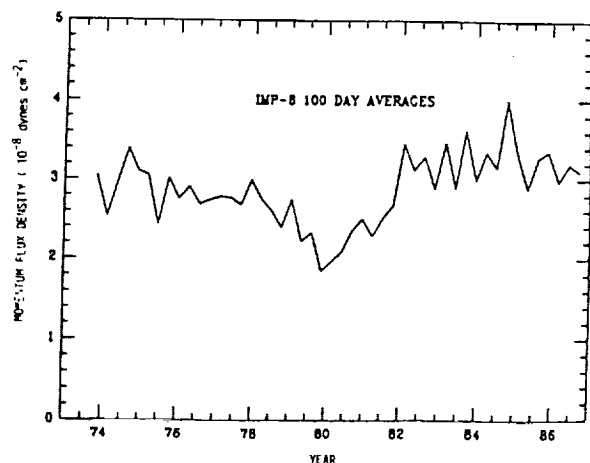


Fig. 40. 100-day averages of the solar wind dynamic pressure p_1^2 over a solar cycle measured in the vicinity of the earth (adapted from [Lazarus and Belcher, 1988]). The dynamic pressure is approximately 50% higher at solar minimum (1976, 1986) than at solar maximum (1980).

occurred during periods of high solar wind dynamic pressure, we can come up with a fairly certain picture. First of all, the dayside ionosphere is highly compressed most of the time. No extensive diffusive equilibrium O^+ layer overlies the O_2^+ layer such as was the case under typical solar maximum conditions. It is reasonable to assume that the ion composition is similar to that illustrated in Figure 4 for orbit 412, an orbit in which the solar wind dynamic pressure was substantially larger than the maximum ionospheric particle pressure. Although O^+ ions will be the dominant ion constituent above an altitude of about 180 km, the scale height of the O^+ ion density will be much smaller than the diffusive equilibrium scale height [Mahajan and Mayr, 1989].

The Nightside Ionosphere

With the dayside O^+ layer effectively removed at solar minimum, the nightside O^+ layer should also be effectively removed since the nightside O^+ layer is almost exclusively produced by O^+ transport. The discrepancy in nightside density at 200 km altitude between that measured by the Venera 9 and 10 radio occultation experiments at solar minimum and that measure by PVO in situ instruments at solar maximum and illustrated in Figure 37 was the first evidence of the missing nightside O^+ layer. Additional evidence is illustrated in Figure 41. Medians of ion density derived from ORPA measurements at solar maximum and at solar minimum exhibit more than an order of magnitude difference in density when extrapolated to a common altitude of 1800 km. The inference is that a large reduction in the nightside O^+

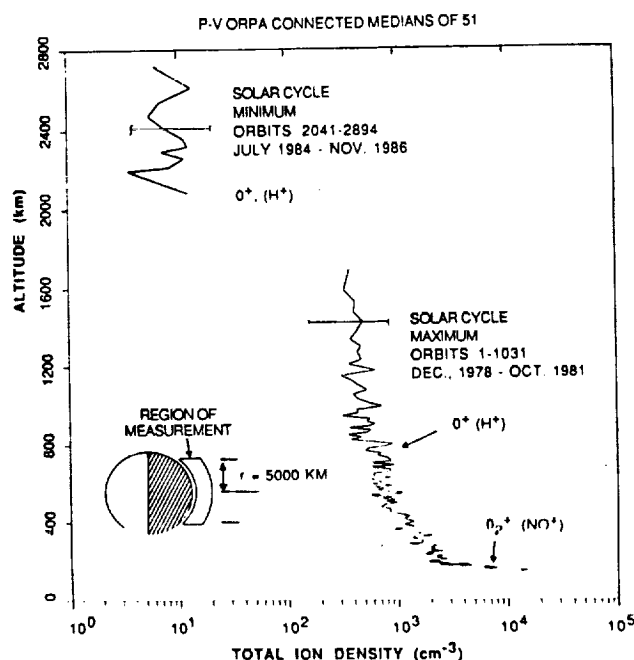


Fig. 41. Nightside median ion density profiles measured at solar maximum and solar minimum by the PVO ORPA experiment (from [Knudsen, 1988]). The curves do not overlap because of PVO periaapsis altitude changes throughout the solar cycle (Figure 3). The ion in parentheses is known or thought to be the most abundant minor ion at the indicated altitude.

layer density has occurred between solar maximum and solar minimum. Brace et al. [1990] have verified that the average plasma density above 2000 km altitude at solar minimum is about 10 cm^{-3} or less.

Brace et al. [1987] have shown that the nightside solar minimum ionosphere above about 2000 km altitude is very structured and consists of filaments ("tail rays") with a plasma density of a few hundred cm^{-3} imbedded in a background plasma ("troughs") with a density of the order of 10 cm^{-3} , as shown in Figures 42 and 43. The filaments are thought to be elongated with their long axis more or less parallel to the sun-Venus axis. Figure 43 illustrates the variation of electron density N_e , magnetic field magnitude B and component vectors B_x , B_y and B_z , suprathermal O^+ density O_{st}^+ , fast ionospheric ions O_f^+ , electron temperature T_e , and total, plasma and magnetic pressures P_T , P_P , and P_B through one nightside passage recorded in Jan 1984 shortly before solar minimum (see Figure 3). Suprathermal ions O_{st}^+ appear to compose most of the ion density in the rays and troughs and are thought to have a temperature in the range 9-16 eV. The fast O^+ ions have an energy of approximately 40 eV and comprise of the order of 2% or less of the total density [Kasprzak et al., 1987]. The electron temperature measured by the PVO electron temperature probe (OETP) is approximately 0.5 eV within the rays, a temperature similar to that in the solar maximum nightside ionosphere at an altitude of 1000 km. The electron temperature in the troughs is approximately one

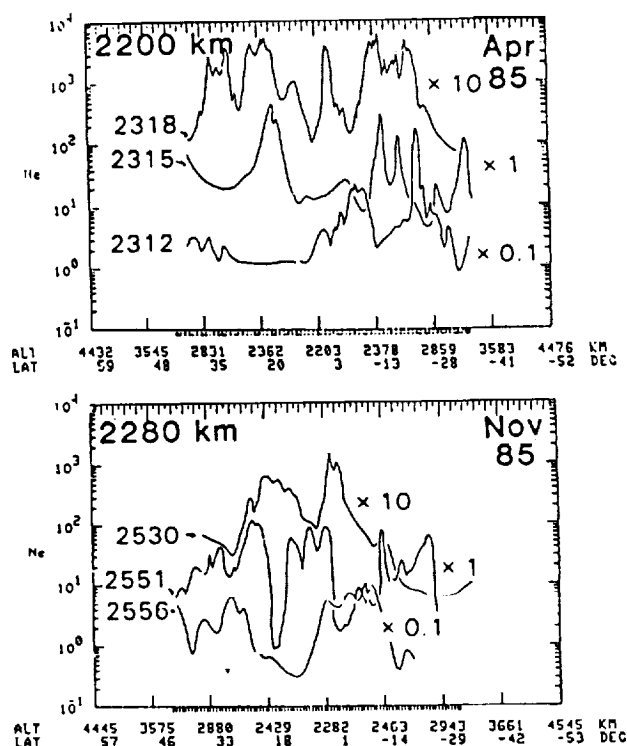


Fig. 42. Structure in the solar minimum nightside electron density at high altitude (adapted from Brace et al. [1987]). The high density intervals are interpreted to be filaments or rays with long dimension approximately parallel to the sun-Venus axis.

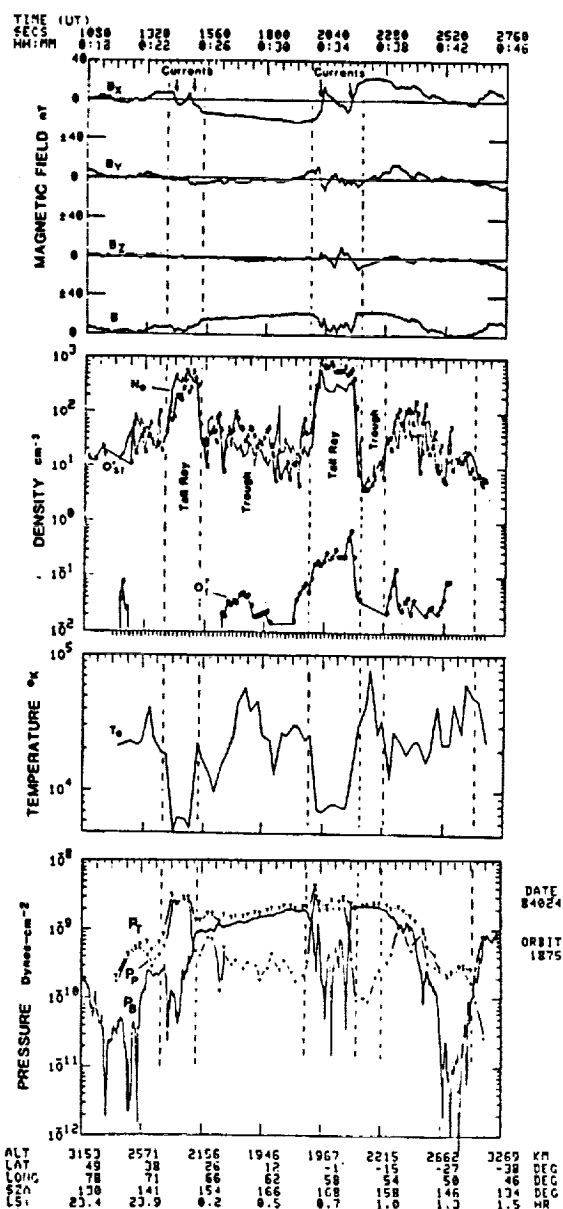


Fig. 43. Composition and some thermal properties of the solar minimum high altitude tail region (adapted from Brace et al. [1987]). The high density intervals are interpreted as tail rays. The electron temperature and magnetic field strength are low in the rays and high in the troughs. The plasma pressure P_T and magnetic field pressure P_B are in approximate balance at the ray edges. The rays and troughs are believed to be composed primarily of O^+ ions (O_m^+) and are inferred to have a temperature between 9 and 16 eV. A component of the O^+ ions O_r^+ has an energy of approximately 40 eV and typically composes less than 1% of the ions.

order of magnitude larger. B is strongest in the troughs and is parallel to the sun-Venus axis.

Vaisberg et al. [1976] have reported Venera 10 measurements of cool ions at about 1800 km altitude with temperatures of a few eV converging toward the sun-Venus axis as shown in Figure 44. The

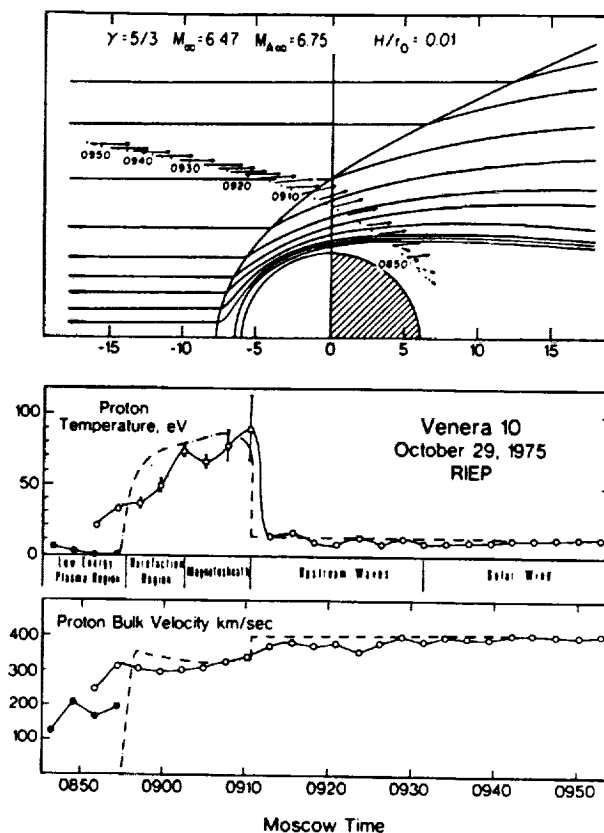


Fig. 44. Direction of flow, temperature, and velocity of ions measured by the RIEP instrument on Venera 10 in Oct. 1975. Location of the shock and boundary of obstacle and flow direction (solid lines in upper portion) are from HD model of Spreiter et al. [1980]. Dashed arrows show the low energy ion flow direction. The temperature and velocity of the low energy component is indicated by dots in the middle and bottom part of the figure, respectively (adapted from Russell and Vaisberg [1983]).

ion temperature is of the order of 1-5 eV and the velocity, if the ions are assumed to be O^+ , is $25\text{--}50\text{ km s}^{-1}$. The typical number density of the heavy component is of the order of 0.5 cm^{-3} . Russell and Vaisberg [1983] have interpreted these ions as having been introduced into the solar wind plasma as it flowed toward the terminator within the plasma mantle. It would appear from the evidence available at this time that the cool, few eV temperature ions observed by Vaisberg et al. [1976] and Brace et al. [1987] are largely O^+ ions produced by photoproduction or charge exchange in the mantle layer above the solar minimum ionopause and carried into the solar minimum wake. The filaments may have arisen from magnetic flux tubes flowing closer to the ionopause than those tubes forming the troughs.

Figure 45 illustrates a nightside solar minimum plasma density profile inferred from Venera and PVO radio occultation profiles and PVO in situ measurements. The O_2^+ peak density is less than it is at solar maximum as a result of the elimination of the solar maximum O^+ transport ionization source and a possible small reduction in the precipitating suprathermal electron flux. Because the O_2^+ peak density varies only as the square root of the ionization

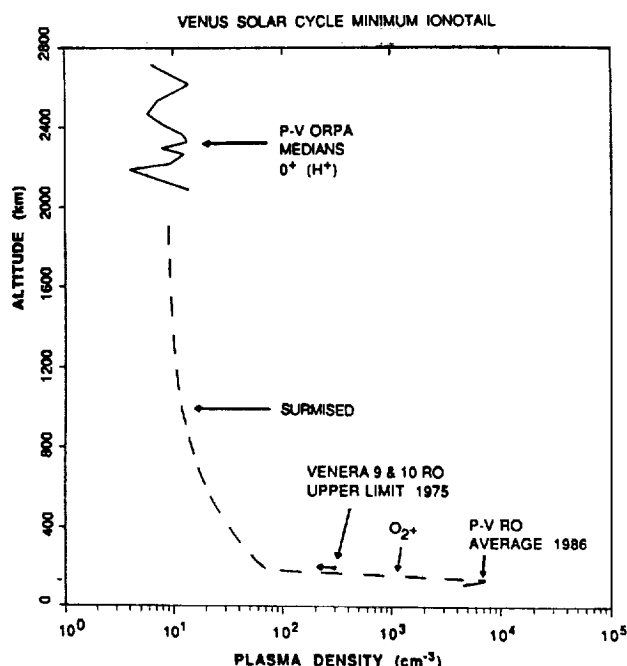


Fig. 45. Nightside median plasma density height profile at solar minimum inferred from Venera and PVO radio occultation measurements and PVO ORPA in situ measurements (from [Knudsen, 1988]).

rate, it is relatively insensitive to changes in the ionization rate. The solar maximum topside O^+ layer is largely missing and is replaced by filaments and troughs of plasma containing O^+ ions and presumably H^+ ions of comparable concentration with ion temperatures of the order of 10 eV. The density, composition and temperature of the topside plasma suggest that the plasma has originated as solar wind plasma flowing within the mantle region and subsequently converging into the near-Venus wake. The O^+ and other ions of Venus origin are added through photoionization, charge exchange and possibly diffusion (turbulence) as the solar wind flux tubes traverse the dayside mantle region.

CONCLUDING REMARKS

PVO and previous NASA and Russian experiments have revealed a Venusian ionosphere dramatically different than that of the earth. The Venusian ionosphere, unprotected and unconstrained by a strong internal magnetic field, exhibits a gross morphology and many processes and features, such as an ionopause; a supersonic, antisunward-directed ion wind; and magnetic flux ropes, that are substantially different from anything observed in the earth's ionosphere. Our reservoir of knowledge concerning the behavior of ionospheric plasma when subjected to constraints different from those imposed at earth has greatly increased as a result of these successful experiments, and we will be better able to predict the behavior of plasmas in new environments.

Although we now have a large body of experimental data defining many of these new processes and features, as is often the case, we need additional, refined measurements to discriminate between or verify current hypotheses as to the physics behind the

processes. Some inadequacies in our present measurements needed for a better understanding of Venus processes include high spatial resolution suprathermal (10^0 - 10^5 eV) electron and ion mass spectrometer three dimensional flux measurements, and high spatial resolution thermal ion bulk velocity measurements. Hopefully, PVO and the Venera missions will not be the last plasma physics missions to Venus.

Acknowledgments. I thank the editor and referees for the considerable contribution they have made to this paper. This work was supported by NASA contract NAS2-12902.

REFERENCES

- Bauer, S. J., Solar control of the Venus ionosphere, *Sitzungsber. Oesterr. Akad. Wiss. Math. Naturwiss. Kl.*, 2, 192(8-10), 309-317, 1983.
- Bauer, S. J., L. H. Brace, H. A. Taylor, Jr., T. K. Breus, A. J. Kliore, W. C. Knudsen, A. F. Nagy, C. T. Russell and N. A. Savich, The Venus ionosphere, *Adv. Space Res.*, 5, 233, 1985.
- Brace, L. H., and A. J. Kliore, The structure of the Venus ionosphere, *Space Sci. Rev.*, 5, 233, 1991.
- Brace, L. H., R. F. Theis, W. R. Hoegy, J. H. Wolfe, J. D. Mihalov, C. T. Russell, R. C. Elphic, and A. F. Nagy, The dynamic behavior of the Venus ionosphere in response to solar wind interactions, *J. Geophys. Res.*, 85, 7663, 1980.
- Brace, L. H., Plasma clouds above the ionopause of Venus and their implications, *Planet. Space Sci.*, 30, 29, 1982a.
- Brace, L. H., R. F. Theis, H. G. Mayr, S. A. Curtis, J. G. Luhmann, Holes in the nightside ionosphere of Venus, *J. Geophys. Res.*, 87, 199, 1982b.
- Brace, L. H., H. A. Taylor Jr., T. I. Gombosi, A. J. Kliore, W. C. Knudsen, and A. F. Nagy, in *Venus*, edited by D. M. Hunten, L. Colin, T. M. Donahue, and V. I. Moroz, pp 779-840, Univ. of Arizona Press, 1983a.
- Brace, L. H., R. C. Elphic, S. A. Curtis, C. T. Russell, Wave structure in the Venus ionosphere down stream of the terminator, *Geophys. Res. Lett.*, 10, 1116, 1983b.
- Brace, L. H., W. T. Kasprzak, H. A. Taylor, R. F. Theis, C. T. Russell, A. Barnes, J. D. Mihalov, and D. M. Hunten, The ionotail of Venus: Its configuration and evidence for ion escape, *J. Geophys. Res.*, 92, 15, 1987.
- Brace, L. H., R. F. Theis, and J. D. Mihalov, Response of nightside ionosphere and ionotail of Venus to variations in solar EUV and solar dynamic pressure, *J. Geophys. Res.*, 95, 4075, 1990.
- Brinton, H. C., H. A. Taylor, Jr., H. B. Niemann, H. G. Mayr, A. F. Nagy, T. E. Cravens and D. F. Strobel, Venus nighttime hydrogen bulge, *Geophys. Res. Lett.*, 7, 865, 1980.
- Bougher, S. W., and T. E. Cravens, A two dimensional model of the nightside ionosphere of Venus: Ion energetics, *J. Geophys. Res.*, 89, 3837, 1984.
- Colin, L., The Pioneer Venus program, *J. Geophys. Res.*, 85, 7575, 1980.
- Cravens, T. E., A. F. Nagy, L. H. Brace, R. H. Chen, and W. C. Knudsen, The energetics of the ionosphere of Venus: A preliminary model based on Pioneer Venus observations, *Geophys. Res. Lett.*, 5, 341, 1979.
- Cravens, T. E., T. I. Gombosi, J. Kozyra, and A. F. Nagy, Model calculations of the dayside ionosphere of Venus: Energetics, *J. Geophys. Res.*, 85, 7778, 1980.
- Cravens, T. E., L. H. Brace, H. A. Taylor, Jr., C. T. Russell, W. C. Knudsen, K. L. Miller, A. Barnes, J. D. Mihalov, F. L. Scarf, S. J. Quenon, and A. F. Nagy, Disappearing ionospheres on the nightside of Venus, *Icarus*, 51, 271, 1982.
- Cravens, T. E., S. L. Crawford, A. F. Nagy, and T. I. Gombosi, A two-dimensional model of the ionosphere of Venus, *J. Geophys. Res.*, 88, 5595, 1983.
- Donahue, T. M., J. H. Hoffman, R. R. Hodges, Jr. and A. J. Watson, Venus was wet: A measurement of the ratio of deuterium to hydrogen, *Science*, 216, 630, 1982.
- Elphic, R. C., C. T. Russell, J. A. Slavin, and L. H. Brace, Observations of

- the dayside ionopause and ionosphere of Venus, *J. Geophys. Res.*, **85**, 7679, 1980.
- Elphic, R. C., C. T. Russell, and J. G. Luhmann, The Venus ionopause current sheet: Thickness length scale and controlling factors, *J. Geophys. Res.*, **86**, 11,430, 1981.
- Elphic, R. C., H. G. Mayr, R. F. Theis, L. H. Brace, K. L. Miller, and W. C. Knudsen, Nightward ion flow in the Venus ionosphere: Implications of momentum balance, *Geophys. Res. Lett.*, **11**, 1007, 1984.
- Fox, J. L., and S. W. Bougher, Structure, luminosity, and dynamics of the Venus thermosphere, *Space Sci. Rev.*, **55**, 357, 1991.
- Fox, J. L., and A. I. E. Stewart, The Venus ultraviolet aurora: a soft electron source, *J. Geophys. Res.*, In Press, 1991.
- Grebowsky, J. M., and S. A. Curtis, Venus nightside ionospheric holes - the signatures of parallel electric field acceleration regions, *J. Geophys. Res. Lett.*, **8**, 1273, 1981.
- Grebowsky, J. M., H. G. Mayr, S. A. Curtis, H. A. Taylor Jr., Venus' nighttime horizontal plasma flow, magnetic congestion, and ionospheric hole production, *J. Geophys. Res.*, **88**, 3005, 1983.
- Gringauz, K. I., M. I. Verigin, T. K. Breus, and T. Gombosi, The interaction of electrons in the optical umbra of Venus with the planetary atmosphere-The origin of the nighttime ionosphere, *J. Geophys. Res.*, **84**, 2123, 1979.
- Hartle, R. E. and H. A. Taylor, Jr., Identification of deuterium ions in the ionosphere of Venus, *Geophys. Res. Lett.*, **10**, 965, 1983.
- Kasprzak, W. T., H. B. Niemann, and P. Mahaffy, Observations of energetic ions on the nightside of Venus, *J. Geophys. Res.*, **92**, 291, 1987.
- Keating, G. M., J. L. Bertaux, S. W. Bougher, T. E. Cravens, R. E. Dickinson, A. E. Hedin, V. A. Krasnopolsky, A. F. Nagy, J. Y. Nicholson III, L. J. Paxton and U. von Zahn, *Adv. Space Res.*, **5**, 117, 1985.
- Kim, J., A. F. Nagy, T. E. Cravens, H. Shinagawa, Temperatures of individual ion species and heating due to charge exchange in the ionosphere of Venus, *J. Geophys. Res.*, **95**, 6569, 1990.
- Kliore, A. J. and L. F. Mullen, The long-term behavior of the main peak of the dayside ionosphere of Venus during solar cycle 21 and its implications on the effect of the solar cycle upon the electron temperature in the main peak region, *J. Geophys. Res.*, **94**, 13339, 1989.
- Knudsen, W. C., Solar cycle changes in the morphology of the Venus ionosphere, *J. Geophys. Res.*, **93**, 8756, 1988.
- Knudsen, W. C., and K. L. Miller, Pioneer Venus suprathermal electron flux measurements in the Venus umbra, *J. Geophys. Res.*, **2695**, 1985.
- Knudsen, W. C., K. Spenner, R. C. Whitten, J. R. Spreiter, K. L. Miller, and V. Novak, Thermal structure and major ion composition of the Venus ionosphere: first RPA results from Venus orbiter, *Science*, **203**, 757, 1979a.
- Knudsen, W. C., K. Spenner, R. C. Whitten, J. R. Spreiter, K. L. Miller, and V. Novak, Thermal structure and energy influx to the day- and nightside Venus ionosphere, *Science*, **205**, 105, 1979b.
- Knudsen, W. C., K. Spenner, P. F. Michelson, R. C. Whitten, K. L. Miller, and V. Novak, Suprathermal electron energy distribution within the dayside Venus ionosphere, *J. Geophys. Res.*, **85**, 7754, 1980a.
- Knudsen, W. C., K. Spenner, K. L. Miller, and V. Novak, Transport of ionospheric O⁺ ions across the Venus terminator and implications, *J. Geophys. Res.*, **85**, 7803, 1980b.
- Knudsen, W. C., K. Spenner, J. Bakke and V. Novak, Pioneer-Venus orbiter planar retarding potential analyzer plasma experiment, *IEEE Trans. Geosci. Remote Sensing*, **GE-18**, 54-59, 1980c.
- Knudsen, W. C., K. Spenner, R. C. Whitten, and K. L. Miller, Ion energetics in the Venus nightside ionosphere, *Geophys. Res. Lett.*, **7**, 1045, 1981a.
- Knudsen, W. C., K. Spenner, and K. L. Miller, Anti-solar acceleration of ionospheric plasma across the Venus terminator, *Geophys. Res. Lett.*, **8**, 241, 1981b.
- Knudsen, W. C., P. M. Banks, and K. L. Miller, A new concept of plasma motion and planetary magnetic field for Venus, *Geophys. Res. Lett.*, **9**, 765, 1982a.
- Knudsen, W. C., K. L. Miller, and K. Spenner, Improved Venus ionopause altitude calculation and comparison with measurement, *J. Geophys. Res.*, **87**, 2246, 1982b.
- Knudsen, W. C., K. L. Miller, and K. Spenner, Median density altitude profiles of the major ions in the central nightside Venus ionosphere, *J. Geophys. Res.*, **91**, 11,936, 1986.
- Knudsen, W. C., A. J. Kliore, and R. C. Whitten, Solar cycle changes in the ionization sources of the nightside Venus ionosphere, *J. Geophys. Res.*, **92**, 13,391, 1987.
- Krehbiel, J. P., L. H. Brace, R. F. Theis, J. R. Cutler, W. H. Pinkus, and R. B. Kaplan, Pioneer Venus orbiter electron temperature probe, *IEEE Trans. Geosci. Remote Sensing*, **GE-18**, 49, 1980.
- Lazarus, A. and J. Belcher, Large scale structure of the distant solar wind and heliosphere, in *Proceeding of the 6th International Solar Wind Conference*, Vol. 2, edited by V. Pizzo, T. Holzer and D. Sime, pp. 533-536, 1988, NCAR/TN-306 Proc., NCAR High Altitude Observatory, Boulder, Colorado.
- Luhmann, J. G., The solar wind interaction with Venus, *Space Sci. Rev.*, **44**, 241, 1986.
- Luhmann, J. G., and T. E. Cravens, Magnetic fields in the ionosphere of Venus, *Space Sci. Rev.*, **55**, 201, 1991.
- Luhmann, J. G., R. C. Elphic, C. T. Russell, J. D. Mihalov, and J. H. Wolfe, Observations of large scale steady magnetic fields in the dayside Venus ionosphere, *Geophys. Res. Lett.*, **7**, 917, 1980.
- Luhmann, J. G., C. T. Russell, L. H. Brace, H. A. Taylor, W. C. Knudsen, F. L. Scarf, D. S. Colburn, and A. Barnes, Pioneer observations of plasma and field structure in the near wake of Venus, *J. Geophys. Res.*, **87**, 9205, 1982.
- Mahajan, K. K., and H. G. Mayr, Venus ionopause during solar minimum, *Geophys. Res. Lett.*, **16**, 1477, 1989.
- Marubashi K., J. M. Grebowsky, H. A. Taylor Jr., J. G. Luhmann, C. T. Russell, and A. Barnes, Magnetic field in the wake of Venus and the formation of ionospheric holes, *J. Geophys. Res.*, **90**, 1385, 1985.
- McComas, D. J., H. E. Spence, C. T. Russell, and M. A. Saunders, The average magnetic field draping and consistent plasma properties of the Venus magnetotail, *J. Geophys. Res.*, **91**, 7939, 1986.
- McCormick, P. T., R. C. Whitten, and W. C. Knudsen, Dynamics of the Venus ionosphere revisited, *Icarus*, **70**, 469, 1987.
- McElroy, M. B., M. J. Prather and J. M. Rodriguez, Escape of hydrogen from Venus, *Science*, **215**, 1614, 1982.
- Mihalov, J. D., and A. Barnes, The distant interplanetary wake of Venus: Plasma observations from Pioneer Venus, *J. Geophys. Res.*, **87**, 9045, 1982.
- Miller, K. L., and R. C. Whitten, Ion dynamics in the Venus ionosphere, *Space Sci. Rev.*, **55**, 165, 1991.
- Miller, K. L., W. C. Knudsen, Spatial and temporal variations of the ion velocity measured in the Venus ionosphere, *Adv. Space Res.*, **7**, 107, 1987.
- Miller, K. L., W. C. Knudsen, K. Spenner, R. C. Whitten, and V. Novak, Solar zenith angle dependence of ionospheric ion and electron temperatures and density on Venus, *J. Geophys. Res.*, **85**, 7759, 1980.
- Miller, K. L., W. C. Knudsen, and K. Spenner, The dayside Venus ionosphere, *Icarus*, **57**, 386, 1984.
- Miller, K. L., W. Zhao, L. Gordon, Evidence of a re-compression shock wave in the nightside ionosphere of Venus, *EOS, Trans. AGU*, **71**, 1515, 1990.
- Moore, K., D. J. McComas, C. T. Russell, S. S. Stahara, and J. R. Spreiter, Gasdynamic modeling of the Venus magnetotail, *J. Geophys. Res.*, **96**, 5667, 1991.
- Nagy, A. F., T. E. Cravens, R. H. Chen, H. A. Taylor Jr., L. H. Brace, and H. C. Brinton, *Science*, **205**, 107, 1979.
- Nagy, A. F., T. E. Cravens, S. G. Smith, H. A. Taylor Jr., and H. C. Brinton, Model calculations of the dayside ionosphere of Venus: Ionic composition, *J. Geophys. Res.*, **85**, 7795, 1980.
- Nagy, A. F., A. Korosmezey, J. Kim, and T. I. Gombosi, A two dimensional, shock capturing, hydrodynamic model of the Venus ionosphere, *Geophys. Res. Lett.*, In Press, 1991.
- Osmolovskii, I. K., N. A. Savich, and L. N. Samoznaev, On the height extent of the Venusian nightside ionosphere, *Radio Sci. Electron.*, **29**, 2302, 1984.

- Phillips, J. L., J. G. Luhmann, W. C. Knudsen, and L. H. Brace, Asymmetries in the location of the Venus ionopause, *J. Geophys. Res.*, **93**, 3927, 1988.
- Phillips, J. L., J. G. Luhmann and C. T. Russell, Growth and maintenance of large-scale magnetic fields in the dayside Venus ionosphere, *J. Geophys. Res.*, **89**, 10,676-10,684, 1984.
- Phillips, J. L., A. I. F. Stewart, and J. G. Luhmann, The Venus ultraviolet aurora: Observations at 130.4 nm, *Geophys. Res. Lett.*, **13**, 1047, 1986.
- Rohrbaugh, R. P., J. S. Nisbet, E. Bleuler, and J. R. Herman, The effect of energetically produced O_2^+ on the ion temperatures of the Martian thermosphere, *J. Geophys. Res.*, **84**, 3327, 1979.
- Russell, C. T., and O. Vaisberg, The interaction of the solar wind with Venus, in *Venus*, edited by D. M. Hunten, L. Colin, T. M. Donahue, and V. I. Moroz, pp. 873-940, The University of Arizona Press, Tucson, Arizona, 1983.
- Savich, N. A., I. K. Osmolovsky, and L. N. Samonznayev, The agreement problem of different Venusian ionosphere measurements, in *Proceedings of the Thirteenth International Symposium on Space Technology and Science*, pp. 1533-1537, AGNE Publishing, Inc., Tokyo, Japan, 1982.
- Singhal R. P. and R. C. Whitten, A simple spectral model of the dynamics of the Venus ionosphere, *J. Geophys. Res.*, **92**, 5735, 1987.
- Shinagawa, H., T. E. Cravens, and A. F. Nagy, A one-dimensional time-dependent model of the magnetized ionosphere of Venus, *J. Geophys. Res.*, **92**, 7317, 1987.
- Spencer, K., W. C. Knudsen, K. L. Miller, V. Novak, C. T. Russell, and R. C. Elphic, Observation of the Venus mantle, the boundary region between solar wind and ionosphere, *J. Geophys. Res.*, **85**, 7655, 1980.
- Spencer, K., W. C. Knudsen, R. C. Whitten, P. F. Michelson, K. L. Miller, and V. Novak, On the maintenance of the Venus nightside ionosphere: Electron precipitation and plasma transport, *J. Geophys. Res.*, **86**, 9170, 1981.
- Spreiter, J. R. and S. S. Stahara, Solar wind flow past Venus: Theory and comparisons, *J. Geophys. Res.*, **85**, 7715, 1980.
- Taylor, H. A. Jr., H. C. Brinton, S. J. Bauer, R. E. Hartle, P. A. Cloutier, R. E. Daniell Jr., T. M. Donahue, Ionosphere of Venus: First observations of day-night variations of the ion composition, *Science*, **205**, 96, 1979.
- Taylor H. A. Jr., H. C. Brinton, S. J. Bauer, and R. E. Hartle, Global observations of the composition and dynamics of the ionosphere of Venus: implications for the solar wind interaction, *J. Geophys. Res.*, **85**, 7765, 1980a.
- Taylor, H. A., Jr., H. C. Brinton, T. C. G. Wagner, B. H. Blackwell, and G. R. Cordier, Bennett ion mass spectrometers on the Pioneer-Venus bus and orbiter, *IEEE Trans. Geosci. Remote Sensing*, **GE-18**, 44, 1980b.
- Theis, R. F., L. H. Brace, R. C. Elphic, and H. G. Mayr, New empirical models of the electron temperature and density in the Venus ionosphere with application to terminator flow, *J. Geophys. Res.*, **89**, 1477, 1984.
- Vaisberg, O. L., S. A. Romanov, V. N. Smirnov, I. P. Karpinsky, B. I. Khazanov, B. V. Polenov, A. V. Bogdanov, and N. M. Antonov, Ion flux parameters in the solar-wind-Venus interaction region according to Venera 9 and Venera 10 data, in *Physics of Solar Planetary Environments*, edited by D. J. Williams, vol. 2, pp. 904-915, AGU, Washington, D.C., 1976.
- Whitten, R. C., B. Baldwin, W. C. Knudsen, K. L. Miller, and K. Spencer, The Venus ionosphere at grazing incidence of solar radiation: transport of plasma to the nightside ionosphere, *Icarus*, **51**, 261, 1982.
- Whitten, R. C., P. T. McCormick, D. Merritt, K. W. Thompson, R. R. Brynsvold, C. J. Eich, W. C. Knudsen, and K. L. Miller, Dynamics of the Venus ionosphere: A two-dimensional model study, *Icarus*, **60**, 317, 1984.
- Whitten, R. C., R. P. Singhal, and W. C. Knudsen, Thermal structure of the Venus ionosphere: A two-dimensional model study, *Geophys. Res. Lett.*, **13**, 10, 1986.
- Zwan, B. Y. and R. A. Wolf, Depletion of solar wind plasma near a planetary boundary, *J. Geophys. Res.*, **81**, 1636, 1976.

APPENDIX B

SUPRATHERMAL ELECTRON FLUX IN VENUS IONOSPHERIC HOLES

BY

W. C. KNUDSEN, K. L. MILLER, L. H. BRACE, AND C. T. RUSSELL

PREPRINT

Suprathermal Electron Flux in Venus Ionospheric Holes

William C. Knudsen¹

Kent L. Miller^{2,5}

L. H. Brace³

C. T. Russell⁴

¹ Knudsen Geophysical Research, Monte Sereno, CA

² Lockheed Research Laboratory, Palo Alto, CA

³ NASA/Goddard Space Flight Center, Greenbelt, MD

⁴ Institute of Geophysics & Planetary Physics,
UCLA, Los Angeles, CA

⁵ Now at Center for Atmospheric and Space Sciences,
Logan, Utah

1. William C. Knudsen
Knudsen Geophysical Research
18475 Twin Creeks Rd.
Monte Sereno, CA 95030
2. Kent L. Miller
Lockheed Palo Alto Research Laboratory
3251 Hanover Street
Palo Alto, CA 94304
3. L. H. Brace
NASA/Goddard Space Flight Center
Greenbelt, Maryland 20771
4. C. T. Russell
Institute of Geophysics and Planetary Physics
University of California
Los Angeles, CA 90024

Abstract. Suprathermal electron density, temperature, integral flux above 58 eV energy and the magnetic field are presented for two Pioneer-Venus orbits passing through the antisolar region of the Venus ionosphere. One of the orbits passed through an ionospheric hole. The second orbit did not exhibit a hole signature and is representative of other orbits examined in the antisolar region. The suprathermal electron properties exhibited by both orbits are consistent with median values and their variation reported for the Venus umbra in a previous study. The suprathermal electron temperature, density, and integral flux within the hole region are similar in magnitude to these same quantities observed exterior to the hole and give no suggestion of the existence of a significant parallel electric field. We infer that ionospheric holes are formed by a less energetic process than the parallel electric fields responsible for aurorae in the auroral zone of the earth. We favor the more benign process of plasma loss through chemical recombination at low altitude as dayside ionospheric plasma with imbedded, weak magnetic field flows toward the antisolar region. The magnetic field intensifies as the plasma density within a tube decreases to maintain pressure balance. The suprathermal electron energy flux

entering the atmosphere within the hole system is estimated at $2.4 \times 10^{-2} \text{ erg cm}^{-2} \text{ s}^{-1}$ and will produce an ionospheric layer with peak density of the order of $1 \times 10^4 \text{ cm}^{-3}$ at an altitude of approximately 145 km. The layer, composed almost entirely of molecular ions, will decrease in density rapidly with altitude, a property exhibited by holes.

1. Introduction

An unusual ionospheric phenomenon observed in the Venus nightside ionosphere has been termed a "hole." A hole is a region in which the electron concentration is strongly depleted and the magnetic field is increased in strength and is approximately radial in direction (Brace et al., 1982, Luhmann et al., 1982). The purpose of this paper is to present suprathermal electron properties measured in a hole by the Pioneer-Venus retarding potential analyzer (RPA), properties not previously published, and to use this new information to limit the range of proposed mechanisms of hole formation.

Grebowsky and Curtis (1981) suggested that holes may be a manifestation of parallel electric fields similar to those observed in the terrestrial auroral ionosphere. More recently, Grebowski et al. (1983) have developed a simple two-dimensional model in which holes develop as plasma, transported from the dayside ionosphere, is lost into the lower ionosphere through normal chemical processes. The magnetic field within the tube concurrently intensifies to maintain pressure balance. Elements of this process were previously suggested by Knudsen et al. (1981, 1982) and Brace et al. (1982).

We present measurements of suprathermal electron properties along two periapsis passes of the Pioneer-Venus spacecraft through the antisolar region of Venus. The spacecraft passed through an ionospheric hole on the one pass and did not encounter a hole on the second. The suprathermal electron properties measured through the hole region do not indicate the presence of a parallel electric field and are typical of properties measured through non-hole regions. We infer from the results of this study and previous studies that ionospheric holes can be formed by processes other than parallel electric fields and that it is unlikely that significant parallel electric fields play a role in forming ionospheric holes.

2. Method of Measurement

The suprathermal electron quantities which we report herein were measured by the Pioneer-Venus retarding potential analyzer while operating in its suprathermal electron mode (Knudsen et al., 1979, 1980). In this mode the instrument records the integral electron current as the retarding potential sweeps from 0 to -50 V. The instrument measures the background current at -58V. Since

the vehicle potential V_{sc} is typically of the order of -1.5 V negative relative to the plasma when the spacecraft is within the ionosphere and in the umbra, the background current is measured at an effective retarding potential of approximately -60 volts. We have shown in a recent study that the electron current-voltage (i - V) curves may be approximated quite accurately by assuming the electron gas to be composed of two Maxwellian components with concentrations N_1 and N_2 and temperatures T_1 and T_2 (Knudsen et al., 1984). N_1 and T_1 approximate the thermal electron density and temperature, respectively. N_2 and T_2 are the density and temperature of a suprathermal electron component and typically have values equal to 3 cm^{-3} and 14 eV , respectively (Knudsen et al., 1984; Gringauz et al., 1979). The suprathermal electron distribution has an energetic tail which may be represented by a third Maxwellian distribution with a typical density N_3 of $\sim 0.1 \text{ cm}^{-3}$ and a temperature of 100 eV (Gringauz et al., 1979; Knudsen et al., 1984). This more energetic component is primarily responsible for the background integral current per unit area i_{58} measured with a retarding potential of -58 V . We shall indicate the variation of N_3 by presenting the variation of i_{58} normalized by π and e , the

electronic charge. $i_{58}/(\pi e)$ is an approximation of the integral electron flux per steradian above 60 eV energy. The exact expression is $(i_{58} - V di/dV)/(\pi e)$. Both terms in the expression are comparable in magnitude.

A more detailed discussion of the least-squares method we use in deriving the parameters N_1 , N_2 , T_1 , T_2 and N_3 from an RPA i-V curve and an example of an i-V curve with least-squares fit has been published previously (Knudsen, et al., 1984). We summarize here some of the uncertainties discussed in more detail in the previous paper. The RPA electrometer root-mean-square current noise is 6×10^{-13} A and yields an uncertainty in the quantity $i_{58}/(\pi e)$ of approximately $1 \times 10^6 \text{ cm}^{-2} \text{ s}^{-1}$. We have estimated that the uncertainty in N_2 and T_2 caused by random noise in the RPA is approximately 25% for the median values of these quantities, $N_2 = 3 \text{ cm}^{-3}$ and $T_2 = 14 \text{ eV}$, observed in the Venus umbra. The uncertainty is estimated to increase to 100% for N_2 equal to or less than approximately 0.5 cm^{-3} .

The vehicle potential within the holes and in other regions where the thermal plasma ($T \sim 1 \text{ eV}$) density is very small ($\leq 10^2 \text{ cm}^{-3}$) is unknown. It may become of the order of $-T_2/e$ where

T_2 is expressed in eV. If the vehicle potential does become this negative in these regions, the value of N_2 derived with the assumption that it is a uniform -1.5 volts will be too small by a factor of $\exp(-T_2/1.5 \text{ eV})$ where T_2 is in eV.

An occasional $N_2 - T_2$ pair may exceed the 25% uncertainty estimated above because the $i - V$ curve from which it is derived by least-squares fitting has one or more erroneous current values caused by telemetry dropout or an electrometer switching transient. These bad current values can be recognized by inspection but the data reduction software is not sufficiently sophisticated to recognize all of them.

3. Experimental Observations

Orbit with Hole

In Figure 1, we have plotted the thermal electron concentration measured by the P-V Langmuir probe N_e (Krehbiel et al., 1980), the supra-thermal electron concentration N_2 with temperature T_2 and the integral current i_{58} . In Figure 2, the total magnetic field $|B|$ and the components B_x , B_y , and B_z measured by the P-V magnetometer (Russell et al., 1980) are presented for the same time period. The coordinate system is centered in Venus with the z axis perpendicular

to the earth's ecliptic plane and directed northward. The sun is contained in the x-z plane with positive x toward the sun. At approximately 1:39 UT, the thermal electron density N_e is strongly depleted relative to the surrounding plasma density, and the magnetic field is enhanced and is primarily in the $+B_x$ direction (toward the sun). These two signatures are those characterizing an ionospheric hole. We observe that $i_{58}/(\pi e)$ does not reflect any significant enhancement as the spacecraft passes through the hole region. N_2 is somewhat depressed relative to the surrounding values. This decrease within the hole may be only apparent because, as explained above, the spacecraft potential may be more negative within the hole than in the surrounding ionospheric region. Two values of T_2 appear somewhat enhanced - 20 eV instead of the typical 14 eV - on the walls of hole region and have correspondingly small values of N_2 . $i_{58}/(\pi e)$ reveals no increase in flux above 60 eV energy. At the present level of our investigation, we are unable to attach any significance to the occurrence of these two values. The least-squares analysis software yielded a standard deviation of 4 eV for the two larger tempera-

tures and 1 eV for the remainder which indicates the two i-V curves were somewhat noisier than the remainder. We interpret these measurements of i_{58} , N_2 , and T_2 as indicating no significant enhancement of electron flux or energization of electrons within the ionospheric hole region.

In Figure 3 we have expanded the time interval near UT 1:39 and plotted the cosine of the average pitch angle θ between the RPA normal (positive in the outward direction) and \bar{B} . The direction of \bar{B} has been calculated only at UT 1:38:30 and is assumed to be approximately constant over the interval 1:37 to 1:40 UT. We have plotted the thermal electron density N_1 measured by the RPA instead of N_e measured by the Langmuir probe because of the exact time coincidence of the N_1 , N_2 , T_2 , and $\cos(\theta)$ values of the RPA. N_1 is calculated with the assumption that the vehicle potential is a constant -1.5 V relative to the plasma potential. N_1 differs in value from N_e because it has not been corrected for the factor $\exp(-eV_{sc}/kT_1)$, but it serves to locate the strong thermal depletion region. The objective of Figure 3 is to reveal any pitch angle anisotropy of the electron flux that may be detectable because of the changing orientation of the RPA with spacecraft spin. Although the P-V RPA is a

planar instrument, its "effective" acceptance solid angle is approximately π steradians, a cone with half-angle of approximately 60° . The RPA normal describes a cone with half-angle of 25° and with axis of the cone directed toward the south ecliptic pole as the spacecraft rotates. Since \bar{B} is approximately parallel to the earth ecliptic plane during the time interval of interest, the RPA primarily samples the electron flux with pitch angles nearer to 90° than to 0° and 180° . The RPA is programmed to record an i-V curve at four celestial longitudes separated by approximately 90° . This cyclical sampling pattern is reflected in the $\cos(\theta)$ curve of Figure 3 with the exception that the instrument did not record (or transmit) the i-V curve at approximately 1:37:15 UT, the time at which $\cos(\theta)$ would have been negative.

The cyclical variation of $i_{58}/(\pi e)$ between 1:37:30 and 1:40:30 UT suggests that some electron flux anisotropy exists in the flux with energy greater than 58 eV. When $\cos(\theta)$ is negative, $i_{58}/(\pi e)$ exhibits a maxima, and when $\cos(\theta)$ is most positive, $i_{58}/(\pi e)$ exhibits a minima. Although the uncertainty in $i_{58}/(\pi e)$ resulting from the electrometer noise level is

comparable in amplitude to the cyclical variation, we believe the cyclical variation to be indicative of a somewhat greater electron flux with energy above 58 eV traveling down the magnetic flux tube toward the atmosphere than that traveling up the flux tube.

There is no clear indication in N_1 or N_2 of flux anisotropy in these lower energy electrons. T_1 is approximately 1 eV within the hole region. These variables show little variation through the hole region except for the two larger values of T_2 and the corresponding small values of N_2 at approximately 1:38 and 1:30 UT.

Orbit without Hole

In Figure 4 we illustrate the thermal electron density from the Langmuir probe and suprathermal electron properties from the RPA for orbit 1197. Figure 5 illustrates the magnetic field for the orbit. The thermal electron density in orbit 1197 is more irregular and depressed below that of orbit 1203 and is essentially absent from UT 1:38 to 1:43. This latter region is not interpreted as an ionospheric hole because the field is not enhanced over the general level of the field elsewhere and is not restricted to being largely in the radial (B_x) direction. We interpret the magnetic field behavior as that of

the interplanetary magnetic field draped over the front of Venus and extending into the magnetic wake with the field in opposite directions on either side of a neutral sheet. The general level of the background electron current measured at -58 V retarding potential is similar to that of orbit 1203. Also, $i_{58}/(\pi e)$ does not exhibit any unusual behavior in the UT interval, 1:38 to 1:43, in which N_e is strongly depleted. The suprathermal electron temperature T_2 exhibits some large values (~ 50 eV) in regions where N_2 is of the order of 1 cm^{-3} . These may be noise values resulting from the least squares fitting process. The background flux $i_{58}/(\pi e)$ does not reflect any unusual corresponding variation.

We have estimated the total energy flux deposited in the atmosphere by the N_2 and N_3 Maxwellian populations by assuming that the flux is isotropic. The energy flux passing through unit area from one side in one second for a Maxwellian distribution is

$$1) \text{ Energy flux} = (2/(\pi m))^{1/2} N (kT)^{3/2}$$

where the symbols have their usual meaning. Using the measured values of N_1 , T_1 , N_2 , T_2 , the largest energy flux we computed for the UT time interval 1:37:30 to 1:39:40 is $2.4 \times 10^{-2} \text{ erg cm}^{-2}$

sec^{-1} . The largest energy flux in the depressed N_e interval of orbit 1197 is $3.4 \times 10^{-2} \text{ erg cm}^{-2} \text{ sec}^{-1}$.

4. Discussion and Conclusions

We interpret the experimental observations presented in Figures 1-5 as evidence that an energetic process such as a significant parallel electric field formed along the radial magnetic field of an ionospheric hole is not responsible for the hole formation. As the Pioneer-Venus spacecraft moved through the hole region in orbit 1203, the integral current i_{58} measured with retarding potential at -58 V reflected no increase in flux. At earth, a spacecraft equipped with a low energy electron detector, such as the soft particle spectrometer on the ISIS 2 spacecraft, shows a definite and substantial increase in total electron flux, energy flux, and mean energy of the flux as the spacecraft passes through an auroral feature (Winningham and Heikkila, 1974; Knudsen et al., 1977). A peak in the differential energy flux develops within the auroral precipitation region at an energy of a few KeV as a result of the electrons dropping through the parallel electric field formed at higher altitude. Although the P-V RPA is incap-

able of measuring the differential electron flux at energies above approximately 45 eV, it would reveal any significant increase in integral flux above 58 eV.

The differential flux below 50 eV is also increased within an auroral form as a result of the production of secondary electrons by the KeV primaries. We observe no increase in N_2 which would signal an increase in the production rate of secondary electrons.

The energy flux of the suprathermal electrons within the ionospheric hole of orbit 1203 has been estimated above at 2.4×10^{-2} erg cm⁻² sec⁻¹. This energy flux is one to two orders of magnitude less than that producing faint, diffuse aurora (IBCl) on earth (Chamberlain, 1961). It is also an order of magnitude less than the typical electron energy flux entering the Earth's cusp region (Heikkila and Winningham, 1971).

The presence of a suprathermal electron flux within hole magnetic flux tubes with magnitude typical of that observed over the nightside Venus ionosphere contributes to our understanding of an observed property of holes. When the Pioneer-Venus spacecraft passes through a hole on both the inbound and outbound legs of a single periap-

sis pass, it passes through the hole on the inbound leg at a lower altitude than the hole on the outbound leg. The plasma density is observed to be less depleted in the inbound hole, which is at lower altitude, than in the outbound hole (Luhmann et al., 1982). The explanation which has been given previously for this observation is that collisions of ions and electrons with neutrals at the lower altitudes permit diffusion of plasma into the hole region from the surrounding denser plasma. We point out here that the supra-thermal flux observed within the hole of orbit 1203 is sufficient to maintain a layer of molecular ions with peak density of the order of $1 \times 10^4 \text{ cm}^{-3}$ at an altitude of approximately 145 km (Spenner et al., 1981; Cravens et al., 1983). The O^+ density produced by the electron flux is less than approximately $1 \times 10^2 \text{ cm}^{-3}$. Hence, if we assume that the O^+ ions initially contained in a flux tube have been lost largely through downward diffusion and recombination, a plasma layer with a topside molecular ion scale height will still be maintained with near-typical peak density at an altitude of approximately 145 km by the supra-thermal electron flux.

We have argued that the suprathermal electron properties measured in one clear example of an ionospheric hole do not reflect the existence of a significant parallel electric field accelerating electrons toward Venus. We have shown that the suprathermal electron properties within the hole region and in the adjacent non-hole region are similar to suprathermal properties measured in an orbit passing through the same general antisolar region six days previously. The properties exhibited in both orbits are consistent with median properties and their variation derived in a previous study of the low altitude Venus umbra (Knudsen and Miller, 1984). The present study, the previous study, and a cursory examination of the suprathermal electron properties in several orbits around 1197 and 1203 all suggest to us that the Venus nightside ionospheric holes are not formed by parallel electric fields of any significant magnitude. We are thus led to favor a less energetic process for forming the holes.

Insufficient data are available to be very specific about the process or processes forming the holes. We do not know the two-dimensional shape of the holes - let alone the three-dimensional shape (Brace et al., 1982; Marubashi et al., 1985). Neither do we know the range of envi-

ronmental conditions under which the holes form or do not form. We do not attempt to be very specific, therefore, but one less energetic process which we suggest is involved in the formation of holes and to which several authors have contributed (Knudsen et al., 1981, 1982; Brace et al., 1982, Grebowsky et al., 1983) is as follows: As high beta plasma from the dayside ionosphere flows supersonically toward the antisolar region, a portion of the plasma is continuously lost through a downward component of flow into the low altitude chemical sink where atomic ions are converted to molecular ions which then recombine. As the plasma density decreases within a magnetic tube, the magnetic field increases to maintain pressure balance across the tube wall. A hole forms when the loss process is sufficiently rapid compared with the horizontal transport time. Slowing of the horizontal plasma flow by passage through a shock (Knudsen et al., 1980) may be essential in forming the holes in which the density is most strongly depleted (Grebowsky et al., 1983).

References

- Brace, L. H., R. F. Theis, H. G. Mayr, S. A. Curtis and J. G. Luhmann, Holes in the night-side ionosphere of Venus, J. Geophys. Res., 199-211, 1982.
- Chamberlain, J. W., Physics of Aurora and Airglow, Academic Press, N.Y., N.Y. 1961.
- Cravens, T. E., S. L. Crawford, A. F. Nagy, and T. I. Gombosi, A two-dimensional model of the ionosphere of Venus, J. Geophys. Res., 88, 5595-5606, 1983.
- Grebowsky, J. M. and S. A. Curtis, Venus nightside ionospheric holes; the signatures of parallel electric acceleration regions? Geophys. Res. Lett., 8, 1273-1276, 1981.
- Grebowsky, J. M., H. G. Mayr, S. A. Curtis, and H. A. Taylor, Jr., Venus' nighttime horizontal plasma flow, magnetic congestion, and ionospheric hole production, J. Geophys. Res., 88, 3005-3012, 1983.
- Gringauz, K. I., M. E. Verigin, T. K. Breus, and T. Gombosi, The interaction of electrons in the optical umbra of Venus with the planetary atmosphere - the origin of the nighttime ionosphere, J. Geophys. Res., 84, 2123-2127, 1979.

- Heikkila, W. J. and J. D. Winningham, Penetration of magnetosheath plasma to low altitudes through the dayside magnetospheric cusps, J. Geophys. Res., 76, 883-892, 1971.
- Knudsen, W. C., P. M. Banks, J. D. Winningham, and D. M. Klumpp, Numerical model of the convecting F^2 ionosphere at high latitudes, J. Geophys. Res., 82, 4784-4792, 1977.
- Knudsen, W. C., J. C. Bakke, K. Spenner, and V. Novak, Retarding potential analyzer for the Pioneer-Venus orbiter mission, Space Sci. Instru., 4 351-372, 1979.
- Knudsen, W. C., K. Spenner, J. Bakke, and V. Novak, Pioneer-Venus orbiter planar retarding potential analyzer plasma experiment, IEEE Trans. Geosci. Remote Sensing, GE-18, 54-59, 1980.
- Knudsen, W. C., K. Spenner, and K. L. Miller, Anti-solar acceleration of ionospheric plasma across the Venus terminator, Geophys. Res. Lett., 8, 241-244, 1981.
- Knudsen, William C., Peter M. Banks, and K. L. Miller, A new concept of plasma motion and magnetic field for Venus, Geophys. Res. Lett., 9, 765-768, 1982.

- Knudsen, William C. and Kent L. Miller, Pioneer-Venus suprathermal electron flux measurements in the Venus umbra, J. Geophys. Res., accepted for publication, 1984.
- Krehbiel, J. P., L. H. Brace, R. F. Theis, J. R. Cutler, W. H. Pinkus, and R. B. Kaplan, Pioneer-Venus orbiter electron temperature probe, IEEE, Trans. Geosci. Remote Sensing, GE-18, 49-53, 1980.
- Luhmann, J. G., C. T. Russell, L. H. Brace, H. A. Taylor, W. C. Knudsen, F. L. Scarf, P. S. Colburn, and A. Barnes, Pioneer Venus observations of plasma and field structure in the near wake of Venus, J. Geophys. Res., 87, 9205-9210, 1982.
- Luhmann, J. G. and C. T., Russell, Magnetic fields in the ionospheric holes of Venus: evidence for an intrinsic field? Geophys. Res. Lett., 10, 409-411, 1983.
- Marubashi, K., J. M. Grebowsky, H. A. Taylor, Jr., J. G. Luhmann, C. T. Russell, and A. Barnes, Magnetic field in the wake of Venus and the formation of ionospheric holes, J. Geophys. Res., 90, 1385-1398, 1985.

- Russell, C. T., R. C. Snare, J. D. Means, and R. C. Elphic, Pioneer-Venus orbiter fluxgate magnetometer, IEEE Trans. Geosci. Remote Sensing, GE-18, 32-35, 1980.
- Spenser, K. W. C. Knudsen, R. C. Whitten, P. F. Michelson, K. L. Miller, and V. Novak, On the maintenance of the Venus nightside ionosphere: electron precipitation and plasma transport, J. Geophys. Res., 86, 9170-9178, 1981.
- Winningham, J. D. and W. J. Heikkila, Polar cap auroral electron fluxes observed with ISIS 1, J. Geophys. Res., 79, 949-957, 1974.

Figure Captions

- Figure 1. Thermal and suprathermal electron properties measured as the P-V spacecraft passed through an ionospheric hole on the nightside of Venus. N_e is the thermal electron density and N_2 and T_2 the suprathermal electron density and temperature, respectively. i_{58} is the integral current measured by the P-V RPA with retarding potential at -58 V.
- Figure 2. Magnetic field measured along the same orbit segment as that in Figure 1. The z coordinate axis points toward the North ecliptic pole and the x-z plane contains the Venus sun vector with positive x toward the sun.
- Figure 3. Thermal and suprathermal electron properties measured in the immediate vicinity of the ionospheric hole of orbit 1203. N_1 is an approximate thermal electron density measured by the P-V ORPA; θ is the angle between the RPA outward pointing axis and the magnetic field vector. The integral current i_{58} variation suggests the electron flux with energy above 58 eV may be anisotropic with the greater flux directed toward the Venus atmosphere.
- Figure 4. Thermal and suprathermal electron properties measured as the P-V spacecraft passed through a region of the nightside ionosphere not exhibiting an ionospheric hole.
- Figure 5. Magnetic field measured along the same orbit segment as that in Figure 4.

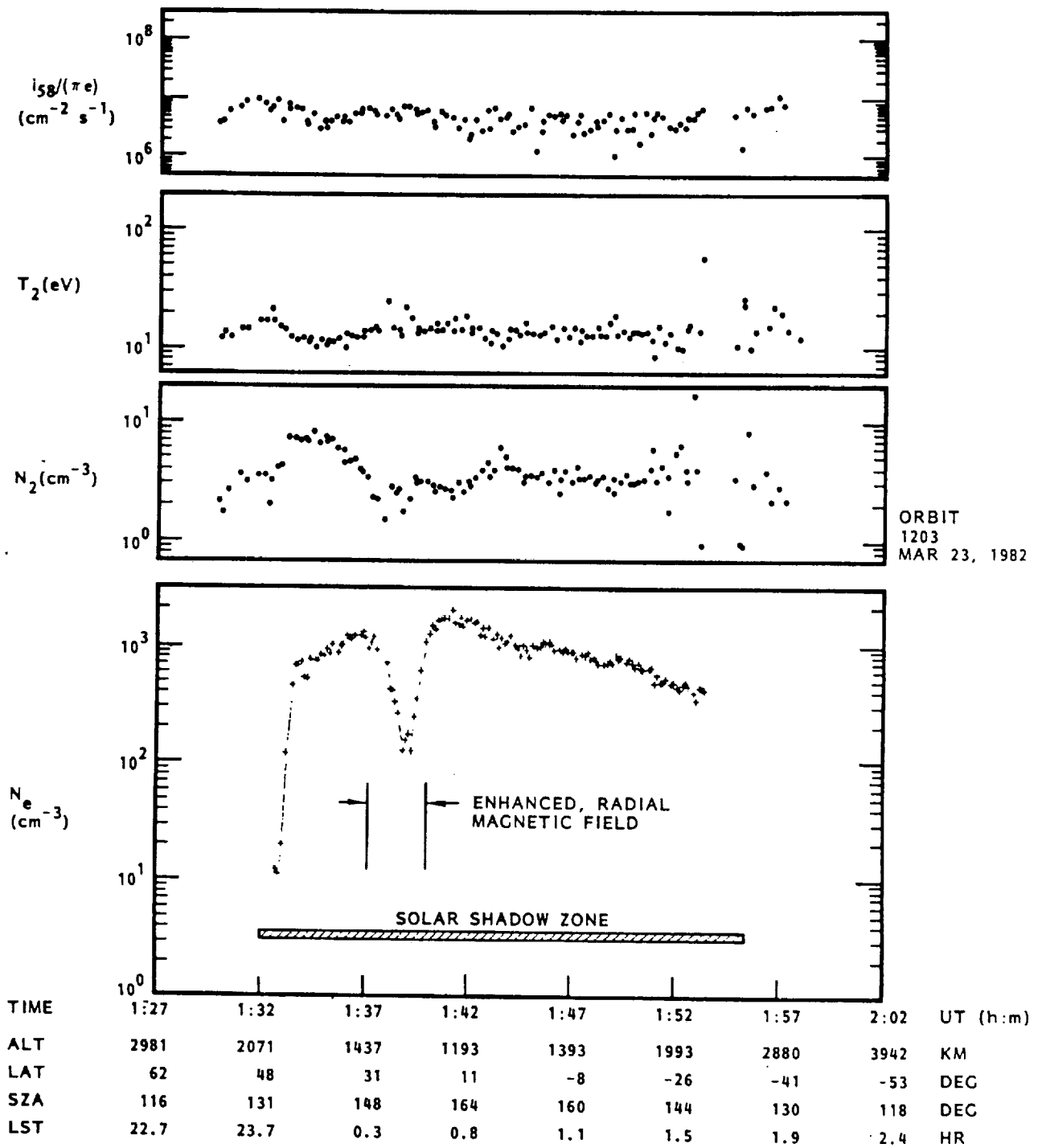


Figure 1

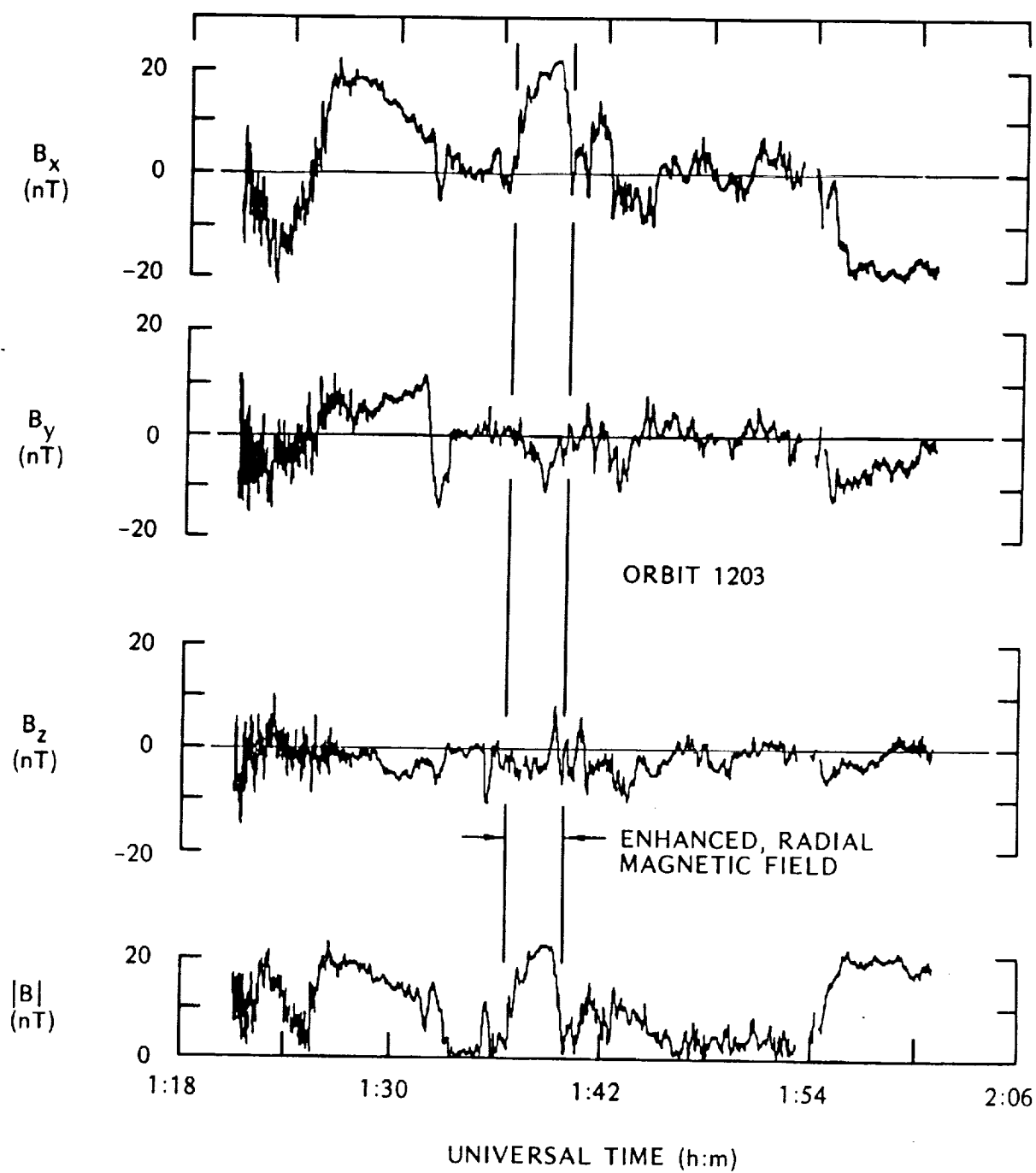


Figure 2

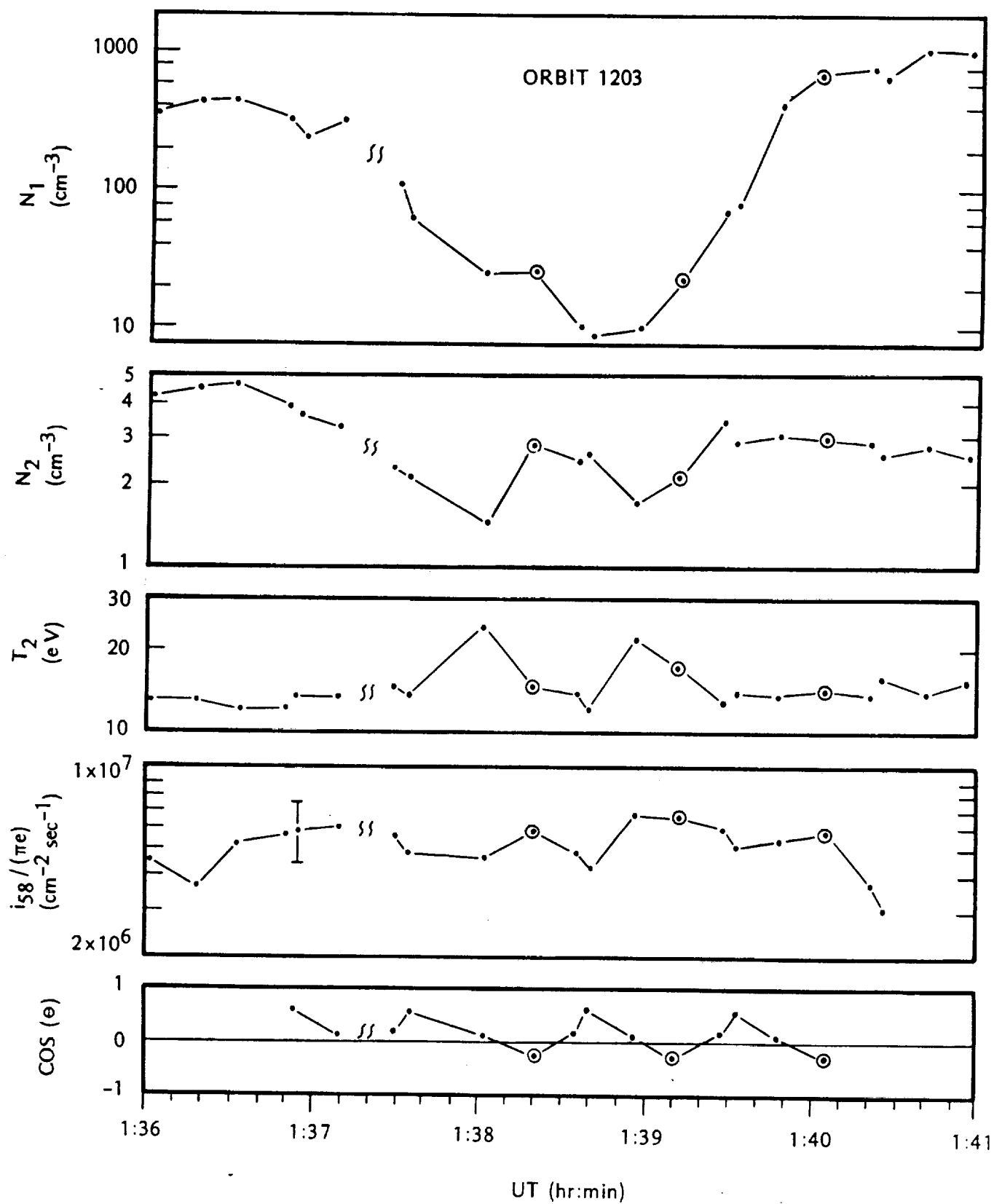


Figure 3

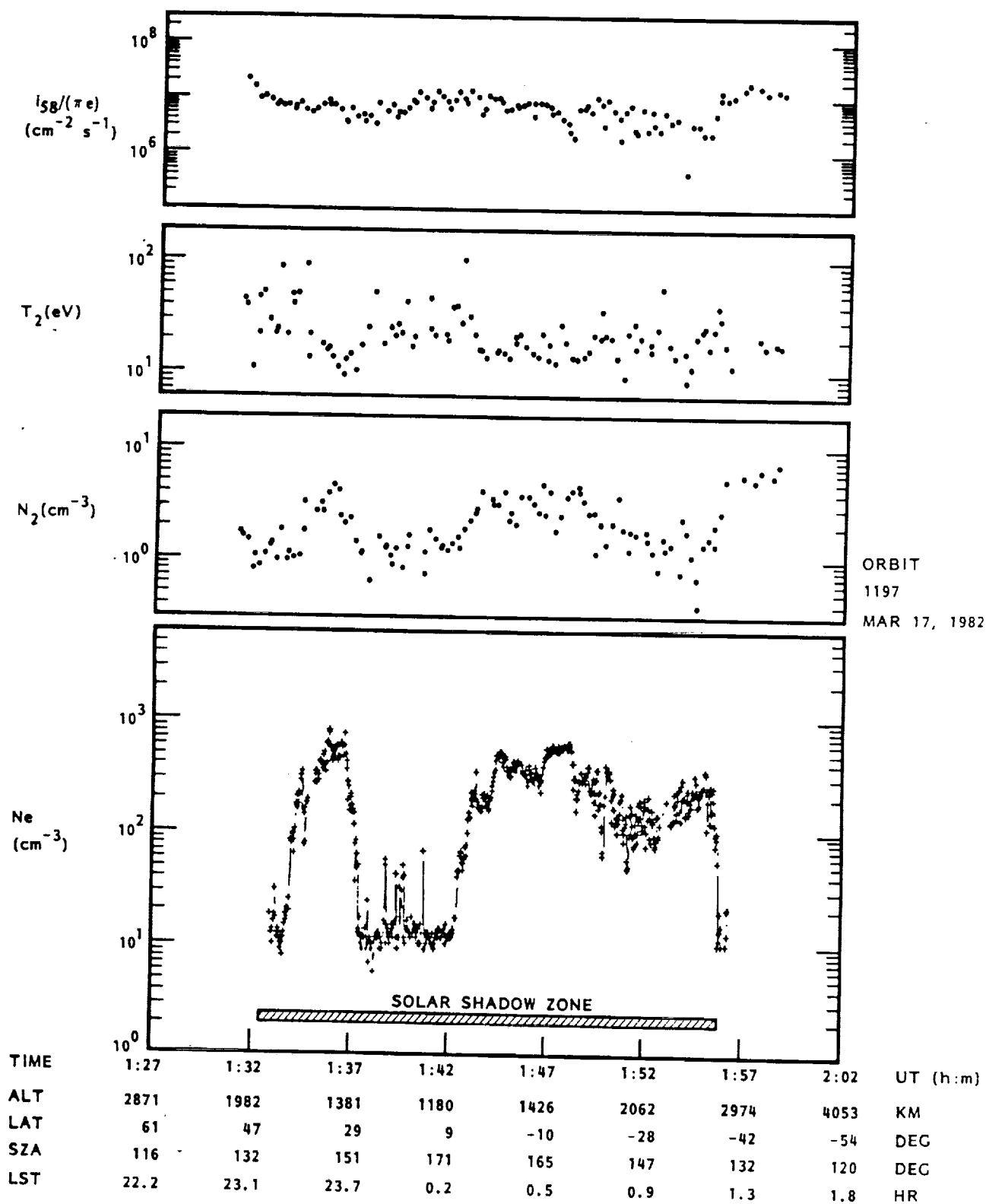


Figure 4

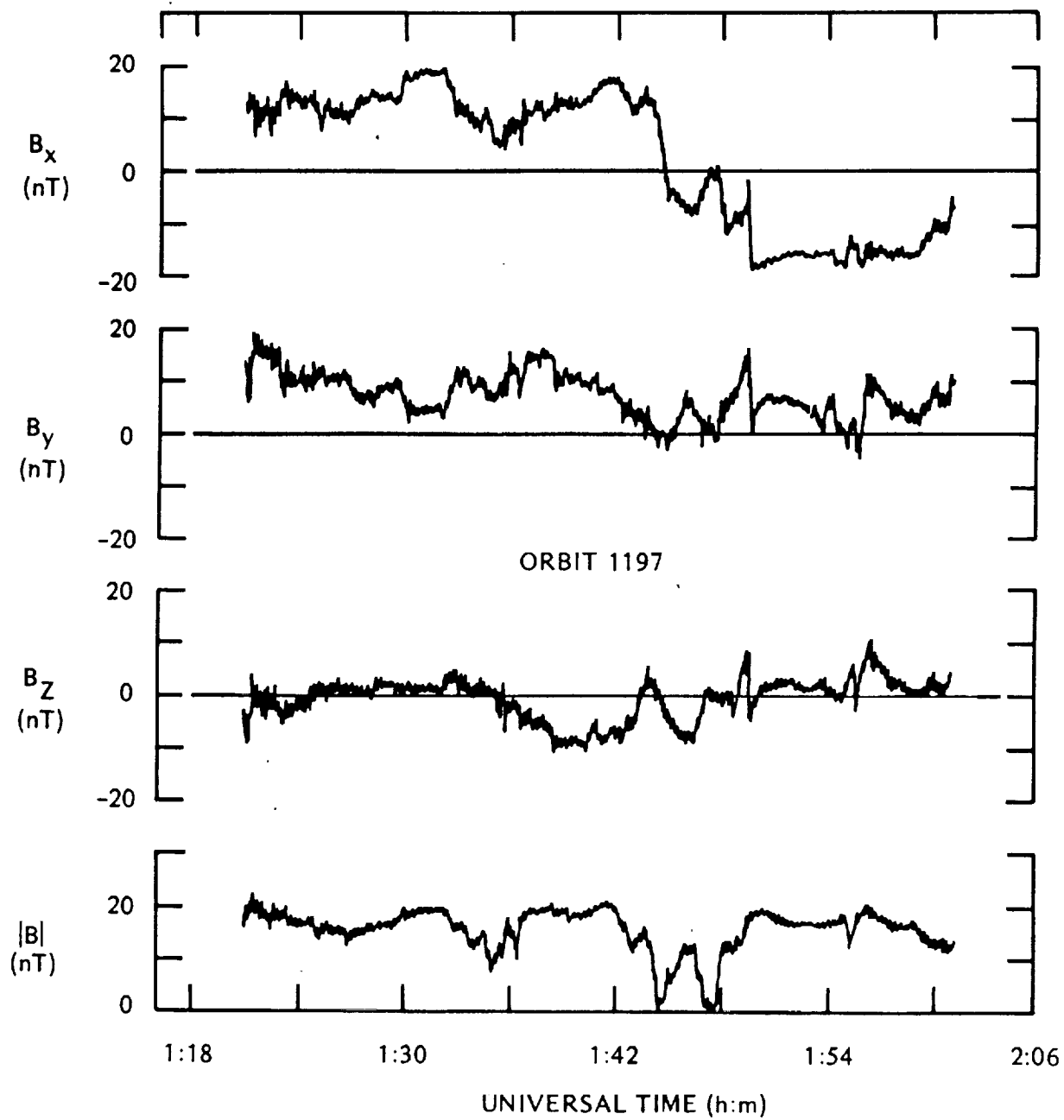


Figure 5

APPENDIX C
NSSDC DATA SUBMISSION

Reply to Attn of: **SSP:244-8**

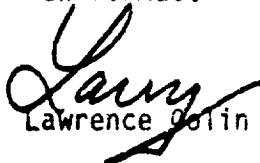
September 7, 1983

TO: Distribution

FROM: Lawrence Colin, Pioneer Venus Project Scientist

SUBJECT: Instructions for Data Submissions to the National Space Science Data Center

Enclosed is a report which defines a new format for submitting your Pioneer Venus data to the National Space Science Data Center. This format should be useful to Data Center users, as well as make it easier for us to fulfill our requirements to archive Pioneer Venus data. Note the deadlines of October 1, 1983 for completing the data sets for orbits 1 to 1000, and November 1, 1983 for replacing the data currently on file at the Data Center with data in the new format.


Lawrence Colin

Enclosure

cc: (w/enc)
NASA Headquarters
EL-4/H. Brinton
EL-4/G. Strobel

GSFC
W. Cameron/601

PIONEER VENUS MISSION

INSTRUCTIONS FOR DATA SUBMISSIONS TO THE
NATIONAL SPACE SCIENCE DATA CENTER

A COMMITTEE REPORT

ROGER A. CRAIG
NASA AMES RESEARCH CENTER
August 11, 1983

I. BACKGROUND

The Unified Abstract Data System, UADS, was developed as a computer based, interactive system to provide Pioneer Venus Orbiter (PVO) experimenters quick and convenient access to data being acquired by the mission. Data were entered into a central facility by each experimenter through local terminals; the UADS software then sorted and cross-filed the data by orbit numbers. Each experimenter could then access any information from the central facility through his local terminal. The UADS proved invaluable in providing quick access to cross-compare results between experiments, especially in the early phases of the mission when rapid feed-back to Mission Control was critical.

The UADS further produced data files on magnetic tape, suitable for archival purposes with the National Space Science Data Center, NSSDC. The files so produced contained Low Frequency Data (LFD), Special Event Data (SED), and Composite Data (CD). Both the SED and CD record formats were defined and controlled by each experimenter. The LFD combined experimental results and orbital information in an unchanging, predefined format. The experimenters were responsible for entering data peculiar to their instrument, while the Pioneer Mission Office (PMO) supplied orbital parameters and experiment pointing information through a subset of the Supplementary Experimenter Data Record (SEDR).

The software for the UADS was developed, under contract, for this purpose by Bendix Corporation and the computing resources of Tymshare Corporation were purchased to serve as the central facility.

As the mission progressed, the need for rapid access to data, cross-referenced by orbit, decreased, and under the pressing need to reduce costs a decision was made by the PMO to terminate the contract with Tymshare Corporation as of January 1981. Without support from Tymshare Corporation the UADS would not be available for preparing NSSDC submissions, so the PMO agreed to develop a substitute system to provide archival data records.

II. PIONEER VENUS ARCHIVAL DATA AT THE NSSDC

In conformance with NASA policy, Pioneer Venus data are archived at the NSSDC, whose charter it is to acquire, store and disseminate space science data for further analysis beyond that provided by the principal investigators.

Pioneer Venus data have been archived with the NSSDC in the format produced by the software of the UADS. Various plans have been suggested to implement the continued submission to the archives now that the UADS has been terminated. Several plans were submitted for consideration to the May 6, 1983 meeting of the OMOP Committee. These were, in brief,

1. The experimenters send their data to the PMO, who periodically contract with a time sharing vendor to run, as a batch job, the archival feature of the UADS. The primary advantage of this would be to produce archival data in the same format as that already at the NSSDC with very little reconfiguration of any existing system. An important drawback is an estimated very high cost (about \$30K for each six months of data processing).

2. The experimenters send their data to the PMO who will arrange to use an existing NASA Ames IBM 4341 computer to run a modified version of the archival feature of the UADS. The primary advantage of this approach would be that it will be relatively inexpensive to use.

Both plans (1) and (2) retain the tape formats used by the UADS. As is discussed below, this was argued to be an important drawback. On the basis of this a third plan was suggested, which is as follows:

3. The experimenters individually send their data directly to the NSSDC. Each experimenter would need to create a self-contained submission which would include experiment data, orbital parameters and experiment pointing information. This concept would result in NSSDC archives organized by experiment rather than by orbit. An advantage of this is that the PMO will no longer need to pay for the elaborate and expensive UADS. Further, data requests to the NSSDC are usually made for a single instrument; this approach would eliminate the need for a requestor to strip out the data of interest from records of all instruments.

This concept would also allow data to be provided to the NSSDC in a tape format which is more convenient to use than that provided by the UADS. The LFD file is recorded on tape both in 32-bit binary format and in IBM 360 floating point format; formats which may present conversion problems for a user employing a small system. Such a user, especially in a remote location, would have great difficulty reading such a tape, or be forced to develop conversion software.

III. COMMITTEE RECOMMENDATIONS

A committee was appointed to consider and recommend a procedure to implement the continued submissions of PVO data to the NSSDC. The committee consisted of:

Peter Ford,	MIT
Larry Brace,	GSFC
Robert Theis,	GSFC
Winifred Cameron	NSSDC
Pat Barclay,	Bendix Corporation
and Roger Craig	ARC, PMO

The committee discussed the above and agreed that the production of archival files which are easily accessible and usable to a variety of users was of high priority. It was agreed that to achieve this it is required that files be generated in a style more consistent with the usual NSSDC submissions, namely organized by instrument rather than by orbit. It was further agreed that in order to broaden the potential user base the UADS format (32-bit binary and IBM 360 floating point) be replaced with a more generally used format.

The results of committee discussions of the above are guidelines for submitting PVO data for the NSSDC. The guidelines are designed to:

1. standardize and improve the data formats for each experiment so that the tapes can be easily read by a requestor.
2. store the data by experiment,
3. provide for orderly updating of data,
4. provide for ultimate replacement of existing UADS generated archival tapes.

A new format was designed which is to be used by each experimenter for PVO NSSDC data experimenter, and can be easily read by computers expected to be accessible to a requester. One major difference between this and the existing LFD format is the use of text (ASCII) data formats, eliminating both binary and IBM floating point formats.

The proposed new submission format is self-defining in the sense that the first three records on each tape define the data parameters, value representations, and missing data (file) indicators. The first tape record defines the order in which the variables appear in the subsequent data records, in a manner similar to that used for SEDR trajectory data (SEDR file 5). The second tape record will contain a FORTRAN-compatible format list describing the field sizes and representations of each data value in the order defined in record 1. This format may be used to decode all subsequent records on the tape.

The third tape record will define a unique value associated with filler (missing) data for all variable fields. It is formatted according to the format used in record 2, and is immediately followed by the start of actual data records (records 4 and beyond).

The following is the proposed new format, with examples as applied to OETP instructions.

PROPOSED PIONEER VENUS NSSDC LOW-FREQUENCY DATA FORMAT

This document describes a suggested format to be used by all investigators for the submission of their data to the National Space Sciences Data Center. The overall specification will require that all data be coded into ASCII, and written onto standard 1/2 inch 1600-bpi 9-track tapes. The logical record length will be fixed for a given tape, as well as the physical blocksize. Blocksizes should be large enough to avoid wasting tape, but should not exceed 8000 bytes in order to avoid making excessive demands on user programs for memory. The first three records of any of these tapes will be formatted as follows:

Record 1: The format to be used is (13,n(1X,A4)) where "n" is the number of data items in each record.

*	4	ELTE	ELNE	MI	VS				(for OETP)
	7	ETEM	SPOT	TONE	TTWO	XVEL	YVEL	ZVEL	(for ORPA)
	↑	↑	↑	↑	↑	↑	↑	↑	
	3	5	10	15	20	25	30	35	

Example 1: The first record in each tape file. Note that new value types with new 4-character designations can be added as necessary. The date, time, orbit and time-tag items are not included in the list, because they are common to all data records.

* number of data items "n"

Record 2: This record contains the format in which all succeeding records are written. The first 4 format items specify the date, time, orbit, and time-tag, and will appear in the same format on all tapes.

(18,19,15,16,4F9.2)	(Appropriate for OETP)
↑	
1	

Example 2: The second record in each tape file

Record 3: This record will contain zeroes for the first four fields (date, time, orbit, and time-tag), and in addition will have a fill value in each data value location. This value will be used by any program reading the data to identify fill data in subsequent input records.

0	0	0	09999999.999999999.99999999.99999999.99
↑	↑	↑	↑
8	17	22	28
			37
			46
			55
			64

Example 3: The third record in each tape file. (Appropriate for OETP).

Record 4 to : These records contain the date, time, orbit, and time-tag for each time which has any non-fill data.

1981207	43527786	879	-1788	2345.67	78543.89999999.99	16.20
↑	↑	↑	↑	↑	↑	↑
8	17	22	28	37	46	55
						64

Example 4: All records after the third in a tape file. (Appropriate for OETP).

As can be inferred from the above example, the date is coded as YEAR, DAY OF YEAR (1-366) with 19 included in the year. The time is in milliseconds of the day, orbit number is self-explanatory, and the time tag is the usual value ranging of the day from -1800 to 1800 in increments of 12.

The project-provided tape of SEDR information would be the source of the official dates and times to be used by all other investigators.

Nothing in the above format would preclude investigators from producing a tape containing the data from more than one experiment.

The external label on the tape should be type-written, and contain the following information:

- o Full name of experiment data contained on tape.¹
- o Start date, time, and orbit number of data on the tape.
- o Stop date, time, and orbit number of data on the tape.
- o Production date of the tape.
- o The density (1600-bpi) and number of tracks (9) at which the tape was recorded.
- o An estimate of the amount of tape used.
- o The physical blocksize used in writing the tape.
- o A name and phone number of the individual responsible for the tape.

¹ Example: "Pioneer Venus Orbiter Electron Temperature Probe".

Each Experimenter will be responsible to modify his software accordingly and when appropriate, submit data tapes to the NSSDC. As data are updated, new tapes should be sent directly to the NSSDC with instructions as to which tapes it replaces, or appends.

Documentation is important in these submissions. All submissions must conform to the NSSDC instructions "Guidelines for Submitting Data to the National Space Science Data Center." These instructions delineate the kinds of documentation which must accompany shipments.

IV TIMETABLE

1. Submissions should be made to the NSSDC for each experiment by October 1, 1983 to complete the data set for orbits 1 to 1000.

2. Submissions should be made to the NSSDC for each experiment by November 1, 1983 to replace all data currently on file in the UADS format. As replacements are received, the NSSDC will destroy the data in the UADS format.

PIONEER VENUS
ORBITER RETARDING POTENTIAL ANALYZER
NSSDC SUBMISSION DOCUMENTATION

WILLIAM C. KNUDSEN

Knudsen Geophysical Research, Inc.
18475 Twin Creeks Rd.
Monte Sereno, CA 95030
Telephone: 408-354-2923

Nov. 4, 1993

INTRODUCTION

This document describes the Pioneer Venus (PV) Retarding Potential Analyzer (RPA) National Space Science Data Center (NSSDC) low frequency data (LFD) experimenter data record (EDR) tapes. These tapes contain one file for each orbit for which data are available. Each file consists of three information records followed by n data records. The value of n is variable for each orbit (file), but does not exceed 721. Each data record consists of four quantities associated with a time tag followed by 25 physical quantities unique to the RPA. The formats for the three information records and the data records are described in the attached report "INSTRUCTIONS FOR DATA SUBMISSIONS TO THE NATIONAL SPACE SCIENCE DATA CENTER, A COMMITTEE REPORT" by Roger A. Craig and dated August 11, 1983. Ephemeris data for the time tags in each record is contained on a supplementary experimenter data record (SEDR) tape supplied to NSSDC by the Pioneer Venus Project Office and will not be described in this document.

The PV RPA is described in considerable detail by Knudsen et al. [1979,1980]. The principles of measurement are also described therein together with some of the factors affecting the accuracy of the derived quantities. Additional information on the theory of measurement by an RPA is presented by Knudsen [1966].

We describe in this documentation the list of 25 quantities provided in the RPA EDR tapes and their limitations appropriate to the submission beginning Nov. 4, 1993.

The PV NSSDC LFD SEDR tapes have time tags at 12 second intervals from 30 minutes prior to periapsis to 30 minutes after periapsis. These time tags are the tags specified in the first four quantities of each of the EDR data records. All PV instruments are to report their data at these common time tags for the purpose of easy inter comparison of data. Principal Investigators (PIs) with instruments with a sampling period much less than 12 seconds are to report the average of measured quantities over a 12 second interval centered on the time tags. The RPA, because of a low telemetry word assignment, records at most one current-voltage (I-V) characteristic curve per spacecraft spin period. Except for one set of 14 orbits, the spin period of the PV spacecraft has been about 12 seconds. Thus, RPA physical quantities are derived at intervals of 12 seconds or more. Since the RPA operates in several modes, a particular quantity such as thermal electron temperature may be typically measured at much longer intervals. The thermal electron temperature is typically measured at either approximately 48 or 60 second intervals. In a few orbits, it was measured at 12 second intervals.

Since the RPA measures its quantities at time intervals of 12 seconds or greater, averaging RPA quantities is meaningless. Consequently, RPA quantities are reported in the EDR data records as derived. The derived value is, for the most part, reported in that data record whose time tag is within plus or minus 6 second of the actual time of measurement. (An individual RPA I-V curve is measured in a time interval of approximately 0.2 seconds. The average time interval between measurement of successive I-V curves is approximately 12 seconds.) The actual time at which the quantity was recorded is given in the record immediately following the four quantities specifying the time tag. Thus, an investigator can use his own scheme of averaging to assign a value to time tags or may plot or otherwise use the quantities at their times of actual recording. When no RPA quantity is available for recording at a specified time tag, no data record for that time tag is written on the NSSDC EDR tape.

RPA quantities may be unavailable for assigning to a specific time tag for several reasons as follows: The spacecraft data format in use at the time may not have contained any words for the RPA. The RPA may have been turned off for power conservation reasons. The spacecraft telemetry bit rate and/or data format may have been such that an RPA I-V curve was recorded only at long time intervals.

RPA MEASURED QUANTITIES

The PV RPA is described together with some of the principles of measurement in some detail by Knudsen et al. [1979,1980]. Many of the factors affecting accuracy are also described therein. We present in this section the quantities recorded on the NSSDC EDR data files following the four time tag quantities, their nominal uncertainty and measurement noise level, and additional limitations of the quantities.

Table 1 lists the symbol, quantity, measurement range with units in which the quantities are quoted, noise level of measurement, and uncertainty of the measurement for the quantities reported by the RPA.

UT: UT is the universal time in milliseconds assigned to the physical quantities recorded in this record. UT will typically, but not always, lie within plus or minus 6 seconds of the time of day assigned to the time tag of this record. UT should be accurate to within plus or minus 0.1 second.

TOTI: TOTI is the total ion density of the plasma in cm^{-3} and is derived from the FORTRAN expression

$$\text{TOTI} = \text{FII} / (\text{VN} * e * \text{Area})$$

where FII is the first ion current measured with zero retarding potential, VN is the component of the ion bulk velocity relative to a coordinate system fixed in the spacecraft and parallel to the RPA axis, e is the electronic charge, and AREA is the effective area of the RPA collector. When a 1st-squares analysis is not possible, VN is assumed to be the component of the spacecraft velocity in ecliptic coordinates parallel to the RPA axis.

H+: H+ is the hydrogen ion density. When the RPA is operating in one of its peaks mode, H+ will be detected and recorded only when its density is greater than approximately 10% of the sum of more massive ion densities. H+ can be the second most abundant ion and still not be recorded when the RPA is operating in its two peaks mode. The uncertainty of the H+ density also depends on its density relative to that of more massive ions. For an H+ density comparable to that of more massive ions, the accuracy should be of the order of 10%. The detection noise level for H+ is estimated at 50 cm^{-3} . Additional discussion of the RPA ion peak detection capability and limitation is given by Miller et al. [1984].

O+: O+ is the oxygen ion density. It will be detected in the presence of more massive ions only when its density is greater than approximately 10% of the sum of more massive ions. The RPA does not resolve C+, N+, or O+. We have assumed in our least-squares fitting that $([\text{C}+] + [\text{N}+])/[\text{O}+]$ is constant at 0.07, a value derived from PV ion mass spectrometer results.

O2+: O2+ is the symbol assigned to the ion with atomic mass of 32. In fitting the RPA I - V curves, it has been assumed that an ion of mass 29 is present in the plasma and has a density that is a fixed fraction of the O2+ ion density at a given altitude. The density ratio of O2+ to the ion of mass 29 varies from approximately 5% at 150 km altitude to 90% at and above 200 km.

CO2+: CO2+ is the density of the carbon dioxide ion with atomic mass of 44.

TI: TI is the ion temperature and is assumed to be the same for all ion masses. It is one of the adjustable variables in the least-squares analysis of ion sweeps.

Vx,Vy,Vz: This vector, specified in the earth ecliptic coordinate system, provides the magnitude ($\text{MAG} = \sqrt{V_x^2 + V_y^2 + V_z^2}$) of the ion bulk velocity in the direction defined by the unit vector ($V_x/\text{MAG}, V_y/\text{MAG}, V_z/\text{MAG}$), and is measured in each ion sweep for which a successful least-squares fit has been obtained. An approximate value of the vector ion bulk velocity can be obtained from three successive vectors obtained in three successive sweeps since the three unit vectors are not parallel to each other.

FII: FII is the saturation (first) current measured in an ion I-V sweep. The retarding potential is programmed to be slightly negative of plasma potential during this measurement. FII is measured relative to the ion current measured with the retarding potential equal to 37V positive [Knudsen et al., 1979].

BKGI: BKGI is the current to the RPA collector measured just before the beginning of an ion sweep with the retarding potential set at approximately +37V relative to plasma potential.

VPI: VPI is the value of the spacecraft potential relative to plasma potential during an ion sweep. The value of VPI is derived from the least-squares fit when two or more ion masses are discernable in the sweep data. Otherwise, VPI is specified with a value interpolated or extrapolated from VPTE or VPI from nearby sweeps.

TOTE: TOTE is the total electron density derived from the thermal electron mode saturation current FIE. The formula used for this present NSSDC submission, in FORTRAN language, is:

$$TOTE = 6.15E9 * MAX(0, -3.5E-9 - FIE) ** 0.847$$

We consider this measure of the total electron density to be approximate and valid only while the PV spacecraft is within the ionosphere. TOTE, TE, and VPTE are stored in the UADS file only if the value of TOTE exceeds $3E+03 \text{ cm}^{-3}$.

TE: TE is the thermal electron temperature derived using equation (1) in Knudsen et al. [1980]. When the spacecraft is positive relative to the plasma potential, a condition existing with the spacecraft in the sun and in a low density plasma, the value of TE is representative of the secondary electrons trapped in the positive spacecraft potential well.

FIE: FIE is the saturation electron current measured at the beginning of a thermal electron mode sweep. The front (retarding) grids are at a potential of +6.8 V relative to the spacecraft ground.

BKGE: BKGE is the current measured by the RPA electrometer at the beginning of the thermal electron mode. The front (retarding) grids of the RPA are held at a potential of -4.6 V during the measurement.

VPTE: VPTE is the spacecraft potential relative to the ambient plasma potential. It is derived from the thermal electron sweep data as described BY Knudsen et al. [1980]. When the spacecraft is in the solar wind and exposed to the sun, its potential is typically a few volts positive with respect to the solar wind plasma potential. VPTE loses its meaning in this situation.

N1: N1 is the density of the low temperature Maxwellian electron distribution used to fit the suprathermal electron I-V curve and is an approximation to the thermal electron density. N1 is stored in the UADS file only when the analysis program thinks the spacecraft is within the ionosphere and assumes the value of VPPE is -1.5V [Knudsen et al., 1985].

T1: T1 is the temperature of the low temperature Maxwellian electron distribution.

N2: N2 is the density of the high temperature Maxwellian electron distribution used to fit the suprathermal electron I-V curve [Knudsen et al., 1985]. It is the density of photoelectrons, primarily, when the spacecraft is within the ionosphere, and is the density of solar wind electrons, primarily, when the spacecraft is above the ionosphere. The spacecraft is assumed to be within the ionosphere when VPPE has the value, -1.5V.

T2: T2 is the temperature of the high temperature Maxwellian electron distribution.

FIP FIP is the electron current measured by the RPA when operating in the suprathermal electron mode with zero retarding potential on the retarding grid.

BKGP: BKGP is the electron current to the RPA when operating in the suprathermal electron mode with the retarding potential on the retarding grid equal to -58V.

VPPE: VPPE is the spacecraft potential relative to the ambient plasma potential when the RPA is sweeping in its suprathermal electron mode. When the spacecraft is in the solar wind and not in the Venus umbra, the spacecraft is positive, and the potential is derived from the suprathermal electron I-V curve. When the spacecraft is within the ionosphere or in the Venus umbra, the potential is assumed to be -1.5V.

The quantities TOTI, H+, O+, O2+, CO2+, TI, N1, T1, N2, T2 and the quantity $\sqrt{V_x^2 + V_y^2 + V_z^2}$ are derived by least-squares fitting a strongly non-linear numerical algorithm to an I-V curve. It is necessary in performing such a fit to supply an initial estimate of the quantities that are to be derived. If the estimates are not sufficiently close to the true least-squares values, the algorithm may yield a grossly erroneous value by converging to a relative minimum of the variance and not to the absolute minimum. Also, it may not converge at all. Although some such erroneous values have been eliminated from our basic tables tapes by checking for the magnitude of the variance, some erroneous values are known to be present. Such values can be way outside the nominal uncertainty quoted in Table 1.

The algorithm that scans the data in an ion I-V curve and computes the initial estimates of the ion quantities must also make a decision as to what ion mass is represented by a peak in delta I (DI) [Knudsen et al., 1979; 1980]. The voltage at which the DI peak occurs for a given mass may be substantially smaller or larger than the nominal value because the Venus ionosphere is moving relative the planet with a velocity that can approach that of the spacecraft. Consequently, some peaks in DI have been assigned the wrong mass. The result is not only an erroneous concentration for that mass but also an erroneous ion velocity and total ion density. It is possible to recognize the incorrect assignments when comparing several I-V curves which are adjacent to each other in time, but the analysis algorithms are not this sophisticated. A few errors in ion quantities are present in the NSSDC files resulting from this difficulty.

The analysis of a suprathermal electron I-V curve is similarly difficult. The interpretation of the electron distributions contributing to the I-V curve depends on the potential of the spacecraft relative to the ambient plasma which, in turn, depends on the location of the spacecraft and the properties of the ambient plasma. The spacecraft is negative in the dense ionospheric plasma. It is positive in the low density solar wind plasma provided the spacecraft is not in the umbra of the planet. An additional complication arises in that the sign of the current to the electrometer occasionally changes from negative to positive during a sweep. This can occur because the background current, with maximum retarding potential applied to the retarding grids, is compensated close to the noise level of the electrometer just before the sweep begins [Knudsen et al., 1979]. If the background current that has been compensated is significant relative to the saturation current and changes in the right direction during the ensuing sweep, the total current will go through zero and the sign change. The background current can change because the orientation of the rotating spacecraft relative to the sun changes, because a purely temporal change occurs or because the location of the spacecraft changes. Switching of the current from one sign to the other with the electrometer in its most sensitive mode produces a noise spike in the electrometer that is digitized and becomes part of the I-V curve. Writing an algorithm that recognizes the noise spike and the change in current sign is difficult because the sign of only the saturation current and background current of a sweep has been retained in the I-V data for reasons of minimizing the telemetry requirements of the RPA. A trained observer, looking at an I-V plot, can rather quickly recognize in most cases when this condition has occurred, but it is difficult to write an algorithm that can recognize all the possible situations and make the necessary adjustments.

In summary, some of the quantities contained in this submittal of RPA data to the NSSDC are erroneous because of bad least-squares fits to the I-V curves. These bad fits have not been detected by our current

algorithms for reduction of the data and have not been removed by a trained observer viewing the I-V curves and making an educated judgment.

REFERENCES

Knudsen, W. C. Evaluation and demonstration of the use of retarding potential analyzers for measuring several ionospheric quantities, *J. Geophys. Res.*, 71, 4669-4678, 1966.

Knudsen, W. C., J. C. Bakke, K. Spenner, and V. Novak, Retarding potential analyzer for the Pioneer-Venus Orbiter mission, *Space Sci. Instrum.*, 4, 351-372, 1979.

Knudsen, W. C., K. Spenner, J. Bakke, and V. Novak, Pioneer Venus orbiter retarding potential analyzer experiment, *IEEE Trans. Geosci. and Remote Sensing, GE-18*, 1, 54-59, 1980.

Knudsen, W. C. and K. L. Miller, Pioneer Venus suprathermal electron flux measurements in the Venus Umbra, *J. Geophys. Res.*, 90, 2695-2702, 1985.

<u>SYMBOL</u>	<u>QUANTITY</u>	<u>RANGE</u>	<u>NOISE LEVEL</u>	<u>UNCERTAINTY</u>
UT	UNIVERSAL TIME OF MEASUREMENT	0 - 8.7E+07 ms	-	0.1 s
TOTI	TOTAL ION DENSITY	10 - 1E+06 cm-3	10 cm-3	10%
H+	HYDROGEN ION DENSITY	50 - 1E+06 cm-3	50 cm-3	10%
O+	OXYGEN ION DENSITY	50 - 1E+06 cm-3	50 cm-3	10%
O2+	SUM DENSITY OF CO+, N2+, NO+, O2+	50 - 1E+06 cm-3	50 cm-3	10%
CO2+	CARBON DIOXIDE ION	50 - 1E+06 cm-3	50 cm-3	10%
TI	ION TEMPERATURE	150 - 20,000 K	-	10%
Vx	BULK ION VELOCITY COMPONENT & DIRECTION *	0 - 7,000 m/s	70 m/s	70 m/s
Vy	BULK ION VELOCITY COMPONENT & DIRECTION *	0 - 7,000 m/s	70 m/s	70 m/s
Vz	BULK ION VELOCITY COMPONENT & DIRECTION *	0 - 7,000 m/s	70 m/s	70 m/s
FII	SATURATION ION CURRENT	0 - 1.3E-04 A	1E-12 A	1%
BKGI	ION BACKGROUND CURRENT	0 - 1.3E-04 A	1E-12 A	1%
VPI	SPACECRAFT GROUND POTENTIAL	-5 - +3 V	-	0.1 V
TOTE	ELECTRON DENSITY	100 - 1E+07 cm-3	-	-
TE	ELECTRON TEMPERATURE	100 - 20,000 K	-	10%
FIE	SATURATION ELECTRON CURRENT	0 - 1.3E-04 A	1E-12 A	1%
BKGE	ELECTRON BACKGROUND CURRENT	0 - 1.3E-04 A	1E-12 A	1%
VPTE	SPACECRAFT GROUND POTENTIAL	-5 - +3 V	-	0.1 V
N1	FIRST SUPRATHERMAL ELECTRON DENSITY	0 - 1E+7	1 cm-3	20%
T1	FIRST SUPRATHERMAL ELECTRON TEMPERATURE	0 - 100 eV	0.1 eV	20%
N2	SECOND SUPRATHERMAL ELECTRON DENSITY	0 - 1E+5	1 cm-3	20%
T2	SECOND SUPRATHERMAL ELECTRON TEMPERATURE	0 - 100 EV	0.2 eV	20%
F1P	SATURATION SUPRATHERMAL ELECTRON CURRENT	0 - 1.3E-04 A	1E-12 A	1%
BKGP	BACKGROUND SUPRATHERMAL ELECTRON CURRENT	0 - 1.3E-04 A	1E-12 A	1%
VPPE	SUPRATHERMAL ELECTRON SPACECRAFT POTENTIAL	-5 - +20 V	-	2 V

* The vector (Vx, Vy, Vz) has a magnitude, m, equal to the component of the bulk ion velocity in the direction (Vx/m, Vy/m, Vz/m). The components of the vectors are given in the earth ecliptic coordinate system.

REFERENCES

- Brace, L. H., Additional Pioneer Venus observations of the precursor to the Venus bow shock (abstract), *EOS Trans. AGU*, 68, 342, 1987.
- Brace, L. H., S. A. Curtis, C. T. Russell, and F. L. Scarf, A precursor to the Venus bow shock (abstract), *EOS Tran. AGU*, 66, 294, 1985.
- Grebowsky, J. M., and S. A. Curtis, Venus nightside ionospheric holes; the signatures of parallel electric field acceleration regions, *Geophys. Res. Lett.*, 8, 1273, 1981.
- Gringauz, K. I., M. I. Verigen, T. K. Breus., and Tom Gomboshi, The interaction of electrons in the optical umbra of Venus with the planetary atmosphere-The origin of the nighttime ionosphere, *J. Geophys. Res.*, 84, 2123, 1979.
- Intriligator, D. S., L. Brace, S. H. Brecht, W. C. Knudsen, F. L. Scarf, R. J. Strangeway, and H. Taylor, Evidence for unusually high densities of plasma in the Venusian ionosheath, *Geophys. Res. Lett.*, 18, 61-64, 1991.
- Knudsen, W. C., Venus bow shock precursor (abstract), *Eos Trans. AGU*, 66, 1024, 1985.
- Knudsen, W. C., Solar cycle changes in the morphology of the Venus ionosphere, *J. Geophys. Res.*, 93, 8756-8762, 1988.
- Knudsen, W. C., Role of hot oxygen in Venusian ionospheric ion energetics and supersonic antisunward flow, *J. Geophys. Res.*, 95, 1097-1101, 1990a.
- Knudsen, W. C., Origin of Suprathermal Electrons in the Venus Ionosphere (abstract), *EOS*, 71, 1431, 1990b.
- Knudsen, W. C., Finite grid radius and thickness effects on RPA- measured suprathermal electron density and temperature, *J. Geophys. Res.*, 97, 13,767, 1992a.
- Knudsen, W. C., The Venus Ionosphere from In-situ Measurements, in Venus and Mars: Atmospheres, Ionospheres, and Solar Wind Interactions, J. G. Luhmann, M. Tatrallyay, and Robert O. Pepin, Eds., pp. 237 - 263, AGU Geophysical Monograph 66, The American Geophysical Union, Wash. DC., 1992b.
- Knudsen, W. C., K. L. Miller, and K. Spenner, Median density altitude profiles of the major ions in the central nightside Venus ionosphere, *J. Geophys. Res.*, 91, 1986.
- Knudsen, W. C., A. J. Kliore, and R. C. Whitten, Solar cycle changes in the ionization sources of the nightside Venus ionosphere, *J. Geophys. Res.*, 92, 13,391, 1987.
- Knudsen, W. C., J. G. Luhmann, C. T. Russell, F. L. Scarf, The Venus precursor: An environmental effect on the Pioneer Venus spacecraft, *J. Geophys. Res.*, 94, 197-207, 1989.
- Knudsen, W. C. and K. L. Miller, The Venus transterminator ion flux at solar maximum, *J. Geophys. Res.*, 97, 17,165, 1992.



Report Documentation Page

1. Report No.	2. Government Accession No.	3. Recipient's Catalog No.	
4. Title and Subtitle Pioneer Venus Data Analysis for the Retarding Potential Analyzer		5. Report Date Oct. 5, 1993	
		6. Performing Organization Code	
7. Author(s) William C. Knudsen		8. Performing Organization Report No.	
		10. Work Unit No. 370-24-11	
9. Performing Organization Name and Address Knudsen Geophysical Research Inc. 18475 Twin Creeks Rd. Monte Sereno, CA 95030		11. Contract or Grant No. NAS2-12902	
		13. Type of Report and Period Covered Final Technical Report Aug., 1988 - Sept., 1993	
12. Sponsoring Agency Name and Address National Aeronautics and Space Administration Washington, D. C. 20546-0001 Ames Research Center, Moffett Field, CA 94035		14. Sponsoring Agency Code	
		15. Supplementary Notes	
16. Abstract <p>This report describes the data analysis and archiving activities, analysis results, and instrument performance of the orbiter retarding potential analyzer (ORPA) flown on the Pioneer Venus Orbiter spacecraft during the period, Aug. 1, 1988 to Sept. 30, 1993. During this period, the periapsis altitude of the Orbiter spacecraft descended slowly from 1900 km altitude, at which altitude the spacecraft was outside the Venus ionosphere, to approximately 130 km altitude in Oct. 1992 at which time communication with the spacecraft ceased as a result of entry of the spacecraft into the Venus atmosphere. The quantity of ORPA data returned during this reporting period was greatly reduced over that recovered in the previous years of the mission because of the reduced power capability of the spacecraft, loss of half of the onboard data storage, and partial failure of the ORPA. Despite the reduction in available data, especially ionospheric data, important scientific discoveries resulted from this extended period of the Pioneer Venus mission. The most significant discovery was that of a strong solar cycle change in the size of the dayside ionosphere and the resulting shutoff of flow of dayside ions into the nightside hemisphere. The large, topside O+ F2 ionospheric layer observed during the first three years of the Pioneer Venus mission, a period of solar cycle maximum activity, is absent during the solar cycle minimum activity period.</p>			
17. Key Words (Suggested by Author(s)) Pioneer Venus Mission, Venus ionosphere		18. Distribution Statement Unclassified - unlimited	
19. Security Classif. (of this report) Unclassified	20. Security Classif. (of this page) Un classified	21. No. of pages 84	22. Price

THE UNIVERSITY OF CHICAGO

1961